

**Structural development of postnatally generated
dentate granule cells in organotypic entorhino-
hippocampal slice cultures**

Dissertation
zur Erlangung des Doktorgrades
der Naturwissenschaften

vorgelegt beim Fachbereich Biowissenschaften
der Johann Wolfgang Goethe-Universität
in Frankfurt am Main

von
Tijana Radić
aus Tuzla, Bosnien und Herzegowina

Frankfurt am Main, 2017

(D30)

vom Fachbereich Biowissenschaften der
Johann Wolfgang Goethe-Universität als Dissertation angenommen.

Dekanin: Prof. Dr. Meike Piepenbring

Gutachter: Prof. Dr. Amparo Acker-Palmer
PD Dr. med. Stephan Wolfgang Schwarzacher

Datum der Disputation:

Teile dieser Arbeit wurden veröffentlicht:

Tijana Radic, Tassilo Jungenitz, Mathias Singer, Marcel Beining, Hermann Cuntz, Andreas Vlachos, Thomas Deller, and Stephan W. Schwarzacher (2017). Time-lapse imaging reveals highly dynamic structural maturation of postnatally born dentate granule cells in organotypic entorhino-hippocampal slice cultures. *Scientific Reports* 7, 43724; doi: 10.1038/srep4372.

Table of Contents

1. ZUSAMMENFASSUNG	11
2. ABSTRACT	19
3. INTRODUCTION	21
3.1. ANATOMY AND FUNCTION OF THE HIPPOCAMPAL FORMATION	22
3.2. STRUCTURE AND FUNCTION OF THE DENTATE GYRUS (DG)	24
3.3. DEVELOPMENT OF THE DG AND THE SUBGRANULAR ZONE	26
3.4. ADULT NEUROGENESIS	28
3.4.1. <i>The hippocampal neurogenic niche</i>	29
3.4.2. <i>Regulation of hippocampal adult neurogenesis</i>	31
3.4.3. <i>Structural development of adult-born dentate granule cells (GCs)</i>	36
3.4.4. <i>Functional development and integration of adult-born dentate GCs</i>	40
3.4.5. <i>Functional relevance of adult-born dentate GCs and clinical implications</i>	45
3.5. POSTNATAL NEUROGENESIS IN ORGANOTYPIC ENTORHINO-HIPPOCAMPAL SLICE CULTURES	48
3.6. AIM AND SCOPE OF THE STUDY	51
4. MATERIALS AND METHODS	53
4.1. ANIMALS AND ORGANOTYPIC ENTORHINO-HIPPOCAMPAL SLICE CULTURE (OTC) PREPARATION	53
4.2. VIRAL TRANSDUCTION OF GCs IN OTCs	54
4.3. TIME-LAPSE IMAGING OF NEWBORN GCs IN OTCs	56
4.4. TWO-PHOTON MICROSCOPY	57
4.5. 3-D RECONSTRUCTION OF LABELED GCs AND MORPHOLOGICAL ANALYSIS	58
4.6. ANTEROGRADE AXONAL TRACING	58
4.7. TRANSCARDIAL PERFUSION AND BRAIN SECTIONING	58
4.8. IMMUNOCYTOCHEMISTRY	59
4.9. CONFOCAL MICROSCOPY	61
4.10. HISTOLOGICAL DATA ANALYSIS	62
4.11. ELECTRON MICROSCOPY.....	63
4.12. STATISTICAL ANALYSIS.....	64

5. RESULTS	65
5.1. EXPRESSION OF DOUBLECORTIN (DCX) AND CALBINDIN IN THE POSTNATAL DG OF MICE AND RATS	65
5.1.1. <i>The distribution of DCX and calbindin in the mouse DG between P7 and P42</i>	65
5.1.2. <i>The distribution of DCX and calbindin in the rat DG between P7 and P42</i>	69
5.1.3. <i>The maturation pattern of the postnatal DG is faster in rats compared to mice</i>	73
5.2. HISTOLOGICAL CHARACTERISTICS AND MARKER DISTRIBUTION IN RAT OTCs	76
5.3. RETROVIRAL TRANSDUCTION ENABLES VISUALIZATION OF COMPLETE POSTNATALLY GENERATED GCs IN OTCs.....	82
5.4. ENTORHINAL PROJECTION FIBERS INNERVATE THE MOLECULAR LAYER IN OTCs DURING THE DEVELOPMENT OF POSTNATALLY GENERATED GCs	84
5.5. TIME-LAPSE IMAGING OF POSTNATALLY GENERATED GCs IN OTCs REVEALS HIGHLY DYNAMIC STRUCTURAL DEVELOPMENT.....	86
5.6. THE FORMATION OF SPINES IN POSTNATALLY GENERATED GCs	100
6. DISCUSSION	103
6.1. EARLY POSTNATAL DEVELOPMENT IN INTACT MOUSE AND RAT BRAINS	104
6.1.1. <i>The distribution of neuronal maturation markers in the DG of mice and rats</i>	104
6.1.2. <i>The maturation time course of the postnatal DG is faster in rats than in mice</i>	106
6.2. POSTNATAL NEUROGENESIS IN OTCs	107
6.2.1. <i>Histology of postnatal rat OTCs, a model for adult neurogenesis</i>	107
6.2.2. <i>Retroviral labeling of newborn GCs in postnatal OTCs</i>	112
6.2.3. <i>Postnatally born GCs mature within an intact entorhino-hippocampal circuitry in OTCs</i>	113
6.3. TIME-LAPSE IMAGING OF NEWBORN GCs IN OTCs UNCOVERS THE DYNAMICS OF DENDRITIC DEVELOPMENT	113

6.3.1. Newborn GC development during the second week is marked by highly dynamic structural changes	114
6.3.2. The third week of GC development is characterized by high dendritic complexity and the emergence of dendritic spines.....	115
6.3.3. Following dendritic pruning, postnatally born GCs reach a state of structural stability by the end of the fourth week of development	117
6.3.4. AAV-Syn-labeled older GCs do not exhibit the strong dynamic structural changes of newborn RV-GFP-labeled GCs	121
6.4. CONCLUSION AND OUTLOOK	122
7. REFERENCES	125
LIST OF ABBREVIATIONS	149
LIST OF FIGURES	153
LIST OF TABLES	155
ACKNOWLEDGEMENTS	157
ERKLÄRUNG	159
CURRICULUM VITAE	161

1. Zusammenfassung

Das Gehirn des Säugetieres, einschließlich des Menschen, hat die Fähigkeit selbst im adulten Organismus neue Nervenzellen aus neuronalen Stammzellen zu generieren. Diese neugebildeten Nervenzellen durchlaufen konkrete Phasen der Maturation, bis sie schließlich in das vorhandene neuronale Netzwerk strukturell und funktionell integriert werden (Eriksson et al., 1998; Espósito et al., 2005; Zhao et al., 2006; Ming and Song, 2011; Wang et al., 2011; Spalding et al., 2013). Adulte Neurogenese findet primär in zwei Hirnregionen statt: in der subventrikulären Zone (SVZ) am Rand des lateralen Ventrikels und der subgranulären Zone (SGZ) des *Gyrus dentatus* (GD) im Hippocampus (Ming and Song, 2011; Gonçalves et al., 2016b). Der Hippocampus ist im Temporallappen des Gehirns lokalisiert, Teil des limbischen Systems und erfüllt eine wesentliche Funktion für das räumliche und deklarative Gedächtnis, einschließlich der Verarbeitung emotionaler und für die räumliche Navigation notwendiger Informationen (Kheirbek and Hen, 2011; Buzsáki and Moser, 2013). Hauptsächlich erhält der GD synaptischen Input vom entorhinalen Cortex (EC) über den *Tractus perforans* und projiziert wiederum zur *Cornu Ammonis* (CA) Region CA3 des Hippocampus. Der GD ist die einzige Struktur des Hippocampus, in dem neue primäre Neurone, die sogenannten Körnerzellen, aus neuronalen Stammzellen lebenslang generiert werden. Eine der faszinierendsten Felder in den Neurowissenschaften beschäftigt sich mit der Zusammensetzung und den Prozessen innerhalb der neurogenen Nische und dem Beitrag neugeborener Körnerzellen zu Netzwerkprozessen und der Verarbeitung von Informationen (Drew et al., 2013). Der GD ist in der Verarbeitung räumlicher Informationen und kontextuellen Objekt-Erkennung involviert und trägt sehr wahrscheinlich vor allem zur Unterscheidung ähnlicher Muster bei. Der Begriff Mustertrennung (engl. *pattern separation*) beschreibt einen informationsverarbeitenden Prozess, bei dem äußerst ähnliche oder überlagernde Muster neuronaler Aktivität in unterschiedliche Repräsentationen getrennt werden. Auf Verhaltensebene manifestiert sich diese neuronale Funktion als Fähigkeit, feine Unterschiede in der Umwelt zu erkennen und sich

dementsprechend zu verhalten und anzupassen. Bisher wurde der Beitrag zur neuronalen Mustertrennung durch adulte Neurogenese hauptsächlich in Verhaltensexperimenten untersucht. Eine Inhibition der Bildung neuer Körnerzellen im GD führt zu Defiziten in der Diskriminierung zwischen sehr ähnlichen Umgebungen (Clelland et al., 2009; Nakashiba et al., 2012; Niibori et al., 2012; Danielson et al., 2016) und im Gegensatz dazu, führt eine Verstärkung der adulten Neurogenese zur besseren kontextuellen Erkennung und Unterscheidung ähnlicher Muster (Sahay et al., 2011; Clemenson et al., 2015). Des Weiteren konnten neurodegenerative Krankheiten (z.B. Alzheimer und Parkinson), sowie psychiatrische Erkrankungen (z.B. Depression und Schizophrenie) mit einer Beeinträchtigung der adulten Neurogenese in Verbindung gebracht werden (Zhao et al., 2008; Christian et al., 2014; Winner and Winkler, 2015).

Um in das neuronale Netzwerk integriert zu werden und zu dessen Funktion beitragen zu können, durchlaufen neurale Stammzellen im GD verschiedene Stadien der Maturation. Die strukturelle Entwicklung verläuft über mindestens 3 - 4 Wochen bis neugeborene Körnerzellen die allgemeine Morphologie von reifen Körnerzellen aufweisen (Zhao et al., 2006; Beining et al., 2016; Gonçalves et al., 2016a). Während der funktionellen Integration durchlaufen adult-geborene Körnerzellen zwischen 4 - 6 Wochen eine sogenannte „kritische Phase“, in der sie einen niedrigen Schwellenwert für synaptische Erregbarkeit aufzeigen, aber gleichzeitig eine schwache GABAerge Inhibition und eine erhöhte synaptische Plastizität (Schmidt-Hieber et al., 2004; Marín-Burgin et al., 2012; Pardi et al., 2015). Es wurde gezeigt, dass die allgemeine Entwicklung adult-geborener Körnerzellen die Entwicklungsphasen der embryonalen Körnerzellen widerspiegelt (Espósito et al., 2005; Piatti et al., 2011). Trotz einer Vielzahl wissenschaftlicher Publikationen sind noch viele Fragen zu den grundlegenden Mechanismen der adulten Neurogenese offen. Aufgrund des großen Potenzials der Neurogenese in regenerativen therapeutischen Ansätzen, ist es von großer Bedeutung einen detaillierten Einblick in die strukturelle Entwicklung und Netzwerkintegration neugeborener Neurone, sowie in die zugrunde liegenden zellulären Mechanismen und Dynamiken zu erhalten.

In der vorliegenden Dissertation wurden postnatal neugeborene Körnerzellen in organotypischen entorhino-hippocampalen Schnittkulturen (engl. „*organotypic entorhino-hippocampal slice cultures*“; OTCs) individuell über einen Zeitraum von mehreren Wochen beobachtet, um ihre strukturelle Entwicklung zu studieren. Die verwendeten OTCs entstammen Tieren, die am postnatalen Tag P4 - 5 präpariert und zunächst histologisch untersucht wurden. Eine Vergleichsstudie zwischen OTCs und fixierten histologischen Präparaten aus Maus und Ratte (P7 bis P42) zeigte eine ähnliche Verteilung des Markers junger Neurone Doublecortin (DCX) und des Markers reifer Körnerzellen Calbindin, sowie des allgemeinen Körnerzellmarkers Prox1. Sowohl *in vitro*, als auch *in vivo* war am frühesten Zeitpunkt der Studie (jeweils DIV 7 und P7) die Mehrheit der Körnerzellen DCX-positiv, während wenige Körnerzellen im äußeren Bereich der Körnerzellschicht Calbindin exprimierten. Zwischen P7 und P21 reduzierte sich die Anzahl der DCX-positiven Zellen *in vivo* graduell, was darauf hindeutet, dass die Rate der Neurogenese abnahm, während die Anzahl der reifen, Calbindin-positiven Körnerzellen anstieg. Ein direkter Vergleich zwischen Maus und Ratte ergab einen Unterschied in der Entwicklungsgeschwindigkeit neugeborener Körnerzellen *in vivo*. In der Ratte zeigten DCX-positiv Körnerzellen einen schnelleren Reifungsprozess im Vergleich zur Maus und dementsprechend einen höheren Anteil Calbindin-positiver Körnerzellen an P14 und P21. Diese Ergebnisse demonstrieren wichtige spezies-spezifische Unterschiede zwischen Mäusen und Ratten, die beim direkten Vergleich von unterschiedlichen Entwicklungsstudien beachtet werden sollten. Im Unterschied zur *in vivo* Situation kam es im OTC zu einer starken Abschwächung in der Neubildung von Körnerzellen mit dem Resultat, dass an DIV 28 nur wenige DCX-positiv Körnerzellen nachgewiesen werden konnten. Im Allgemeinen war die zelluläre Struktur des OTC und die generelle Verteilung der oben genannten neuronalen Marker jedoch vergleichbar mit dem postnatalen Zustand *in vivo*.

Zur vollständigen Visualisierung und Rekonstruktion neugeborener Körnerzellen im OTC, wurde ein retroviraler (RV) Vektor unter Verwendung einer lokalen Injektionstechnik direkt in den GD von OTCs injiziert (van Praag et

al., 2002; Zhao et al., 2006). Das verwendete RV transduziert ausschließlich teilungsaktive Zellen (Osten et al., 2007) und markiert diese mit einem grün-fluoreszierenden Protein (GFP). Das GFP wird unter einem zelltyp-unspezifischen CAG-Promotor exprimiert und markiert deshalb sowohl Neurone als auch Gliazellen. Die RV-markierten Zellen mit neuronaler Morphologie befanden sich hauptsächlich in der SGZ, den inneren Schichten der Körnerzellschicht und exprimierten den Körnerzellmarker Prox1 und den neuronalen Marker DCX. Zusätzlich war die RV-GFP-Markierung auch in Zellen vorhanden, die eine gliale Morphologie aufwiesen und weder DCX noch Prox1 exprimierten. Aufgrund ihrer unterschiedlichen morphologischen und immunzytochemischen Eigenschaften konnten Gliazellen leicht von RV-GFP-markierten Neuronen unterschieden werden. Die morphologischen Merkmale von jungen RV-GFP/Prox1-positiven Zellen in OTCs stimmten mit den Charakteristika der RV-markierten Körnerzellen überein, die zuvor in fixiertem *in vivo* Gewebe der Maus beschrieben wurden (Espósito et al., 2005; Zhao et al., 2006).

Neugeborene Körnerzellen in postnatalen OTCs differenzieren sich in einer organotypischen Umgebung. Für eine korrekte Körnerzell-Entwicklung ist die Anwesenheit von afferenten Fasern, die aus dem EC in die Molekularschicht (engl. *molecular layer*, ML) des GD projizieren, und somit eine funktionierende synaptische Verschaltung wichtig (Zafirov et al., 1994; Drakew et al., 1999; Frotscher et al., 2000). Bei der OTC-Präparation werden jedoch axonale Fasern aus dem EC unvermeidlich durchtrennt. Jedoch konnte in früheren Studien bereits gezeigt werden, dass die entorhino-hippocampale Verbindung in OTCs innerhalb von drei Tagen nach der Kultivierung wieder hergestellt wird, da axonale Fasern aus dem EC die ML des GD erneut innervieren (Li et al., 1994; Kluge et al., 1998). Um die Anwesenheit dieser EC-Projektionen in die ML zu frühen Beobachtungszeitpunkten zu verifizieren, wurde eine anterograde Markierung von entorhinalen Projektionsfasern mit dem biotinylierten Dextranamin Mini Ruby durchgeführt. Die Ergebnisse bestätigten die Existenz von Fasern des *Tractus perforans* zu einem frühen Zeitpunkt der Untersuchung (DIV 8) in der äußeren ML (engl. „*outer molecular layer*“; OML). Zu diesem

Zeitpunkt zeigten neugeborene Körnerzellen apikale dendritische Prozesse in der ML, die jedoch noch nicht die afferenten Fasern in der OML erreichten. An DIV 20 wiesen neugebildete Körnerzellen Dendriten in der OML auf, die dort Kontakt mit entorhinalen Fasern herstellten. Diese Beobachtung zeigt, dass die analysierten postnatal gebildeten Körnerzellen in eine bestehende entorhinale Terminationszone hineinwachsen und in einem intakten entorhino-hippocampalen Schaltkreis reifen. Dies ist sehr ähnlich zu der Situation im erwachsenen Gehirn, in dem sich neugeborene Körnerzellen in einem bereits etablierten entorhino-hippocampalen Netzwerk entwickeln und sich schließlich vollständig hinein integrieren.

Die erfolgreiche RV-Markierung von neugeborenen Körnerzellen in OTCs ermöglichte die tägliche Beobachtung von einzelnen Neuronen über einen längeren Zeitraum. Während der frühen postnatalen Entwicklungsphase in der zweiten Woche war die strukturelle Entwicklung durch eine hohe Dynamik der dendritischen Elongation und Retraktion gekennzeichnet. Ab der dritten Woche verringerte sich diese beobachtete Dynamik und dendritische Bäume zeigten eine komplexe dendritische Verzweigung und Merkmale fortgeschrittener Reifung: Distale dendritische Prozesse der meisten RV-GFP-markierten Körnerzellen endeten in der OML, erreichten die hippocampale Fissur und zeigten sehr komplexe dendritische Bäume mit der höchsten Anzahl von Verzweigungspunkten (engl. „*branch points*“) im Vergleich zu allen anderen Zeitpunkten. Etwa zur gleichen Zeit (ab Tag 16) konnte die Entstehung dendritischer Dornen (engl. *spines*) in den proximalen und distalen Teilen der dendritischen Bäume beobachtet werden und bestätigte bisherige *in vivo* Befunde über den Zeitpunkt der Dornenentstehung (Zhao et al., 2006; Ohkawa et al., 2012). Mit Hilfe von ultrastruktureller Bildgebung konnten synaptische Kontakte zwischen RV-GFP-markierten dendritischen Dornen und unmarkierten axonalen Terminalen nachgewiesen werden. Diese Beobachtung liefert ein weiteres Indiz für eine organotypische Entwicklung und synaptische Integration überlebender postnatal generierter Körnerzellen in OTCs. Zwischen der dritten und der vierten Woche zeigten neugeborene Körnerzellen eine verstärkte Reduktion (engl. „*pruning*“) dendritischer Segmente. Diese Beobachtung könnte

darauf hinweisen, dass Segmente ohne etablierte synaptische Kontakte reduziert werden, während Segmente mit einer kritischen Anzahl an Synapsen bestehen bleiben. Dieser Prozess dient möglicherweise einer dynamischen synaptischen Verschaltung und Optimierung. In der vierten Entwicklungswoche durchliefen neugeborene Körnerzellen eine Phase der strukturellen Stabilisierung, die durch eine Verfeinerung des dendritischen Baumes charakterisiert war. Die Dynamik dendritischer Fortsätze war stark reduziert und es gab nur wenig Veränderung in der gesamten dendritischen Struktur. Zwischen 3 - 4 Wochen zeigten RV-GFP-markierten Zellen die charakteristische Morphologie reifer Körnerzellen (van Praag et al., 2002; Espósito et al., 2005; Zhao et al., 2006; Jungenitz et al., 2014; Radic et al., 2015; Beining et al., 2016).

Durch einen Synapsin-1-tdTomato exprimierenden Adeno-assoziierten Virus (AAV-Syn) wurden ältere, sehr wahrscheinlich perinatal generierte Körnerzellen markiert, strukturell analysiert und neugeborenen RV-GFP-markierten Zellen gegenübergestellt. Im Gegensatz zu neugebildeten Körnerzellen blieben die morphologischen Eigenschaften der AAV-Syn-markierten Körnerzellen über den gesamten Zeitraum relativ stabil und zeigten selbst während der frühen Kultivierungsperiode keine hohe Dynamik. In der Phase der strukturellen Stabilisierung der vierten Woche erreichten die neugeborenen Körnerzellen einen ähnlichen strukturellen Zustand wie AAV-Syn-markierte Körnerzellen. Im direkten Vergleich zeigten die beiden Zellpopulationen während dieser Zeit keine signifikanten Unterschiede in der durchschnittlichen dendritischen Länge oder der durchschnittlichen Gesamtanzahl der Verzweigungspunkte.

Diese Beobachtungen deuten darauf hin, dass die Phase der hohen dendritischen Dynamik spezifisch bei jungen neugebildeten Körnerzellen auftritt und möglicherweise eine notwendige Voraussetzung für die korrekte Reifung und Herstellung von synaptischen Kontakten darstellt. Neue Körnerzellen zeigen vermutlich eine Elongation ihrer Prozesse um synaptische Partner zu suchen und eine Retraktion, wenn keine Verbindungen hergestellt werden können. Der dynamische Entwicklungsverlauf könnte einen Mechanismus

darstellen, der dazu dient, Dendriten zu ihren korrekten synaptischen Partnern zu leiten. Diese dynamische strukturelle Organisation könnte daher einen komplizierten Wegfindungsmechanismus widerspiegeln, der für die Herstellung von Kontakten mit präsynaptischen entorhinalen Fasern notwendig ist und so die Integration neugeborener Körnerzellen in das bestehende entorhino-hippocampale Netzwerk ermöglicht. Insgesamt zeigt diese Arbeit eine unerwartet hohe strukturelle Dynamik während der Entwicklung junger Körnerzellen auf. Darüber hinaus erweist sich die direkte Beobachtung viral-markierter postnataler Körnerzellen im OTC als ein geeignetes Modell um Prozesse der Neurogenese zu studieren.

2. Abstract

In the dentate gyrus (DG) of the mammalian hippocampus, neurogenesis continues to take place throughout an organism's life. Adult neurogenesis includes proliferation and differentiation of neural stem cells into dentate granule cells (GCs) that mature and integrate into the existing cellular network. This thesis work presents a novel approach that enables longitudinal examination of living postnatally generated GCs in their endogenous niche by using retroviral (RV) labeling in organotypic entorhino-hippocampal slice cultures (OTCs). Older GCs were fluorescence-labeled with an adeno-associated virus controlled by the synapsin 1 promoter (AAV-Syn). The combination of time-lapse imaging and 3-D reconstruction of newborn developing GCs and older, more mature GCs enabled comparative analyses of dendritic growth and cellular dynamics as well as investigations of spine formation and the establishment of synaptic contacts.

Postnatal neurogenesis was studied in the mouse and rat DG *in vivo* by analysis of the distribution of chemical neuronal maturation markers doublecortin (DCX) and calbindin in combination with the GC marker Prox1 between P7 and P42. The marker expression patterns at different time points indicated that the number of mature GCs increased gradually over time and that young, immature GCs were added to the inner layers of the granule cell layer (GCL), as is the case in the adult brain. The most substantial shift in GC maturation took place between P7 and P14, though GCs in the rat DG matured faster (i.e. by ~5 days) than GCs in the mouse. Immunocytochemical *in vitro* analysis in OTCs at DIV 7, 14, and 28 exhibited a distribution of marker expression over time that was comparable to *in vivo*, though the number of DCX-expressing GCs was low at DIV 28, indicating a considerable decrease in neurogenesis rate over time in the OTC. Nevertheless, RV-labeling of newborn GCs at DIV 0 yielded successful visualization and enabled time-lapse imaging of complete developing GCs up to 4 weeks after mitosis. During the second week of development, newborn GCs exhibited a high level of structural dynamics, including extension and retraction of dendritic segments. In the third week, newborn GCs displayed high dendritic complexity which was followed by

pronounced dendritic pruning. Finally, a phase of structural stabilization and local refinement could be observed during the fourth week. Older AAV-Syn-labeled GCs did not exhibit such dynamic structural remodeling. Anterograde tracing of entorhinal projection fibers using the biotinylated dextran amine Mini Ruby showed innervation of the outer molecular layer (OML) by entorhinal axons at early time points, i.e. DIV 8 when newborn GCs started to extend dendrites into the ML, as well as at DIV 20 when RV-labeled GCs exhibited elaborate dendritic trees with processes in the OML intermingling with entorhinal fibers. This shows that newborn GCs in the OTC grow into an area of existing entorhinal axon terminals, which is highly similar to the situation in the adult brain. Hence, the results show that postnatal neurogenesis can be studied effectively in the OTC system as a model of adult neurogenesis. The first appearance of spine-like protrusions in newborn GCs was observed two weeks post RV injection. Ultrastructural electron-microscopic images revealed that spines established synaptic contacts with axonal boutons. These findings suggest that newborn GCs are successfully integrated into the existing cellular circuitry in the OTC system. The high level of structural flexibility found in this study might be a necessary requisite of new neurons for successful dendritic maturation and functional integration into a neuronal network. Thus, live imaging of postnatally born GCs in the OTC appears as a useful novel approach to elucidate the mechanisms that affect cellular dynamics of neurogenesis.

3. Introduction

The mammalian brain possesses the ability to produce new neurons throughout the entire lifespan of the animal, including humans (Eriksson et al., 1998; Wang et al., 2011; Spalding et al., 2013). During the process of neurogenesis, proliferating neural stem cells (NSCs) are capable to differentiate into neurons that undergo distinct developmental steps to mature and integrate into the existing neuronal network. One of the major neurogenic niches in the postnatal and adult brain is the subgranular zone (SGZ) of the hippocampus. New granule cells (GCs) are continuously generated in this region just below the granule cell layer (GCL) of the dentate gyrus (DG). These newborn GCs migrate into the GCL where they eventually become structurally and functionally integrated into the DG cellular circuit and hence become involved in hippocampal-dependent functions pertaining to learning, memory, and emotion (Madsen et al., 2003; Clelland et al., 2009; Deng et al., 2010; Aimone et al., 2011; Sahay et al., 2011; Christian et al., 2014; Kempermann et al., 2015). Impairment of hippocampal adult neurogenesis appears to be implicated in various neurological and neuropsychiatric disorders including Alzheimer's disease and other forms of dementia, epilepsy, depression, and anxiety (Lie et al., 2004; Sahay and Hen, 2007; Braun and Jessberger, 2014; Hill et al., 2015; Lucassen et al., 2015; Miller and Hen, 2015; Winner and Winkler, 2015). Therefore, detailed understanding of physiological processes underlying structural and functional maturation and integration of newborn GCs is essential for the development of regenerative therapeutic approaches. This work presents original data on the early postnatal development of the DG and a novel approach to longitudinal observation of living developing newborn GCs in the postnatal DG using organotypic entorhino-hippocampal slice cultures (OTCs). Combining retroviral (RV) labeling and time-lapse imaging, I was able to study the course of structural dynamics and maturation of individual postnatally generated GCs and their integration into the existing hippocampal cellular circuit.

3.1. Anatomy and function of the hippocampal formation

The hippocampal formation is an ensemble of structures in the limbic system located in the medial temporal lobe of the brain. It is comprised of the entorhinal cortex (EC), the dentate gyrus (DG), the hippocampus proper that includes the Cornu Ammonis (CA) regions CA1, CA2, and CA3, as well as the subiculum, parasubiculum, and the presubiculum (Amaral and Witter, 1989; Amaral et al., 1990; Ishizuka et al., 1990; Witter, 1993; Andersen et al., 2006). The hippocampal formation contains a large number of place cells that fire only at particular locations within a given space and thus provide information about the animal's specific position in the environment (O'Keefe and Dostrovsky, 1971; O'Keefe, 1976; Moser et al., 2008). The so-called grid cells in the EC construct a spatiotemporal neural representation of the environment through their spatial firing structure with each grid cell exhibiting multiple firing fields that are organized in a hexagonal lattice (Hafting et al., 2005). In addition, the EC contains head direction cells, border cells, and speed cells which contribute to computation of spatial information and path integration (Sargolini et al., 2006; Solstad et al., 2008). Although the medial EC (MEC) is primarily involved in spatial information processing and the lateral EC (LEC) mainly conveys information related to specific objects and events, both parts of the EC are involved in context and item learning and memory (Hunsaker et al., 2013; Knierim et al., 2013; Keene et al., 2016). Therefore, the entorhino-hippocampal circuit has an essential function in spatial coding, navigation, and path integration (Moser et al., 2008; Igarashi, 2016) as well as episodic memory and planning (Buzsáki, 2005; Buckner, 2010; Buzsáki and Moser, 2013).

The entorhino-hippocampal cellular network is distinguished by the organization of principal cell layers and its laminar flow of information in the circuit (Witter, 1993; Strange et al., 2014). The EC receives a large part of the neocortical input to the hippocampal formation. While the stellate and pyramidal neurons from the superficial layers of the EC (layers II and III) provide some input to several regions of the hippocampal formation, including the distal apical dendrites of pyramidal neurons in the CA3 field, they mainly project axons

through the perforant path to the molecular layer (ML) of the DG where they synapse onto dentate GCs. Whereas axons from neurons in the LEC terminate in the outer ML (OML), those from MEC cells project to the middle ML (MML). The principal cells of the DG, the GCs, project their axons, the mossy fibers, to the CA3 area and form strong synapses with the pyramidal neurons. The latter then connect with other pyramidal neurons in CA3, as well as CA2 and CA1 via their axons, the so-called Schaffer collaterals. The CA1 neurons provide major input to the subiculum, but also project to the deep layers of the EC. The subiculum mainly projects to the EC but also provides input to the pre- and parasubiculum. For an illustration of the major connections in the entorhino-hippocampal circuit, see Figure 1. The DG is the only structure of the hippocampal formation in which the production of new neurons takes place throughout life. One of the major intriguing topics in neuroscience and adult neurogenesis research pertains to the special qualities of the DG that makes it capable to sustain and benefit from the continuous addition of new neurons (Drew et al., 2013).

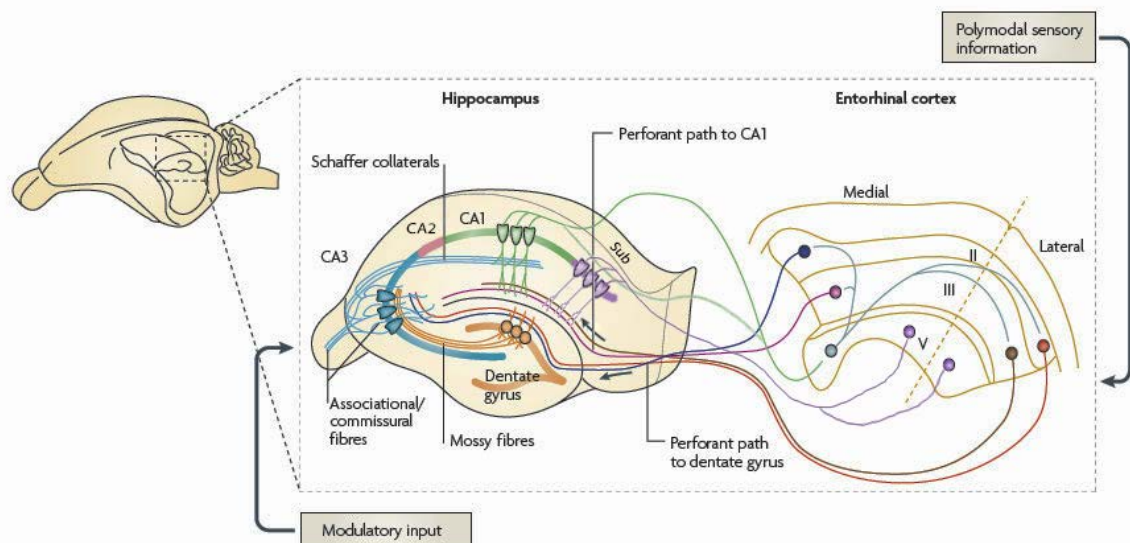


Figure 1. Principal neuron circuitry within the entorhino-hippocampal network. Polymodal sensory input is received by neurons of the entorhinal cortex (EC) layers II and III which then project fibers mainly to the molecular layer (ML) of the dentate gyrus via the perforant path. Dentate granule cells (GCs) receive input from the medial EC primarily in the middle ML and input from the lateral EC mainly in the outer ML. GCs project their axons, the mossy fibers, to CA3 pyramidal cells which extend their axons, the Schaffer collaterals to ipsilateral CA3, CA2, and CA1 pyramidal cells and

contralateral CA regions via associational and commissural fibers, respectively. In addition, the hippocampus receives strong modulatory input from subcortical areas. CA1 neurons provide input to the subiculum (Sub) and the deep layers of the EC. Neurons from the subiculum send connections to the EC as well as to the para- and the presubiculum (not shown) which project fibers to the EC as well. Image adapted from Neves et al. (2008).

3.2. Structure and function of the dentate gyrus (DG)

The DG is organized in a laminated fashion consisting of three main layers. Most superficially, the ML, which is subdivided into the outer (OML), middle (MML), and inner (IML) parts, mainly contains the apical dendrites of DG's principal neurons, the dentate GCs, and axonal projections that provide synaptic input to GCs (Amaral and Witter, 1989; Amaral et al., 1990, 2007). In addition, some inhibitory interneurons including MOPP (molecular layer perforant path-associated) cells and chandelier cells are found in the ML. Deep to the ML is the granule cell layer (GCL) that mainly contains the densely packed somata of GCs (Andersen et al., 2006). A subset of GCs, the so-called semilunar GCs, which have a distinct morphology and firing properties, are located at the border of the ML and the GCL (Williams et al., 2007; Larimer and Strowbridge, 2010). Together, the ML and the GCL form a V or U shape that is distinguished into the suprapyramidal blade located between the CA1 and the CA3 areas, the crest that forms the cleft in the V or U shape, and the infrapyramidal blade on the opposite side. Finally, the polymorphic layer, or hilus, is the third layer of the DG that consists of large glutamatergic mossy cells, GABAergic hilar interneurons, and mossy fibers that project through the hilus to CA3. The hilus contains a number of different GABAergic interneurons, including parvalbumin-expressing basket cells, and the somatostatin-expressing HIPP (hilar perforant path-associated), and HICAP (hilar commissural-associational pathway) interneurons (Amaral et al., 1990; Andersen et al., 2006). The diversity of cell types implies the intricate information processing within the DG. GCs do not only project to CA3 neurons but also transmit strong input to mossy cells and interneurons which in turn provide feedforward and/or feedback inhibition onto GCs. Mossy cells are also strongly activated by semilunar GCs and project their own axons into the ipsi- and contralateral IML

where they provide excitatory input to GCs and interneurons. The complex DG circuit is further elaborated by the constant addition of new GCs in the SGZ which is located just below the GCL. The structure, physiology, and connectivity of the DG are closely associated with its supposed functions within the hippocampal formation. Since GCs display particularly sparse activation (Chawla et al., 2005; Neunuebel and Knierim, 2012) and drastically outnumber the amount of EC cells that provide input to the DG as well as target neurons in the CA3 region (Amaral et al., 1990), it has been proposed that the DG mainly functions as a pattern separator (O'Reilly and McClelland, 1994; Kesner, 2007; Hunsaker and Kesner, 2013). Pattern separation is a process by which highly similar or overlapping input patterns of neuronal activity are separated into more distinct output firing patterns. This allows for similar input from the EC to be arranged into distinct representations in CA3 neuron ensembles to form and retrieve discrete memories (Leutgeb et al., 2007). In addition, the DG is thought to play a role in contextual and conjunctive encoding, and context-object recognition (Xavier and Costa, 2009; Kesner, 2013). Interestingly, the functions of the DG diverge along the septotemporal axis, with the septal (dorsal) DG being implicated in spatial memory and learning while the temporal (ventral) DG contributes to information processing related to emotion and motivation (Fanselow and Dong, 2010; Kheirbek and Hen, 2011). This is presumably mainly due to differential connectivity patterns, as the ventral hippocampus receives more considerable serotonergic input and projects to the nucleus accumbens, prefrontal cortex, the amygdala, and the hypothalamic-pituitary-axis, thus modulating circuits involved in reward, emotion, and stress response (Sahay and Hen, 2007; Kheirbek and Hen, 2011). Since the ongoing adult neurogenesis is a prominent element that greatly influences the cytoarchitecture and circuitry in both DG regions (Sahay and Hen, 2007; Bekiari et al., 2015), it is crucial to examine in what ways newborn GCs affect DG information processing and how they may perform or contribute to its specific functions.

3.3. Development of the DG and the subgranular zone

In rodent thymidine autoradiography studies, the development of the DG was described in remarkable detail (Angevine, 1965; Bayer and Altman, 1974; Schlessinger et al., 1975; Altman and Bayer, 1990). In the rat, first dentate GCs are generated around embryonic day 16 (E16) from the primary dentate neuroepithelium which consists of proliferating cells located around a ventricular indentation, the dentate notch. By day E18, the secondary dentate matrix of proliferative cells emerges in the subventricular area and starts to extend toward the formative DG in the so-called “first dentate migration” following a subpial course while continuing to proliferate. The secondary dentate matrix first forms the outer layers of the suprapyramidal blade of the DG and then adds new GCs to the infrapyramidal blade. By E22, a distinct population of migrating precursor cells, the “second dentate migration,” begins to add new GCs to the inner parts of the developing GCL. During this time, cell proliferation in the secondary dentate matrix decreases substantially while a new pool of locally dividing cells, the tertiary dentate matrix, arises within the hilar area of the DG and reaches its proliferative peak during the first postnatal week, at P5 - 8 (Schlessinger et al., 1975; Altman and Bayer, 1990). By P5, the GCL is established for the most part, although the infrapyramidal blade continues to expand and generally contains more immature GCs compared with the suprapyramidal blade. New GCs are still produced by both the second dentate migration and the tertiary dentate matrix, though the latter is prominent within the DG. This cell population forms the SGZ between P7 and P14 and continues to generate new GCs throughout the lifetime of the animal (Altman and Bayer, 1990; Nicola et al., 2015). For an overview of DG development, see Figure 2.

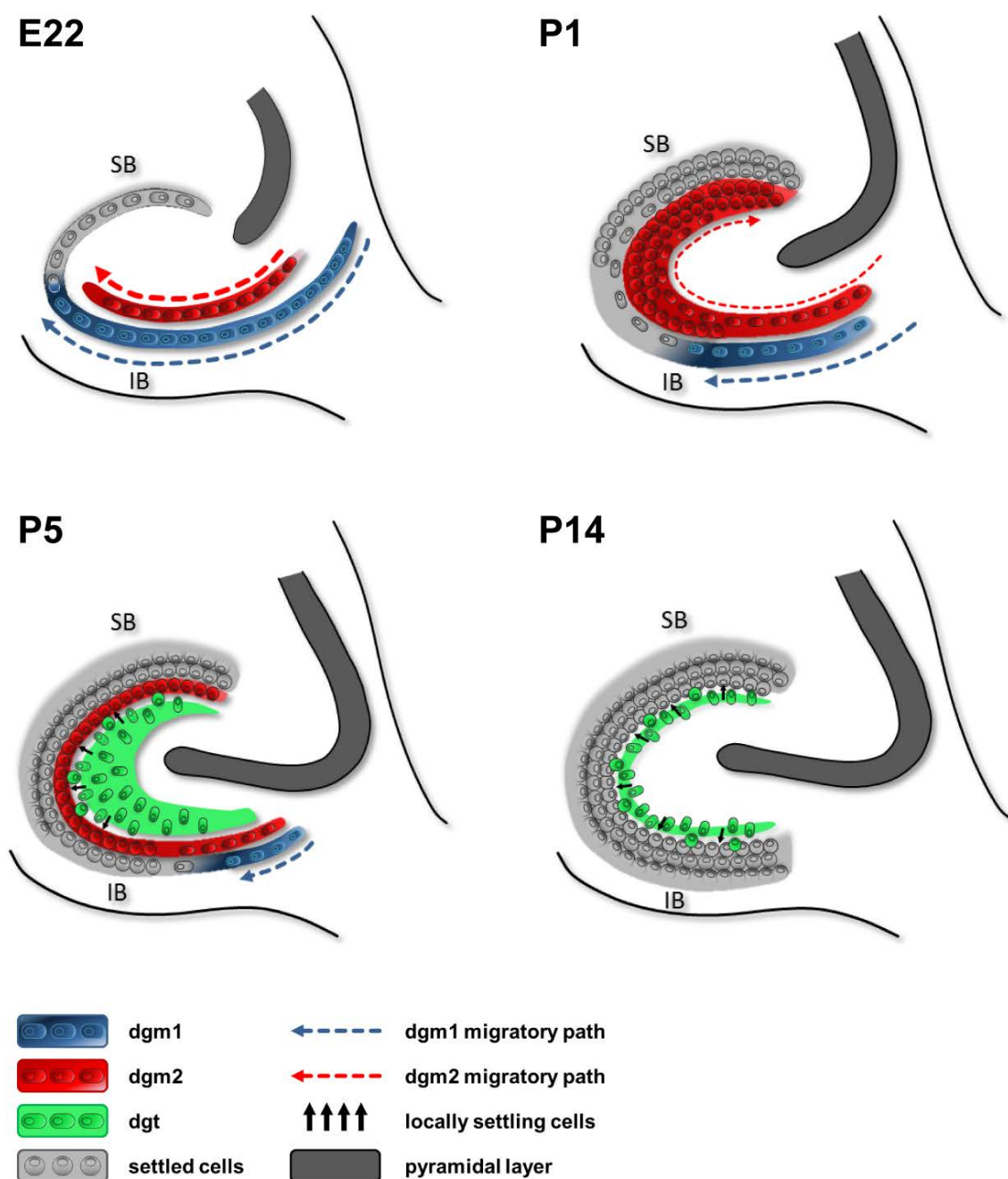


Figure 2. Development of the dentate gyrus (DG). First dentate granule cells (GCs) are generated from the primary dentate neuroepithelium near the lateral ventricle and the secondary dentate matrix that consists of proliferative neural stem cells migrating from the subventricular area toward the formative granule cell layer (GCL) called the first dentate migration (dgm1). Between E18 and E22, new GCs settle in the suprapyramidal blade (SB) of the GCL, then GCs are added to the infrapyramidal blade (IB). On E22, the migration is partitioned and the second dentate migration (dgm2) begins to add new GCs to the inner parts of the forming GCL. By P1, the secondary dentate matrix has decreased substantially, while dgm2 is still prominent and a new pool of locally proliferating cells, the tertiary dentate matrix (dgt) starts to emerge in the

hilar area. By P5, dgm2 has decreased considerably while cells of the dgt reach their proliferative peak and continue to add new GCs in the formative subgranular zone (SGZ). By P14, the SGZ is established as the neurogenic niche of the DG in which new GCs continue to be generated throughout life (Altman and Bayer, 1990; Nicola et al., 2015). Image designed after Altman and Bayer (1990).

3.4. Adult neurogenesis

The fact that the mammalian brain holds NSCs capable of self-renewal and the generation of new neurons in the adult organism was not generally accepted until very recently. The first major evidence of neurogenesis in the adult rat hippocampus and the olfactory bulb was presented in [³H]thymidine radiogram studies by Joseph Altman and Gopal D. Das (Altman and Das, 1965; Altman, 1969). Their findings were met with great skepticism by the scientific community as the dogma of non-regenerative neurons in the adult brain that had been postulated by Ramón y Cajal (1913) was still a wide-held belief. It wasn't until the 1980's, when adult neurogenesis was shown to occur in the tectum of song birds (Goldman and Nottebohm, 1983) that this topic started to receive more scientific attention. With the development of new cell birth marking techniques and neuronal markers improving the study of adult neurogenesis, it has since become the subject matter of extensive research in which its existence could be demonstrated in numerous animals, including humans (Miller and Nowakowski, 1988; Reynolds and Weiss, 1992; Cameron et al., 1993; Okano et al., 1993; Seki and Arai, 1993; Kuhn et al., 1996; Gould et al., 1997; Eriksson et al., 1998; Kornack and Rakic, 1999). There are two distinct regions in the brain that provide a unique suitable environment in which neurogenesis can be sustained throughout life: the subventricular zone (SVZ) which lines the lateral ventricles, and the subgranular zone (SGZ) in the DG (Altman, 1969; Altman and Bayer, 1990; Doetsch et al., 1997; Gage, 2000; Ming and Song, 2011). In the first study that revealed evidence of adult neurogenesis in humans, postmortem brain tissue of cancer patients who had been treated with the thymidine analog bromodeoxyuridine (BrdU) for diagnostic purposes was analyzed (Eriksson et al., 1998). BrdU is incorporated into the cell nucleus of mitotic cells during DNA synthesis and can be detected with

immunocytochemical staining (Miller and Nowakowski, 1988). By identifying BrdU-labeled cells that co-expressed neuronal markers such as neuron-specific nuclear protein (NeuN), calbindin, and neuron specific enolase (NSE), the production and survival of newborn neurons could be demonstrated in the adult human DG (Eriksson et al., 1998). A recent innovative approach enabled the examination of adult neurogenesis and cell turnover in humans in more detail. During the Cold War, in 1955–1963, nuclear bomb testing caused a high concentration of the isotope ^{14}C in the atmosphere around the globe. Since ^{14}C is integrated in the genomic DNA of mitotic cells in a concentration that corresponds to that in the atmosphere, the measurement of ^{14}C levels in postmortem brain tissue could be used for cell birth dating in adult humans. The study revealed a substantial amount of neurogenesis throughout life in the human DG with only a minor decline with aging, and thus suggests that adult neurogenesis may have an important function in the human brain (Spalding et al., 2005, 2013). Moreover, it was discovered that adult-born neurons in humans are also found in the striatum as opposed to the olfactory bulb as is the case in rodents (Bergmann et al., 2012; Ernst et al., 2014). This implies that in the second adult neurogenic niche, the SVZ, newborn neurons may serve differential purposes in rodents and humans.

3.4.1. The hippocampal neurogenic niche

The SVZ and the SGZ are the only two stem cell regions that provide a unique environment for the maintenance of adult neurogenesis (Altman, 1969; Altman and Bayer, 1990; Doetsch et al., 1997; Seri et al., 2004; Fuentealba et al., 2012). In the adult murine brain, newly generated neuronal precursors in the SVZ form a chain and migrate along the rostral migratory stream to the olfactory bulb where they differentiate into granular or periglomerular interneurons. In the SGZ, newborn neurons develop into excitatory dentate GCs that migrate a short distance into the GCL of the DG (Lois and Alvarez-Buylla, 1994; Seri et al., 2004; Ming and Song, 2011). However, NSCs have characteristic properties that include self-renewal and multipotency. This means that they can divide to

generate new NSCs as well as neurons, astrocytes, and oligodendrocytes (Reynolds and Weiss, 1992). It was shown that adult NSCs in the SVZ can differentiate into olfactory bulb neurons or oligodendrocytes that contribute to myelination in the corpus callosum. In contrast, adult NSCs in the SGZ generate mainly new neurons or astrocytes (Lois and Alvarez-Buylla, 1993; Seri et al., 2004; Bonaguidi et al., 2011; Ortega et al., 2013; Bond et al., 2015). The rate of proliferation, differentiation, and development of NSCs is regulated by a variety of factors and signals present in the microenvironment of the neurogenic niche.

The hippocampal neurogenic niche is characterized by a distinctive cellular and molecular composition (Seri et al., 2004; Fuentealba et al., 2012; Bond et al., 2015; Kempermann et al., 2015). The extracellular matrix generates a framework that maintains the niche structure and contains a variety of signaling molecules that have profound effects on neurogenesis. Blood vessels and vascular cells are further important components of the SGZ because they secrete factors and provide signals that impact NSC self-renewal, maintenance as well as quiescence (Ottone et al., 2014). Local astrocytes and microglia are glial cells that affect the development and survival of new NSCs in the SGZ (Bond et al., 2015). Microglia take up apoptotic NSCs and activated microglia can reduce neurogenesis (Ekdahl et al., 2003; Sierra et al., 2010; Sultan et al., 2015). The effects and regulatory mechanisms of the cellular and molecular components of the niche are discussed in more detail in section 3.4.2.

During the course of adult neurogenesis, NSCs in the SGZ undergo distinct developmental and maturation phases to become fully integrated dentate GCs (Kempermann et al., 2004, 2015; Seri et al., 2004). NSCs or type 1 radial glia-like (RGL) cells are largely quiescent but can become activated by particular environmental signaling cues to self-renew or produce intermediate progenitor cells (IPCs), otherwise known as type 2 cells. The highly proliferative IPCs are categorized into type 2a precursors which express the same stem cell and glial markers as type 1 cells, i.e. intermediate filament protein nestin, sex-determining region Y-box 2 (Sox2), glial fibrillary acidic protein (GFAP), and brain lipid-binding protein (BLBP), and type 2b cells that start to express

neuronal lineage markers such as neuronal differentiation factor 1 (NeuroD1), Prospero homeobox protein 1 (Prox1), polysialylated neural-cell-adhesion molecule (PSA-NCAM), and doublecortin (DCX) (Kempermann et al., 2015). DCX, a microtubule-associated protein, continues to be expressed for up to 4 weeks after cell division and is extensively used as a proxy marker for adult neurogenesis (Brown et al., 2003; Rao and Shetty, 2004; Couillard-Despres et al., 2005). It largely overlaps with PSA-NCAM which plays a role in synaptogenesis and hippocampal plasticity (Muller et al., 1996; Dityatev et al., 2004). Prox1 is a specific granule cell marker that continues to be expressed by GCs throughout their lifespan (Lavado and Oliver, 2007; Lavado et al., 2010). After a few rounds of division, type 2 cells give rise to type 3 cells, or neuroblasts, which continue to proliferate, albeit to a lesser degree. When these developing cells exit the cell cycle, they begin to express postmitotic neuronal markers such as the neuron-specific nuclear protein NeuN (Mullen et al., 1992). Calbindin is a calcium-binding protein that is expressed in GCs from about 3 weeks on and is commonly used as a marker for mature neurons (Brandt et al., 2003; Snyder et al., 2009; Jungenitz et al., 2014). For a summary of expression patterns of important developmental markers see Figure 3. The overall maturation process until newborn GCs are completely structurally and functionally integrated into the hippocampal network and are almost indistinguishable from other mature GCs is believed to take at least 5 weeks following mitosis (van Praag et al., 2002; Ambrogini et al., 2004; Jungenitz et al., 2014; Kempermann et al., 2015; Beining et al., 2016). The differentiation and development of NSCs to mature GCs is dynamically regulated by a variety of intrinsic factors and mechanisms and influencing extrinsic cues in the SGZ neurogenic niche.

3.4.2. Regulation of hippocampal adult neurogenesis

The SGZ stem cell niche consists of a variety of different cell types, molecules, and signaling mechanisms that exert an influence on newborn cells which can target different stages of their development (Doetsch, 2003; Alvarez-

Buylla and Lim, 2004; Seri et al., 2004; Ma et al., 2005; Fuentealba et al., 2012). Morphogens that play an essential role in embryonic development also greatly affect NSCs in adult tissue. One of the major morphogens that regulate multiple levels of adult neurogenesis is Notch signaling which is necessary for self-renewal, while blockade of the Notch pathway leads to neuronal differentiation and a depletion of the progenitor cell pool. In addition, Notch1 is important for neuronal structural development at later stages of maturation. However, the effects of Notch sometimes appear to be divergent, as its function is context-dependent (Gonçalves et al., 2016b). Along the same lines, sonic hedgehog (Shh) signaling induces proliferation of progenitor cells and is hence involved in the formation and expansion of postnatal progenitors. Activation of Wnt signaling also has an essential function in self-renewal and maintenance of early progenitors, but it also promotes neuronal differentiation of IPCs as well as dendritic development and radial migration at later developmental stages (Bond et al., 2015; Gonçalves et al., 2016b). In contrast, bone morphogenetic proteins (BMPs) generally promote NSC quiescence and control of GC maturation rate. However, BMP signaling is also involved in a variety of functions related to cell survival, proliferation, and fate specification, but these are very context-dependent (Gonçalves et al., 2016b). In addition, adult neurogenesis is influenced by a variety of neurotrophic and growth factors, including brain-derived neurotrophic factor (BDNF) which stimulates dendritic growth and arbor complexity, vascular endothelial growth factor (VEGF) which induces self-renewal of NSCs, fibroblast growth factor (FGF-2) and epidermal growth factor (EGF) which stimulate proliferation and neurogenesis, and neurotrophin-3 (NT-3) which promotes quiescence (Delgado et al., 2014; Bond et al., 2015). The regulation of adult neurogenesis and neuronal development is highly dependent on intracellular transcriptional control (Hsieh, 2012; Beckervordersandforth et al., 2015; Bond et al., 2015). The transcription factor Sox2 is essential for NSC maintenance and plays a vital role in balancing proliferation and differentiation (Julian et al., 2013). Achaete-scute homolog 1 (Ascl1) or Mash1 is involved in the activation of NSCs by influencing cell-cycle regulators and the induction of the neuronal fate (Andersen et al., 2014). The transcription factor NeuroD1, a

target of Wnt signaling, is also essential for neuronal differentiation of NSCs as well as the survival and maturation of developing GCs (Lee et al., 1995; Pleasure et al., 2000; Gao et al., 2009). Prox1 is a transcription factor that is crucial for granule cell type specification and development (Lavado and Oliver, 2007; Lavado et al., 2010) and maintenance of dentate GC identity (Iwano et al., 2012).

Since communication with other NSCs as well as vascular endothelial cells or astrocytes is important during NSC development, cell-cell signaling molecules are essential components of the neurogenic niche. For example, connexins make up gap junctions with which NSCs are connected and Cx30 and Cx43 have been found to be critical for NSC pool maintenance (Kunze et al., 2009; Bond et al., 2015). Ephrin ligands and Eph receptors have also been implicated in NSC regulation, albeit with differential functions in different niches. For example, ephrinB2 expressed by endothelial cells in the SVZ induces NSC quiescence and prevents differentiation. On the other hand, ephrinB2 expressed by astrocytes in the SGZ binds to the EphB4 receptor and stimulates transcription factor upregulation that induces neuronal differentiation (Ashton et al., 2012; Ottone et al., 2014). Astrocytes have a particularly vital role in adult neurogenesis and the development of newborn neurons. Astrocytic release of cytokines IL-1 β and IL-6 induce neuronal differentiation of NSCs (Barkho et al., 2006). Developing neurons are located in close proximity to astrocytic processes which was found to be essential for adult-born GC survival, proper dendritic development, and synaptic integration, presumably via astrocytic release of D-serine (Shapiro et al., 2005; Sultan et al., 2013, 2015). The structure of adult NSCs with the long radial process that branches out into many individual segments in the ML enables NSCs to sense and integrate a variety of regulatory signals including neurotransmitters that are released by the surrounding network of mature neurons (Berg et al., 2013; Bond et al., 2015).

Neurotransmitters, in particular the typically inhibitory γ -aminobutyric acid (GABA), exert a major influence on NSCs which contain GABA and glutamate receptors very early on (Espósito et al., 2005; Ambrogini et al., 2006).

Essentially, GABA released by parvalbumin-expressing interneurons inhibits cell-cycle progression and thus maintains quiescence of inactive NSCs (Fernando et al., 2011). However, GABA has a depolarizing effect on active NSCs (type 2 and type 3 cells) and young newborn neurons since these have a high concentration of intracellular Cl^- due to a strong expression of the $\text{Na}^+/\text{K}^+/\text{Cl}^-$ co-transporter NKCC1 (imports Cl^-) and very few K^+ -coupled Cl^- transporters KCC2 (which export Cl^-) (Ben-Ari, 2002; Ge et al., 2006). In this manner, GABA stimulates the expression of NeuroD and induces CREB signaling, thus promoting differentiation, survival, and integration of newborn GCs (Tozuka et al., 2005; Ge et al., 2006; Jagasia et al., 2009; Song et al., 2012, 2013; Alvarez et al., 2016). Other neurotransmitters may exert an influence on NSCs, as it was shown in the SVZ that dopamine seems to induce quiescence (Kippin et al., 2005) while serotonin and acetylcholine promote NSC activation (Paez-Gonzalez et al., 2014; Tong et al., 2014). At later developmental stages, from approximately 2 weeks of cell age on, activation of N-Methyl-D-aspartate receptors (NMDARs) by the excitatory neurotransmitter glutamate becomes crucial for newborn GC survival, structural development, and network integration (Tashiro et al., 2006; Mu et al., 2015). Newborn GCs receive excitatory input from hilar mossy cells very early on, starting 5 - 10 days after birth (Vivar et al., 2012) and later from projection fibers of the EC (Deshpande et al., 2013; Song et al., 2016). These data support the notion that the development, survival, and integration of newly generated GCs are highly dependent on network activity and thus experience (Dranovsky et al., 2011; Piatti et al., 2011; Alvarez et al., 2016).

Physiological stimuli have distinctive effects on adult neurogenesis and accordingly affect cognitive performance. Voluntary exercise drastically stimulates the proliferation of NSCs in the SGZ while the exposure to an enriched environment increases the survival rate of newborn GCs (Kempermann et al., 1997; van Praag et al., 1999b). As a result, both stimuli have shown to improve spatial memory and an enriched environment also had a positive effect on recognition memory (van Praag et al., 1999a; Farmer et al., 2004; Bruel-Jungerman et al., 2005; Tashiro et al., 2007; Creer et al., 2010;

Vivar et al., 2013; Garthe et al., 2015). On the contrary, chronic stress and aging seem to impair adult neurogenesis and thus have a negative effect on learning and memory, although different studies regarding stress and learning have yielded inconsistent results (Shors, 2004; Zhao et al., 2008). As learning itself stimulates neural activity and may require involvement of newborn GCs, it has a positive effect on the survival and integration of newborn GCs. However, only some hippocampus-dependent learning tasks such as spatial learning in the Morris water maze contribute to these effects and only during distinct phases of GC development (Döbrössy et al., 2003; Dupret et al., 2007). Pathological conditions that involve heightened neural activity such as seizures also increase proliferation of both progenitors and neuroblasts. However, seizures cause aberrant morphological development, including an increased number of basal dendrites as well as mossy fiber sprouting, and ectopic migration into the hilus (Jessberger et al., 2007; Walter et al., 2007). Following stroke, the production of neurons is considerably increased in both the SGZ and the SVZ. Newborn cells from the SVZ can migrate toward the site of injury and assume the neuronal phenotype specific to that area. However, it is not clear to what extent this process can compensate for any stroke-related damage (Thored et al., 2007; Lindvall and Kokaia, 2011). On the other hand, inflammation causes a profound decrease in neurogenesis, as it inhibits proliferation and neuronal fate commitment of precursor cells in addition to stimulating microglial activation which further protracts the inhibition of neurogenesis (Ekdahl et al., 2003; Monje et al., 2003; Ming and Song, 2011).

Taken together, the interplay of a variety of intra- and extracellular factors greatly affects the generation, survival, development, and integration of newborn NSCs in very different ways depending on the subject's experience. In any case, a large proportion of newborn cells, approximately 75%, undergo apoptosis during either an early or a late critical stage (Christian et al., 2014). During the "early survival phase" which occurs within the first 4 days following mitosis, only a very small fraction of newborn cells survives (Kempermann et al., 2003, 2015; Mandyam et al., 2007; Snyder et al., 2009; Sierra et al., 2010). This process seems to be mainly mediated by activity-dependent BDNF

signaling and neurotransmission of GABA by parvalbumin-expressing interneurons (Tozuka et al., 2005; Bergami and Berninger, 2012; Dieni et al., 2013; Song et al., 2013; Kempermann et al., 2015). During the "late survival phase" at 2 - 3 weeks, the loss of neurons is not as drastic and survival highly depends on NMDAR activation (Tashiro et al., 2006; Mu et al., 2015). It appears that survival is contingent upon network activity during both phases, even early on before new GCs establish any pre- or post-synaptic contacts. Surviving newborn GCs that eventually become integrated into the hippocampal network undergo distinct developmental steps until they reach full structural and functional maturity (Kempermann et al., 2004, 2015).

3.4.3. Structural development of adult-born dentate granule cells (GCs)

With the development of the retroviral (RV) labeling technique in which the sequence for a fluorescent protein is inserted into an RV vector that can only transduce cells that are in the midst of undergoing mitosis, it became possible to visualize complete newborn GCs and determine their day of birth (van Praag et al., 2002; Osten et al., 2007). Several studies ensued in which animals were injected with an RV solution *in vivo* and sacrificed after different time intervals so that complete dendritic structures of adult-born GCs could be analyzed in fixed brain sections at particular time points of development (van Praag et al., 2002; Espósito et al., 2005; Zhao et al., 2006). Two days following RV injection, labeled cells are found in the SGZ and adjacent inner part of the GCL, suggesting that these newborn cells are the progeny of SGZ NSCs (van Praag et al., 2002). At 7 days old, most newborn GCs are located in the SGZ or the inner GCL, and express DCX or both DCX and NeuN, while merely a small fraction expresses NeuN only. Structurally, there are two different classes of newborn neurons: "Class A" GCs display a plump, irregular soma with either no neurites or short processes extending in parallel to the GCL, while "class B" GCs have an oval soma with longer neurites that run horizontally to or into the GCL (Espósito et al., 2005). Moreover, during the first week of development, newborn GCs begin to extend axons, the mossy fibers, through the hilus toward

the target zone CA3 area (Hastings and Gould, 1999; Sun et al., 2013). At 10 days post injection (dpi), axonal processes of newborn GCs are present in the hilus, and 11-16 dpi they continually move further into the CA3 region where they establish synapses with pyramidal neurons (Toni et al., 2008; Sun et al., 2013). Mossy fiber growth and innervation of pyramidal cells and interneurons in the CA3 region as well as local DG and hilar interneurons, is completed by 3 weeks of cell age (Zhao et al., 2006; Sun et al., 2013). The dendritic development at 10 dpi also progresses substantially as apical arbors begin to branch out more extensively and reach through the GCL into the IML (Zhao et al., 2006). At 14 dpi, almost 50% of all RV-labeled cells express both DCX and NeuN, while less than 5% express only DCX or NeuN. The morphology is more elaborate, and dendrites, which typically don't contain any spines yet, extend into the MML. Moreover, the majority of newborn GCs have migrated into the inner layers of the GCL by this time and many exhibit basal dendrites extending toward the hilus (Espósito et al., 2005). The emergence of first dendritic spines in adult-born GCs generally starts at approximately 16 dpi. At 21 dpi, some GCs already exhibit elaborate dendritic arbors resembling mature GCs and don't seem to structurally change considerably thereafter (Zhao et al., 2006; Beining et al., 2016). At 28 dpi, the majority of newborn GCs express NeuN only and their somata are positioned in the inner and middle GCL. Their dendrites contain numerous spines and reach the OML at this point (Espósito et al., 2005) (for a summary see Figure 3). Even though the basic morphology appears to be established by this time, some studies have reported continuous additional dendritic growth, branching, or pruning, as well as an increase in spine density over the course of several months (van Praag et al., 2002; Jungenitz et al., unpublished). Interestingly, even though matured adult-born GCs morphologically largely resemble prenatally generated GCs, they possess a few distinct morphological features. Their dendrites are more curved and contain a higher number of short terminal segments (STS). In addition, they exhibit differences in the branching pattern, as they display a higher number of branch points in the IML and the OML, and fewer branches in the MML. These

differences may be attributed to dendritic pruning during structural development and postnatal growth of the DG (Beining et al., 2016).

In recent research, dendritic development of newborn GCs was examined in a dynamic manner by the employment of time-lapse imaging of living cells. In an *in vitro* paradigm, slice cultures of adult mice were used to label newborn GCs with an RV vector and follow the development of their neurites in 24 hour intervals from day *in vitro* (DIV) 2 or 3 up to DIV 9. Neurite growth was generally very variable between individual GCs. However, most cells developed a primary apical dendrite around DIV 4 that continued to extend toward the ML until DIV 9 (Kleine Borgmann et al., 2013). More recently, time-lapse imaging was performed over an extended period of time *in vivo* in adult mice. Newborn RV-labeled GCs were followed from 15 up to 60 dpi. Their morphological development within that time frame showed rapid dendritic growth during the third and fourth week post injection after which there was only little change in dendritic length. During early time points, dendritic segments were simultaneously added and withdrawn whereby there was a net increase in branching during the third week, whereas in the fourth week, there was a strong reduction in the number of branches and almost no structural change in the fifth week. This indicates that newborn GCs first go through a period of over-branching followed by extensive dendritic pruning until they reach a stable structural state (Gonçalves et al., 2016a). Interestingly, the developmental pattern could be modulated by experience. When animals were exposed to an enriched environment, newborn GCs displayed longer dendrites and more branching during the third week of development compared to the control group. However, by the fifth week, i.e. at 31 dpi, there were no significant differences in total dendritic length or number of branches between the two groups. This indicates that GCs that showed higher growth and branching as a result of increased activity also underwent a higher level of dendritic pruning. Similarly, when dendritic growth of newborn GCs was impaired by blockade of Wnt signaling, the manipulated GCs initially exhibited both faster dendritic growth and higher branching during the third week, while at 31 dpi, they had a shorter total dendritic length but a comparable number of branches as controls. These

results show that dendritic branching patterns are affected by extrinsic stimuli such as activity and extracellular signals, but are homeostatically regulated via pruning which is possibly governed by intracellular mechanisms (Gonçalves et al., 2016a).

In general, the morphological findings reveal that adult-born GCs follow a highly similar course of maturation as GCs generated during ontogenesis (Espósito et al., 2005), although the developmental progression in the adult brain appears to be slightly slower, i.e. by approximately 4 days (Zhao et al., 2006). However, a number of studies have shown that there is substantial variability in the onset and speed of structural development between individual GCs which should be taken into account (Plümpe et al., 2006; Kleine Borgmann et al., 2013; Jungenitz et al., 2014; Radic et al., 2015). Using BrdU and DCX staining to visualize adult-born GCs in the mouse DG at 4 hours, 1 day, 3 days, 1 week, 2.5 weeks, and 4 weeks post mitosis, Plümpe et al. (2006) observed newborn GCs of varying morphological states at each time point. The adult-born GCs were classified into six morphological categories ranging from cells with no or very short neurites to cells exhibiting a mature dendritic structure. A quantitative analysis revealed that while the percentage distribution of labeled GCs showed an age-related progression through the six categories over time, the BrdU/DCX-positive GCs displayed a range of morphologies associated with different categories at each individual time point (Plümpe et al., 2006). Along similar lines, in a rat study performed in our laboratory, BrdU-marked DCX-expressing adult-born GCs were morphologically categorized into six developmental stages: stage 1 for cells with the soma located within the SGZ and containing no processes, stage 2 for cells with short processes in the SGZ, stage 3 when the primary dendrite extended into the inner half of the GCL, stage 4 when it reached the outer half of the GCL, stage 5 when it extended into the IML, and stage 6 when it reached the OML. Although the analysis of DCX-positive GCs at 7 and 14 dpi showed a clear correlation between age and the proportion of cells with an immature morphology (stages 1 - 4) at 7 dpi, and a more mature morphology (stages 5 - 6) at 14 dpi, it was also marked by a high structural variability between individual GCs at both time points (Jungenitz et al.,

2014). Similar results were obtained in a Thy1-GFP transgenic mouse model in which DCX-positive adult-born GCs were analyzed at 7, 14, 21, and 28 days post injection with BrdU. At 7 dpi, the majority of GCs were in stages 1 - 4, at 14 dpi, most GCs were classified as stage 5, and finally, at 21 and 28 dpi, the vast majority of GCs were classified as stage 6, though, again, there was a considerable level of variability at each time point (Radic et al., 2015). These findings show that the time course of structural maturation is variable between individual GCs and therefore appears to be governed by very specific regulatory mechanisms (Plümpe et al., 2006). As a result, analysis of structural development should ideally be performed via observation of individual GCs over time in order to effectively track dendritic growth and dynamic morphological changes.

In addition to the variability between individual GCs, there are differences in GC speed of maturation between distinct parts of the hippocampus, as adult-born GCs in the temporal DG seem to undergo slower development compared to adult-born GCs in the septal DG which appears to be mainly due to differences in neural activity patterns (Piatti et al., 2006, 2011). This may reflect differential demand and subsequent integration of newborn GCs into the existing DG network.

3.4.4. Functional development and integration of adult-born dentate GCs

In a characterization of functional development of newborn GCs in the adult mouse, electrophysiological properties of RV-labeled GCs were recorded from 1 - 29 dpi in acute brain slices (Espósito et al., 2005). Between 1 - 7 dpi, newly generated GCs displayed typical passive physiological properties of immature neurons marked by a high input resistance and a low membrane capacitance (Owens et al., 1996; Carleton et al., 2003; Zhang, 2004; Overstreet Wadiche et al., 2005; Ye et al., 2005). The potential presence of afferent inputs was assessed by analysis of evoked synaptic responses of young cells to extracellular stimulation of the GCL. Newborn GCs exhibited neither postsynaptic evoked responses nor spontaneous synaptic activity within this

time frame and were therefore described as “silent.” However, they already expressed both GABA and glutamate receptors, as direct application of either neurotransmitter elicited a response from the young neurons. From the second week of development on, newborn GCs exhibited a lower input resistance and higher membrane capacitance than silent neurons. Depolarizing currents evoked individual few spikes but not repetitive action potentials that are typical for mature GCs. First afferent connections were detected at 8 dpi as extracellular stimulation of the GCL elicited slow inward currents that could be blocked by the GABA_A receptor antagonist bicuculline methiodide, but not by the glutamate receptor blocker kynurenic acid. The same was true for spontaneous activity marked by a low frequency and long rise and decay times, which shows that the first synaptic input to adult-born GCs is GABAergic and therefore stems from local interneurons (Espósito et al., 2005; Song et al., 2013). The slow kinetics of post-synaptic currents (PSCs) suggest that the GABAergic input is of dendritic rather than perisomatic origin (Espósito et al., 2005).

First glutamatergic input originates from hilar mossy cells and occurs at 10 dpi (Deshpande et al., 2013; Chancey et al., 2014). During the second week of development, new GCs also receive input from cells in the ML and external long-range projections from the medial septum and the nucleus of the diagonal band of Broca (Deshpande et al., 2013). Starting at 18 dpi, newborn GCs start to receive first glutamatergic input from the EC and fast perisomatic GABAergic input. In addition, they begin to display fast spontaneous PSCs. These fast synaptic responses continue to become more abundant at later maturation stages, starting at 25 dpi. Depolarizing current steps elicit repetitive spiking with a high frequency and large amplitude at this time. The membrane capacitance is much higher compared to more immature neurons which indicates an increase in the number of leak channels (Espósito et al., 2005). In the third week, as Cl⁻ transporter channels NKCC1 have gradually become replaced by KCC2, GABAergic inputs become inhibitory (Ben-Ari, 2002; Espósito et al., 2005; Ge et al., 2006). During the first month, newly generated GCs receive transient input from mature GCs as well as back-projections from the CA3 area

(Vivar et al., 2012) and input from the subiculum. At 4 weeks, innervation by inhibitory interneurons is rare, therefore new GCs receive relatively weak feedforward and feedback inhibition (Marín-Burgin et al., 2012; Temprana et al., 2015). Although at this point newborn GCs display mature firing patterns and are integrated in the DG network, it takes several additional weeks for newborn GCs to reach full electrophysiological maturity and exhibit the same properties and functions as mature GCs (van Praag et al., 2002; Ambrogini et al., 2004; Mongiat et al., 2009; Jungnitz et al., 2014; Yang et al., 2015) (for a summary see Figure 3). Similarly to structural maturation, the physiological development may be variable between individual GCs (Espósito et al., 2005) as well as between GCs generated in the septal and temporal areas of the DG (Piatti et al., 2011; Snyder et al., 2012). In general, however, the sequence of physiological maturation and timing of afferent input of adult-born GCs is strikingly similar to GCs during hippocampal development (Espósito et al., 2005). Interestingly, in a recent study it was shown that the connectivity patterns of new GCs heavily depend on the animal's experience (Bergami et al., 2015). As mentioned before, exposure to an enriched environment, voluntary exercise, and spatial learning increases the number of newborn GCs that integrate into the pre-existing hippocampal network (Kempermann et al., 1997; van Praag et al., 1999a; Vivar et al., 2013; Garthe et al., 2015). Bergami et al. (2015) found that experience also modulates the number of local and distant synaptic inputs to new GCs. Using exposure to an enriched environment at different times during GC development and tracing first-order presynaptic partners, they found that innervation by local and CA interneurons and by cortical projections, particularly from the EC, drastically increased when enriched environment was provided specifically during 2 - 6 weeks following GC birth. This implies that experience has a profound effect on GC connectivity only during a critical time window. Furthermore, when animals were returned to standard housing for an additional 7 weeks, innervation by all interneurons returned to control conditions, while the enhanced cortical inputs persisted. This finding suggests that once cortical connections (particularly from the EC) have been established during a critical period in GC development, they remain stable thereafter despite

changes in experience (Bergami et al., 2015). Interestingly, voluntary running between 2 - 6 weeks similarly caused augmentation in cortical projections to newborn GCs, but had no effect on innervation by local DG and hippocampal interneurons (Bergami et al., 2015; Vivar et al., 2016). Recently, Alvarez et al. (2016) have provided insight into the mechanism of experience-dependent enhancement in integration of newborn GCs. Exposure to an enriched environment led to strong activation of the mature GC network. Subsequently, activated mature GCs synapsed onto parvalbumin-expressing interneurons which then provided depolarizing GABAergic input to newborn developing GCs. As a result, newborn GCs that were about 9 days old at the time of the exposure to an enriched environment displayed greater dendritic complexity, an increased number of spines, and accelerated functional integration into the network (Alvarez et al., 2016). These findings suggest that the process of attaining functional relevance and recruitment might be modulated by experience during an early period (i.e. 9 days) before new GCs obtain adequate cortical synaptic input (Alvarez et al., 2016). Under basal conditions, newborn GCs are generally able to contribute to functional processing after about 4 weeks of age (Ge et al., 2007; Marín-Burgin et al., 2012),

During their development, newborn GCs undergo a critical period at 4 - 6 weeks in which they exhibit hyper-excitability and increased synaptic plasticity (Schmidt-Hieber et al., 2004; Ge et al., 2007). In this time period, new GCs are highly excitable and very active, as they receive only weak inhibitory input from interneurons (Marín-Burgin et al., 2012; Temprana et al., 2015; Danielson et al., 2016). At the same time, they have a lower threshold for the induction of long-term potentiation (LTP) and display a high amplitude while undergoing LTP which is linked to the expression of the NR2B subunit of the NMDA receptor and weak feedforward inhibition (Schmidt-Hieber et al., 2004; Ge et al., 2007) (see Figure 3). In addition, they are less spatially tuned than mature GCs which causes firing in response to a broad range of stimuli (Danielson et al., 2016). Furthermore, the critical period coincides with the time window during which experience has a profound effect on the establishment of synaptic connections with hippocampal and cortical afferents (Bergami et al., 2015; Vivar et al.,

2016). Altogether, these unique properties are thought to contribute to a specific function of newborn GCs in new memory formation and recall, context encoding, and pattern separation during the critical phase.

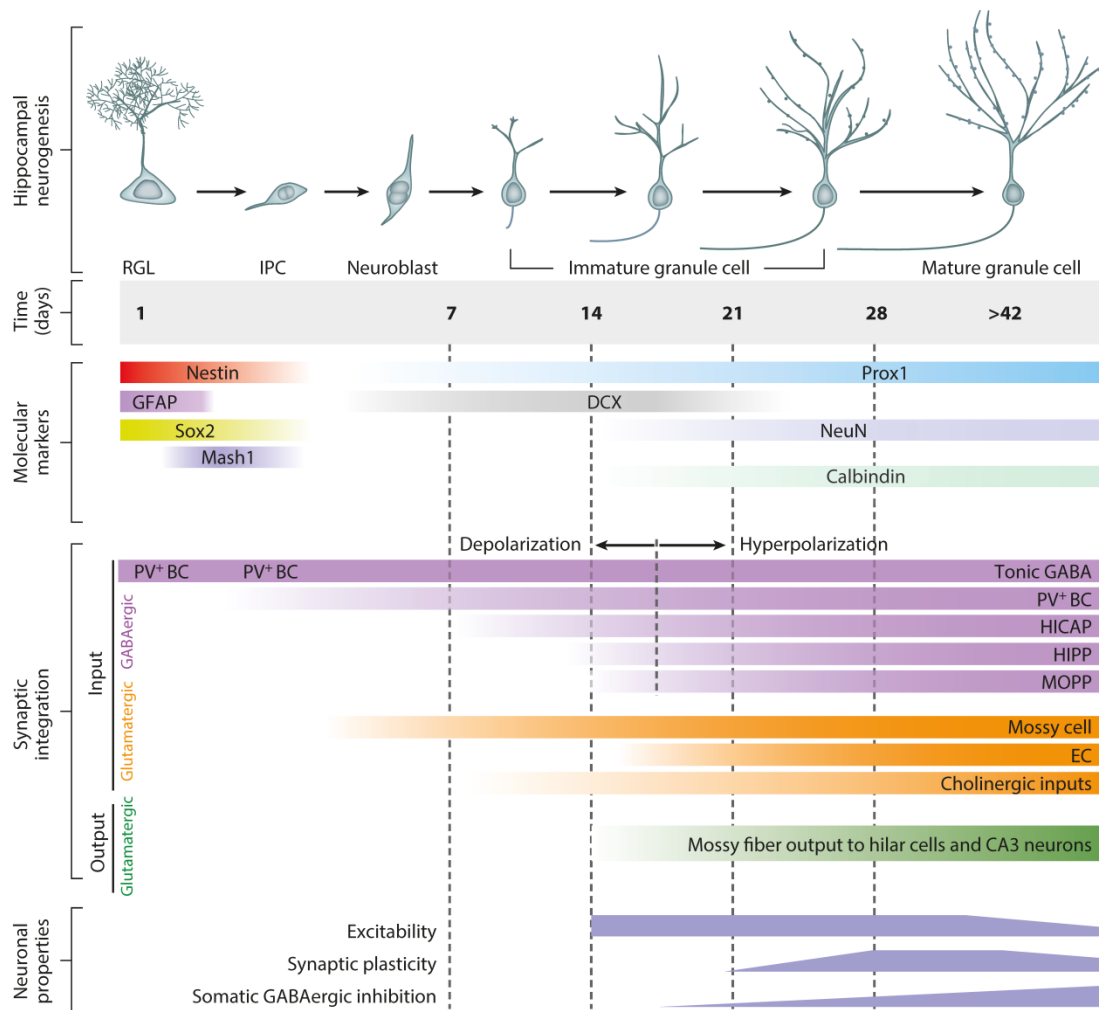


Figure 3. The structural and functional development of newborn dentate granule cells (GCs). A schematic summary of developmental stages during structural and functional maturation of newborn GCs including a timeline of morphological change, marker expression, synaptic input and output, and the unique properties that newborn GCs display during the critical period. BC, basket cells; EC, entorhinal cortex; HICAP, hilar interneuron with commissural-associational pathway-associated axon terminals; HIPP, hilar perforant path-associated interneurons; IPCs, intermediate progenitor cells; MOPP, molecular-layer perforant pathway cells; PV⁺, parvalbumin-expressing interneurons; RGL, radial glia-like cell. Image adapted from Christian et al. (2014).

3.4.5. Functional relevance of adult-born dentate GCs and clinical implications

Since the development and functional integration are experience- and activity-dependent, it is possible that the function of newborn GCs depends on particular network demands and connectivity (Gonçalves et al., 2016b). The role of adult-born GCs in hippocampal function has been linked to spatial and context-dependent memory (Snyder et al., 2005; Saxe et al., 2006; Wojtowicz et al., 2008; Ko et al., 2009; Tronel et al., 2012, 2015; Danielson et al., 2016), memory resolution (Aimone et al., 2011), cognitive flexibility (Burghardt et al., 2012), decline of remote memories (Arruda-Carvalho et al., 2011), and forgetting (Akers et al., 2014). Computational model theories propose an involvement of newborn GCs in temporal memory coding, the reduction of interference of old memories with new learning, and the distinction of memories that were acquired at different time points (Aimone et al., 2006; Rangel et al., 2014). The perhaps most compelling theory of newborn GC function has been associated with the computational concept of pattern separation (Aimone et al., 2010; Deng et al., 2010; Sahay et al., 2011; Johnston et al., 2015). As mentioned before, pattern separation enables greater distinction between highly similar input representations of neuronal activity by the production of more separated output patterns. On a behavioral level, pattern separation facilitates discrimination between very similar yet distinct experiences and hence enables precision in memory encoding. Therefore, it plays an important role in the ability to recognize and adapt to changes in the environment (Aimone et al., 2011). So far, the role of adult-born GCs in pattern separation has been tested in several different behavioral paradigms. Ablation of adult neurogenesis in the mouse DG leads to deficits in the discrimination between very similar contexts and adjacent navigation choices (Clelland et al., 2009; Nakashiba et al., 2012; Niibori et al., 2012; Danielson et al., 2016). Conversely, enhanced adult neurogenesis is associated with a better performance in contextual discrimination tasks (Sahay et al., 2011; Clemenson et al., 2015). However, the mechanism of this function is still the subject of ongoing research. Recent findings indicate that the activity

of newborn GCs affects the overall activity of the DG network. Impairment in adult neurogenesis has been linked to an increase in mature GC activity and gamma oscillations (Burghardt et al., 2012; Lacefield et al., 2012; Ikrar et al., 2013). As immature GCs go through a hyper-excitable phase during which they receive only weak inhibition, they synapse onto inhibitory interneurons of the DG which imposes feedback inhibition onto the mature GC population (Drew et al., 2016). Thus, while being particularly active, newborn GCs maintain the low activity pattern of mature GCs and thus contribute to sparse coding which is regarded as an essential prerequisite for pattern separation (Johnston et al., 2015; Lepousez et al., 2015; Gonçalves et al., 2016b). Impairment in adult neurogenesis and the consequent deficits in pattern separation have been linked to certain neurological and psychiatric conditions, including anxiety disorders such as panic and post-traumatic stress disorder. Deficiency in pattern separation could result in failure to distinguish between contextual information associated with a new ambiguous threat and a previously stored memory as well as a loss of precision in remote memories, and thus lead to overgeneralization of fear (Besnard and Sahay, 2016). When fear is not restricted to a specific representation of traumatic experience, it can be induced by partial elements related to the original aversive memory (Acheson et al., 2012) so that disambiguation of threat and safety becomes difficult. Poor pattern separation has also been correlated with depression in human subjects (Déry et al., 2013; Shelton and Kirwan, 2013; Leal et al., 2014). In general, research on adult neurogenesis related to depression has yielded varying results (Sahay and Hen, 2007; Miller and Hen, 2015). Whereas in some models of anxiety and depression involving exposure to chronic stress, adult neurogenesis seemed to be impaired (Lucassen et al., 2015), other studies have found no such effects (Hanson et al., 2011). What seems to be consistent is that adult neurogenesis is enhanced by antidepressants in animal models of stress (Malberg et al., 2000; Miller and Hen, 2015). However, it is still unclear whether antidepressant action is dependent on adult neurogenesis, as suggested in some mouse models (Santarelli et al., 2003) but could not be reproduced in other strains (Holick et al., 2008; Huang et al., 2008). Recently, it

has been shown that enhanced adult neurogenesis had a substantial effect on thwarting behaviors related to anxiety and depression in stressed mice, though not under baseline conditions (Hill et al., 2015). Further research is needed to resolve the conflicting findings of different depression models and elucidate the mechanisms involved in antidepressant effects and their relation to adult neurogenesis. Other clinical implications of adult neurogenesis dysfunction pertain to temporal lobe epilepsy, fragile X disorder, and schizophrenia (Parent et al., 1997; Duan et al., 2007; Jessberger et al., 2007; Faulkner et al., 2008; Luo et al., 2010; Guo et al., 2011; Murphy et al., 2011; Kim et al., 2012; Christian et al., 2014; Lee et al., 2015) as well as neurodegenerative disorders including Alzheimer's, Huntington's, and Parkinson's disease (Demars et al., 2010; Christian et al., 2014; Schlachetzki et al., 2015; Winner and Winkler, 2015; Salvi et al., 2016). Additional research is necessary before it can be determined whether improvement of neurogenesis and enhanced integration of new neurons can restore cognitive deficits and other symptoms associated with neurological and mental disorders (Ehninger et al., 2008; DeCarolis and Eisch, 2010; Richetin et al., 2015; Winner and Winkler, 2015). Because of the great potential of neurogenesis in regenerative therapy, it is of great importance to gain detailed insight into the development and network integration of newborn neurons as well as the underlying cellular mechanisms and dynamics. This requires experimental approaches that enable controlled manipulation and longitudinal observation of newborn neurons in their organotypic milieu. In the current work, I established time-lapse imaging of RV-labeled postnatally generated GCs in organotypic entorhino-hippocampal slice cultures (OTCs) to observe the dynamics of structural development and integration of new GCs in their endogenous niche.

3.5. Postnatal Neurogenesis in organotypic entorhino-hippocampal slice cultures

Although numerous studies have convincingly shown that adult-born GCs become integrated into the DG network and contribute to its function, there is still a variety of open questions that need to be addressed before therapeutic approaches can be developed. The dynamic cellular processes underlying successful GC maturation and integration into existing circuits need to be investigated in more detail. The use of OTCs offers many advantages, as they can be easily prepared and accessed and enable chronic manipulation and detailed longitudinal observation of the entorhino-hippocampal network all the while the organotypic conditions are largely preserved (Gähwiler, 1984; Heimrich and Frotscher, 1991; Stoppini, 1991; Gähwiler et al., 1997; Del Turco and Deller, 2007). Previous work has established the presence and persistence of neurogenesis in mouse and rat OTCs (Kamada et al., 2004; Raineteau et al., 2004, 2006; Chechneva et al., 2005; Sadgrove et al., 2006; Namba et al., 2007, 2011). Using BrdU and neuronal markers such as NeuN to label newborn neurons in mouse OTCs, Raineteau and colleagues (2004) have shown that neurons were generated at 2.5 weeks *in vitro* and were located in the inner parts of the GCL when cultures were fixed 2 weeks later. The authors also demonstrated that the addition of new GCs to the GCL followed an outside-in layering pattern as described *in vivo* (Altman and Bayer, 1990), since older GCs were located in the outer parts of the GCL and new GCs were added to the inner layers. Finally, the study revealed that OTCs could be used to directly administer chronic treatment to modify neurogenesis, as application of EGF significantly increased the rate of neurogenesis (Raineteau et al., 2004). In a follow-up study, Raineteau et al. (2006) used a conditional transgenic mouse model in which newborn GCs were labeled with GFP under a neurogenin2 promoter at DIV 3. Morphological and physiological properties of newborn GCs were analyzed at 10 and 20 days. The findings indicate that newborn GCs advanced structurally, as the total dendritic length and axonal branching increased over time and resembled *in vivo* data. Furthermore, new GCs

matured functionally and were synaptically integrated since they exhibited both GABAergic and glutamatergic miniature postsynaptic currents at 20 days (Raineteau et al., 2006).

A number of studies have reported a strong reduction in neurogenesis in mouse and rat OTCs within the first week of cultivation (Sadgrove et al., 2006; Namba et al., 2007; Gerlach et al., 2016) which may be due to increased glial differentiation in response to inflammation (Gerlach et al., 2016). However, labeling at later time points, e.g. at DIV 7, still yielded BrdU labeling of neurons, albeit at low numbers. Nevertheless, a number of neurons that were generated at this time point persisted over several weeks (Namba et al., 2007; Gerlach et al., 2016). Hence, even though the rate of neurogenesis decreases over time in OTCs, the survival of the newborn neurons does not seem to be affected (Gerlach et al., 2016). Additional findings have shown that new GCs are generated even after 2 weeks *in vitro* (Kamada et al., 2004; Raineteau et al., 2004; Chechneva et al., 2005). In one of these studies, rat OTCs were injected with an RV-GFP vector at DIV 14 which yielded GFP-labeled cells co-expressing neuronal markers including Tuj1, NeuN, and calbindin at 4 weeks post injection (Kamada et al., 2004). The RV injection was performed after 2 weeks *in vitro* in order to allow the OTC to mature and thus achieve a state that is more comparable with the *in vivo* situation. However, as the rate of neurogenesis decreases over time, the observation of new neurons after several weeks *in vitro* becomes technically challenging, which may contribute to the lack of detailed follow-up research.

As slice cultures prepared from adult animals can only be cultivated for short periods of time (Kleine Borgmann et al., 2013), OTC preparations need to be generated from young animal tissue in order to remain viable (Gähwiler et al., 1997; Del Turco and Deller, 2007). Hence, using this system, newborn neurons can only effectively be studied during the early postnatal period. Therefore, the question arises whether the investigation of new neurons generated in immature brain tissue is valid for the study of the integration of adult-born GCs into the existing hippocampal network. There are several reasons that

substantiate the use of OTCs for this purpose: (1) The general hippocampal structure and the entorhino-dentate circuitry in OTCs appear to resemble the *in vivo* situation very closely (Gähwiler et al., 1997; Kluge et al., 1998; Raineteau et al., 2004; Del Turco and Deller, 2007). However, due to the lack of detailed studies of the early postnatal DG using modern experimental methods and markers, this notion has yet to be corroborated. Thus, in the current work, a detailed histological analysis of the cellular organization in the early postnatal DG was performed *in vivo* and compared to the situation in the OTC. (2) The course of maturation of adult-born GCs largely follows the development of prenatally generated GCs, including the structural development as shown in fixed tissue, changes in membrane excitability, and the establishment of synaptic connections (Espósito et al., 2005; Laplagne et al., 2006; Piatti et al., 2006). (3) A recent study indicates that the SGZ, the source of lifelong neurogenesis of GCs, is established during an early postnatal period which further supports the notion that adult neurogenesis is essentially a continuation of neonatal neurogenesis (Nicola et al., 2015). (4) Since the entorhino-hippocampal circuitry should already be established in OTCs (Li et al., 1994; Kluge et al., 1998), newborn neurons would have to differentiate in and grow into an existing afferent network which resembles the conditions in the adult brain. As a result, it is plausible that postnatal neurogenesis in OTCs can serve as a good model for adult neurogenesis.

Taken together, previous studies have shown that postnatal neurogenesis persists in OTCs and that RV-labeling of newborn neurons is generally possible which makes the OTC system a valuable tool for the study of neurogenesis. However, all of the aforementioned prior work provided only snapshots of GC development in fixed OTCs which offers no information on the dynamic developmental processes driving structural maturation. Due to the fact that OTCs are easily accessible, they can be used as a tool for online observation of individual cells over extended periods of time. In the current dissertation RV-labeling in OTCs was combined with live cell time-lapse imaging in order to study the dynamics of structural development of newborn GCs.

3.6. Aim and scope of the study

The focus of the present work was to investigate the dynamics and hallmarks of structural development of individual living postnatally generated dentate GCs. In order to achieve that, I applied the method of RV labeling in OTCs to fully visualize complete newborn GCs in the postnatal rat hippocampus. Since OTCs are generated from young animals, the distribution of neuronal maturation markers was examined during an early postnatal period (i.e. between P7 and P42) both *in vivo* and *in vitro* which showed that OTCs contain an organotypic cellular composition that was comparable to the according maturation levels *in vivo*. Successful RV labeling in OTCs enabled time-lapse imaging of individual newborn GCs from 8 dpi until 28 dpi in order to observe structural changes of developing GCs during a time period from when they first extended dendritic processes toward the ML until they reached an elaborate and mature dendritic structure. In addition, I confirmed the presence of afferent fibers in the ML projecting from the EC using anterograde tracing and showed that newborn GCs grow into an existing layer of axon terminals which is highly similar to the situation in the adult brain. The development of newborn GCs was compared to structural dynamics of older, presumably prenatally generated GCs that were labeled with an adeno-associated viral (AAV) vector under the synapsin 1 promoter. The findings reveal a very dynamic course of structural development in newborn GCs. More specifically, three distinct phases of morphological development were identified: the first phase of rapid dendritic growth and a high level of dynamic structural reorganization, including extension and retraction of branches during the second week of development, a second phase of maximum structural complexity during the third week followed by dendritic pruning, and a third phase of structural stabilization during the fourth week. In contrast, older GCs, which exhibited a mature morphology from the earliest time point on, remained structurally stable throughout the imaging period. Furthermore, the emergence of dendritic spines was observed between 14 and 16 dpi with continuously increasing spine density over time. Using electron microscopy, it was confirmed that newly formed spines of postnatally generated GCs established synaptic contacts with unlabeled axonal boutons. The results

indicate that the highly dynamic structural reorganization and flexibility is unique to newly generated GCs and may reflect a complex pathfinding process that is necessary for the establishment of contacts with presynaptic entorhinal fibers and thus enable integration of newborn GCs into the existing entorhino-hippocampal network.

4. Materials and Methods

4.1. Animals and organotypic entorhino-hippocampal slice culture (OTC) preparation

Sprague Dawley rats and C57BL/6J mice were bred and housed at the animal facility “Zentrale Forschungseinrichtung” (ZFE) of the Goethe-University hospital Frankfurt/Main. They were housed under standard conditions in a 12 hour dark/light cycle with food and water available *ad libitum*. Animal care and experimental procedures were performed in agreement with the German law on the use of laboratory animals (animal welfare act; TierSchG; §4 par 3) and approved by the animal welfare officer of Goethe-University, Faculty of medicine.

Organotypic entorhino-hippocampal slice cultures (OTCs) were generated from Sprague Dawley rats of either sex at postnatal days 4 - 5 (P4 - 5; day of birth was considered as P0) by applying the interface method (Stoppini, 1991). After the animal was sacrificed by decapitation, the head was disinfected with 70% ethanol and transferred onto a sterile laminar flow bench so that the remainder of the procedure was performed under sterile conditions. The brain was explanted from the skull and the cerebellum was dissected off. Next, the brain was glued onto a vibratome stage with the posterior side facing upward. The stage was placed inside a tray containing preparation medium (4°C, pH 7.40) that was comprised of 95% minimum essential medium (MEM) containing Hanks' salts and L-glutamine, 0.65% glucose, 25 mM HEPES, 0.1 mg/ml streptomycin (Sigma-Aldrich, Steinheim, Germany), 100 U/ml penicillin (Sigma-Aldrich), and 2 mM glutamax (all reagents were obtained from Gibco, Invitrogen, Karlsruhe, Germany unless otherwise noted). Using a vibratome (Leica VT1200 S, Leica Biosystems, Wetzlar, Germany) rat brains were sliced horizontally into 300 µm thick sections at low speed (0.10-0.15 mm/s) and high vibration frequency (80-90 Hz). Brain sections were transferred into a 30 mm petri dish with preparation medium. The hippocampi with attached entorhinal

cortices were dissected with scalpels and placed onto sterile membrane culture inserts (Millicell-CM, 0.4 μm pore size, 30 mm diameter) (Millipore, Schwalbach, Germany). Subsequently, the membranes were transferred into six-well plates (BD Falcon, Heidelberg, Germany) containing pre-incubated slice culture incubation medium (1 ml per well, 35°C, adjusted to pH 7.30 with NaOH) that consisted of 42% MEM, 25% Basal Eagle Medium containing Earle's salts, 25% heat-inactivated normal horse serum, 0.65% glucose, 25 mM HEPES, 0.1 mg/ml streptomycin (Sigma-Aldrich), 100 U/ml penicillin (Sigma-Aldrich), 0.15% sodium bicarbonate, and 2 mM glutamax (all reagents were obtained from Gibco Invitrogen unless otherwise noted). OTCs were cultivated in a humidified environment (95% air, 5% CO₂, at 35°C) in an incubator (Hera Cell 240, Thermo Fisher Scientific, Waltham, MS, U.S.A.), and the medium was changed every 2 to 3 days until further processing.

4.2. Viral transduction of GCs in OTCs

To label and visualize complete newborn cells in OTCs, cultures were transduced with a Moloney murine leukemia virus (MMLV) based retroviral (RV) vector that included sequences encoding green fluorescent protein (GFP) controlled by the CAG promoter (van Praag et al., 2002; Zhao et al., 2006). The RV vector was generated by transfection of a HEK293T (human embryonic kidney-derived) cell line with the plasmid pCAG-GFP and the helper plasmids pCMV-GP and pCMV-VSVG. The plasmids were kindly provided by Sebastian Jessberger (ETH, Zürich) and viral production was performed by Tassilo Jungenitz (Goethe-University, Frankfurt). Briefly, HEK293T cells were grown in T-175 cell culture flasks (BD Falcon) in culture medium that consisted of DMEM + glutamax basal medium, 10% fetal calf serum, 1% L-glutamine (all reagents obtained from Gibco, Invitrogen), and 1% penicillin/streptomycin (Sigma-Aldrich). When they were approximately 80% confluent (at a density of 4.5-5x10⁶ cells per 10 cm plate), they were transfected with a DNA solution containing the plasmids (pCAG-GFP (150 μg), pCMV-GP (102 μg), and pCMV-VSVG (48 μg) in a 3 x 2 x 1 ratio) by calcium-phosphate precipitation. After

incubation for 2 days at 35°C, virus-containing supernatant was collected in a 50 ml polystyrene conical tube (BD Falcon) and centrifuged for 10 minutes at 4000 rpm (Eppendorf centrifuge 5810R, HOST, Hamburg, Germany). Next, the solution was filtered with a 50 ml perfusion syringe (BD Luer-Lok Tip, Heidelberg, Germany) and a syringe driven filter unit (Millex-GP, 0.22 µm pore size, 33 mm diameter; Millipore). The centrifugation at 4000 rpm for 10 minutes and the filtering steps were repeated once more. Subsequently, the solution was concentrated by ultracentrifugation in 34 ml polyallomer open-top centrifuge tubes (Beckmann Coulter, Krefeld, Germany) at 30,000 rpm for 2 h at 4°C (Thermo Fisher Scientific Sorvall Ultracentrifuge WX-80 Ultra). The supernatant was discarded, and the pellet was re-suspended in 200 µl sterile PBS (AppliChem), divided into 10 µl aliquots in 0.2 ml SafeSeal micro tubes (Sarstedt, Nümbrecht, Germany), and stored at -80°C.

RV transductions were performed via local injection of RV solution directly into the hilar area of the DG of each culture. For that, each membrane insert containing 3 - 4 OTCs was placed in a 30 mm petri dish containing 1 ml pre-warmed (37°C) imaging medium (Modified Edi's Recording Medium; MERM) which consisted of 129 mM NaCl, 4 mM KCl, 1 mM MgCl₂, 2 mM CaCl₂, 4.2 mM glucose, 10 mM HEPES, 0.1 mM Trolox (Sigma-Aldrich), 0.1 mg/ml streptomycin, 100 U/ml penicillin (all reagents were obtained from Gibco Invitrogen unless otherwise noted), with a pH of 7.4. The osmolarity of the imaging medium was adjusted to 365 mOsm/kg with sucrose to match the osmolarity of the incubation medium. The cultures were placed under a stereo microscope (Zeiss Stemi 2000-C, Göttingen, Germany). To visualize the area of interest in the OTCs, a camera (ColorView II, Soft Imaging System, Münster, Germany) and the software AnalySIS 2677 (Olympus, Münster, Germany) were used. Using a manual micromanipulator, approximately 0.2 µl of RV solution was injected with a NanoFil syringe (World Precision Instruments, Sarasota, FL, USA) containing a 35-gauge beveled needle (World Precision Instruments) directly into the hilar area of the DG.

As a control group to newborn GCs, older GCs that had presumably been generated prenatally were labeled with an adeno-associated viral (AAV) vector

encoding for tdTomato under the synapsin 1 promoter. The AAV-Syn vector was generated and kindly provided by Nadine Zahn (Goethe-University, Frankfurt). Briefly, calcium-phosphate precipitation was used to co-transfect HEK293T cells with pDP1rs, pDG, and tdTomato-vector plasmid (2.4:1.6:1) necessary for reproduction of the full viral vector (Kügler et al., 2001, 2003). Transfected HEK293T cells were collected 48 h after transfection and washed twice with PBS. Cells were scraped in PBS, centrifuged at 800 rpm for 4 min, and resuspended in PBS. Four freeze (-80°C) and thaw (37°C) cycles were performed to set the viral particles inside the cells free. Subsequently, cells were spun down at 1000 rpm for 5 min. The supernatant was collected and centrifuged at 10,000 rpm for 10 min to remove cell debris. The supernatant was collected, aliquoted, and stored at -80°C.

A cocktail of the RV-CAG-GFP (5 µl) and the AAV-Syn-tdTomato (3 µl) vectors was injected in the same manner as described above in order to simultaneously label newborn as well as older, more mature GCs in the same cultures.

4.3. Time-lapse imaging of newborn GCs in OTCs

Live imaging of individual GCs was performed with an upright confocal laser scanning microscope (Zeiss LSM 5 Pascal version 3.2 SP2, Jena, Germany; 488 nm and 543 nm excitation lasers) and the AIM software version 3.2 (Advanced Imaging Microscopy, Zeiss). Individual membrane inserts containing the OTCs were placed in a 30 mm petri dish and submerged into warm (37°C) MERM (see section 4.2.). The petri dish was placed onto a temperature-regulated stage (37°C) of the microscope. Using a 10x water immersion objective lens (numeric aperture (NA) 0.3; Zeiss) for overview, RV- or AAV-labeled GCs were identified within each OTC. High resolution (1024 x 1024 pixels) image stacks (30 - 40 images per stack; z-axis interval between consecutive frames: 2 µm) of individual GCs were obtained with a 40x water immersion objective lens (0.8NA; Zeiss). Imaging of individual dendritic segments and spines was performed with a 63x water immersion objective lens

(0.9NA; Zeiss), applying a 4x field zoom (15 - 25 images per stack; z-axis interval between consecutive frames: 0.5 μm). OTCs were imaged once per day, or twice per day when imaging of spines was performed, for less than 10 min per culture in order to keep exposure time minimal and avoid phototoxic damage. After imaging, cultures were transferred back into the 6-well plate containing incubation medium and returned to the incubator (Hera Cell 240, Thermo Fisher Scientific).

Editing of images was done with Fiji (Image Processing and Analysis in Java, version 1.48s; Schindelin et al., 2012) and/or Adobe Photoshop CS6 version 13.0 x64 (Adobe, San Jose, CA, USA) for contrast, background reduction, rotation, and selection of region of interest. Figures were prepared with Adobe Illustrator CS6 version 16.0.0.

4.4. Two-photon microscopy

Live imaging sequences of newborn RV-GFP-labeled GCs was performed every hour in an 11-hour interval with a custom-built two-photon microscope based on Sutter Instruments Movable Objective Microscope (Sutter Instruments, Novato, CA, USA). High resolution (1024 x 1024 pixels) image stacks (30 - 35 images per stack; z-axis interval between consecutive frames: 2 μm) were acquired using a 40x water immersion objective (Olympus XLUMPlan FI, 0.80NA; Olympus, Shinjuku, Tokyo, Japan) and the software ScanImage 3.8.1 (Pologruto et al., 2003). GFP was excited with a MaiTai HP Ti-sapphire mode-locked laser (Spectra-Physics, Darmstadt, Germany) tuned to a wavelength of 890 nm. Images were processed with the Fiji software (Image Processing and Analysis in Java, version 1.48s; Schindelin et al., 2012) for contrast, rotation, and selection of region of interest. Figures were prepared with Adobe Illustrator CS6 version 16.0.0.

4.5. 3-D reconstruction of labeled GCs and morphological analysis

Three-dimensional computer reconstruction of complete apical dendritic trees of both newborn (RV-GFP-labeled) and older (AAV-Syn-labeled) GCs was performed from confocal image stacks (30 - 40 images per stack; z-axis interval between consecutive frames: 2 μm , magnification: 40x, see section 4.3.) in a blinded manner using the software TREES Toolbox (Cuntz et al., 2010, 2011) in Matlab (MathWorks, Natick, MA, U.S.A.). To trace individual dendrites, anchor nodes were placed starting at the soma and following each dendritic branch from the branch point to the termination point in 3 dimensions. All reconstructions were resampled to an internode distance of 1 μm . Dendritic diameter (“quaddiameter tree”) and soma thickness (“soma tree”) were individually adjusted according to the image. Morphological analyses were performed using the TREES Toolbox (Cuntz et al., 2011) and custom written programs in Matlab (MathWorks) by Mathias Singer and Marcel Beining (Goethe-University, Frankfurt).

4.6. Anterograde axonal tracing

Anterograde tracing of axons originating in the EC was performed with the neurotracer Mini Ruby, a biotin-conjugated 10kD dextran amine (MoBiTec, Göttingen, Germany). A few Mini Ruby crystals were placed on the surface of RV-transduced and untreated OTCs in layers II and III of the EC. Cultures were treated with Mini Ruby on DIV 3 and DIV 15 and fixed on DIV 8, DIV 17, or DIV 20 before they were processed for immunocytochemistry (see section 4.7.).

4.7. Transcardial perfusion and brain sectioning

Male Sprague Dawley rats and C57BL/6J mice were sacrificed with an overdose of isoflurane (Forene, Abbott, Wiesbaden, Germany) and subsequently placed onto an aluminum foil covered cork block. After ensuring that the animal was dead by checking for a response to a noxious stimulus, all 4

limbs were pinned to the cork surface in the supine position for stability. Using forceps, the skin around the xiphoid process area was lifted up and an incision was made through the skin from just under the xiphoid process along the thoracic area to the clavicle. A similar incision was performed laterally in order to expose the entire thoracic field. Starting just below the xiphoid process, a superficial cut was made to the diaphragm. The diaphragm was cut from one side to the other to expose the thoracic cavity. Next, cuts were made laterally through the rib cage to expose the heart. Holding the heart with forceps, a cut was made through the atrial chamber and a 21-gauge butterfly needle attached to an infusion container set was inserted into the left ventricle to begin infusion of 0.9% NaCl (Sigma-Aldrich) in dH₂O. Once the liquid became clear and the liver turned paler, the perfusion was continued with 4% paraformaldehyde (PFA; Sigma-Aldrich) in phosphate-buffered saline (PBS; AppliChem), pH 7.40, for 15 minutes. Following perfusion, the animal was decapitated and the brain was removed. Subsequently the brain was postfixed with 4% PFA in PBS at 4°C overnight. On the following day, brains were transferred into TRIS-buffered saline (TBS) (0.1 M TRIS; AppliChem, in dH₂O, pH 7.40) + 0.01% NaN₃ (Merck, Darmstadt, Germany). Before sectioning, brains were embedded in 5% agar (AppliChem) in dH₂O, glued onto a vibratome stage with RotiColl superglue (Carl-Roth, Karlsruhe, Germany) which was placed into a vibratome tray containing TBS + 0.01% NaN₃, and sliced into 50 µm thick frontal sections with a vibratome (Leica VT1000 S, Bensheim, Germany) at a speed of 0.25-0.50mm/s and a frequency of 80 Hz. Brain sections were stored in cryoprotection solution consisting of 30% ethylene glycol (Sigma-Aldrich), 25% glycerol (AppliChem), and 0.01% NaN₃ in 0.1 M PBS at -20°C until further processing.

4.8. Immunocytochemistry

To identify cellular phenotypes and determine the distribution of mature and immature neurons in brain sections and OTCs, the following chemical markers were used: the immature neuronal marker DCX, the mature neuronal marker calbindin, and the granule cell marker Prox1 (see section 3.4.1.). OTCs, still

attached to the membrane inserts, were fixed in 4% PFA (Sigma-Aldrich)/4% sucrose in PBS (AppliChem), pH 7.40, for 1 hour at room temperature and 2% PFA/30% sucrose in PBS overnight at 4°C. After fixation, the membrane inserts were washed with TBS (AppliChem) in dH₂O, pH 7.40 + 0.01% NaN₃ (Merck) and glued onto a 5% agar (AppliChem) in dH₂O block with RotiColl superglue (Carl-Roth). The block was then glued onto a vibratome stage and placed into the vibratome tray containing TBS + 0.01% NaN₃. Cultures were re-sliced into 50 µm thick sections using a vibratome (Leica VT1000S) at a speed of 0.25-0.50 mm/s and a frequency of 80 Hz.

Free-floating OTC and frontal brain sections containing the dorsal DG (3 sections per animal; see section 4.10.) were placed into 24-well plates, washed 3 times in TBS + 0.01% NaN₃ for 5 minutes, and blocked with 5% bovine serum albumin (BSA; Carl-Roth) + 0.5% Triton X-100 (VWR Prolabo, Darmstadt, Germany) in TBS for 1 hour at room temperature. Next, sections were placed in primary antibody solution containing the relevant antibodies (for a list of all antibodies and dilutions, see Table 1) in TBS + 0.01% NaN₃, 0.1% Triton X-100, and 1% BSA overnight at room temperature. Sections were washed in TBS + 0.01% NaN₃ 3 times for 5 minutes and then incubated with secondary antibodies that were conjugated with fluorescent dye (see Table 2 for a list of secondary antibodies and dilutions) in TBS + 0.01% NaN₃, 0.1% Triton X-100, and 1% BSA for 4 hours at room temperature. Next, sections were washed 3 times in TBS + 0.01% NaN₃. For nuclear staining, sections were incubated with TO-PRO[®]-3 IODID (Invitrogen) for 15 min during the first wash with TBS + 0.01% NaN₃. Finally, sections were mounted onto glass slides (Engelbrecht, Edermünde, Germany) with DAKO fluorescent mounting medium (DakoCytomation, Hamburg, Germany) and stored at 4°C until further use.

Primary Antibody	Host	Type	Dilution	Company
α-Prox1	rabbit	polyclonal	1:1000	ReliaTech
α-calbindin	mouse	monoclonal	1:1000	Swant
α-doublecortin	goat	polyclonal	1:500	Santa Cruz
α-GFP (Alexa488-conjugated)	mouse	monoclonal	1:1000	Sigma-Aldrich

Table 1. Primary antibodies and working concentrations used in immunostainings.

Host	Antigen	Conjugation	Dilution	Company
donkey	goat	Alexa Fluor 633 [®]	1:1000	Molecular Probes
donkey	mouse	Alexa Fluor 568 [®]	1:1000	Molecular Probes
donkey	mouse	Alexa Fluor 488 [®]	1:1000	Molecular Probes
donkey	rabbit	Alexa Fluor 568 [®]	1:1000	Invitrogen
donkey	rabbit	Alexa Fluor 488 [®]	1:1000	Molecular Probes
donkey	rabbit	Alexa Fluor 647 [®]	1:1000	Molecular Probes

Table 2. Secondary antibodies and working concentrations used in immunostainings.

4.9. Confocal microscopy

Confocal images of brain and fixed OTC sections were obtained with a confocal laser scanning microscope (Nikon Eclipse 80i; 488 nm and 561 nm excitation lasers) equipped with a camera (Nikon D-Eclipse C1) and the software EZ-C1 3.60 at a resolution of 1024 x 1024 pixels. Overlapping image stacks (4-5 stacks per OTC section; 10 - 20 images per stack; z-axis interval between consecutive frames: 1 μm) were obtained using a 4x (0.2NA; Nikon), 10x (0.3NA), 20x (0.75NA), or 40x oil immersion lens (1.3NA). Image stacks

belonging to each section were saved in the ics/ids (Image Cytometry Standard) file format and analyzed with the Fiji software (Image Processing and Analysis in Java, version 1.48s; Schindelin et al., 2012). Images were edited with Fiji and/or Adobe Photoshop CS6 version 13.0 x64 for contrast, rotation, and selection of region of interest. Figures were prepared with Adobe Illustrator CS6 version 16.0.0.

4.10. Histological data analysis

Confocal images of histological frontal sections (50 μm) including the dorsal DG (3 sections per animal) were used for the analysis of chemical marker distribution in the postnatal DG of male Sprague Dawley rats (P7: n=3; P14: n=3; P21: n=4; P28: n=3; P35: n=3; and P42: n=4) and male C57BL/6J mice (P7: n=4; P14: n=3; P21: n=3; P28: n=5; P35: n=5; and P42: n=3). Sections were collected from the first section in which both the supra- and infrapyramidal blades of the dorsal DG were clearly visible. From there, every 6th section within the first millimeter was selected. For 7-day-old brains, every 5th section was selected. In each section, three adjacent, non-overlapping regions of interest (medial, middle, and lateral), were chosen for imaging along the suprapyramidal blade of the DG (bilaterally) starting directly laterally from the crest where the supra- and infrapyramidal blades clearly separate. Image z-stacks (30 - 35 images per stack; z-axis interval between consecutive frames: 1 μm) were oriented perpendicular to the longitudinal axis of the GCL. Image stacks belonging to each section were saved in the ics/ids (Image Cytometry Standard) file format and analyzed with the Fiji software (Image Processing and Analysis in Java, version 1.48s; Schindelin et al., 2012). All Prox1-positive cells were counted, including the following: DCX+/CB-, CB+/DCX-, DCX+/CB+, and DCX-/CB- which were normalized against the total number of Prox1-positive cells and presented as “% of Prox1+ cells.” Cells were counted in single images chosen from the z-stack and co-localization was determined by overlapping signals in each individual channel using Fiji. A monoexponential function fit was used to determine the average age at which 50% of Prox1-positive cells was

DCX-positive as well as the age when 50% of Prox1+ cells was CB-positive (i.e. $t_{50\%}$) for both, mice and rats using the following model: $Y = (Y_0 - \text{Plateau}) * \exp(-K * X) + \text{Plateau}$ in GraphPad Prism 6 (Graphpad Software, San Diego, CA, U.S.A.).

4.11. Electron microscopy

Slice cultures were fixed with 0.1 M sodium cacodylate buffer (CB) containing 4% paraformaldehyde and 2% glutaraldehyde for 1.5 h while still attached to membrane inserts. Fixed cultures were resliced to 50 μm with a vibratome (Leica VT1000S) at a speed of 0.25-0.50mm/s and a frequency of 80Hz as described in section 4.7. Subsequently, free floating OTC sections were washed with TBS and blocked with 5% BSA in 0.1% NaBH₄ (Sigma-Aldrich) for 1 h at room temperature. For detection of GFP-labeled cells, sections were treated with anti-GFP (goat, 1:500; Acris, Herford, Germany) primary antibody and 2% BSA in 0.1M TBS for 18 h at room temperature and subsequently incubated with a biotinylated anti-goat IgG (1:200; Vector Laboratories, Burlingame, CA, USA) secondary antibody for 60 min at room temperature. Next, sections were washed with TBS, then incubated in avidin-biotin-peroxidase complex (ABC-Elite, Vector Laboratories) for 90 min at room temperature, and reacted with a diaminobenzidine solution (Vector Laboratories) for 2 - 15 min at room temperature. Silver-intensification of sections was done by incubation in 3% hexamethylenetrarnine (Sigma-Aldrich), 5% silvernitrate (AppliChem) and 2.5% di-sodiumtetraborate (Sigma-Aldrich) for 10 min (60°C); 0.05% tetrachlorogold (AppliChem) solution for 3 min, and 2.5% sodium thiosulfate (Sigma-Aldrich) for 3 min. Between each of the aforementioned steps, sections were washed with dH₂O.

Upon completion of GFP staining, sections were washed in 0.1 M CB which was followed by osmication for 30 min with 0.5% OsO₄ (Plano, Wetzlar, Germany) in 0.1 M CB, dehydration with 1% uranyl acetate (Serva, Heidelberg, Germany) and 70% ethanol in dH₂O for 60 min. Next, OTC sections were embedded in Durcupan (Sigma-Aldrich) for ultrathin sectioning (60 nm) which

was performed with an ultramicrotome (Ultracut, Leica UCT). Finally, ultrathin sections were collected on single-slot Formvar-coated copper grids that were contrast enhanced with lead citrate for 4 min and examined using a Zeiss electron microscope (Zeiss EM 900) at 20,000× magnification. Electron microscopy was performed by Anke Biczysko (Goethe-University, Frankfurt).

4.12. Statistical analysis

Statistical analysis was performed using Microsoft Excel (Microsoft, Redmond, Washington, U.S.A.) and GraphPad Prism 6. Statistical testing was done with the two-way ANOVA followed by a *post hoc* Bonferroni test and a non-parametric Wilcoxon signed-rank test, two-tailed. Significance level was set to $P < 0.05$, denoted by an asterisk (*). Results are expressed as mean \pm SEM.

5. Results

5.1. Expression of doublecortin (DCX) and calbindin in the postnatal DG of mice and rats

To assess the cytological structure of the DG and gain an overview of the distribution of young, immature and mature dentate GCs during the postnatal period before animals reach adulthood, the expression patterns of DCX, which is a marker for immature neurons that is commonly used for the study of neurogenesis (Brown et al., 2003; Couillard-Despres et al., 2005) and calbindin, a marker for mature neurons (von Bohlen Und Halbach, 2007), were examined with immunohistochemistry at P7, 14, 21, 28, 35, and 42. Although calbindin expression was quite heterogeneous within each brain section, calbindin-immunoreactive cells could be clearly distinguished from calbindin-negative cells. Prox1, a GC-specific marker, was used to identify GCs and calculate the relative percentage values of DCX- and calbindin-positive GCs.

5.1.1. The distribution of DCX and calbindin in the mouse DG between P7 and P42

At P7, DCX expression was very prominent in GCs throughout the GCL of the mouse DG, whereas only the very outer part of the GCL exhibited calbindin expression in GCs (Figure 4A). Therefore, the majority of Prox1-positive cells expressed DCX ($78.57 \pm 2.44\%$ of all Prox1-positive cells) while only a small percentage of GCs was calbindin-positive ($3.56 \pm 0.33\%$; Figure 5A). In addition, Prox1-positive cells co-expressing both, DCX and calbindin were observed ($9.62 \pm 0.57\%$) as well as a small number of cells that were not labeled by either maturity marker ($8.25 \pm 2.19\%$; Figure 5B). Hence, at an early postnatal time point, when the development of the DG is barely completed and the establishment of the “adult” neurogenic niche in the subgranular zone (SGZ) has only begun (Nicola, et al 2015), the vast majority of dentate GCs is young and immature. At P14, when the adult neurogenic niche is established (Nicola

Results

et al., 2015), and animals begin to open their eyes and start to become active, still a majority of all GCs is DCX-positive ($49.60 \pm 3.49\%$) compared to calbindin-expressing GCs ($41.54 \pm 3.08\%$; Figures 4B, 5A). Only a small percentage of Prox1-positive cells were also labeled with both, DCX and calbindin ($5.67 \pm 1.12\%$), or expressed neither ($3.19 \pm 0.52\%$; Figure 5B). At P21, the distribution of immature and mature GCs started to shift, as $34.47 \pm 1.32\%$ of GCs were labeled with DCX, while the majority ($49.52 \pm 3.50\%$) was calbindin-positive (Figures 4C, 5A). Only $1.01 \pm 0.27\%$ expressed both, DCX and calbindin, while $15.01 \pm 2.98\%$ exhibited neither maturity marker (Figure 5B). At P28, when the SGZ was distinctly observable just below the GCL, young, immature DCX-positive cells were found in the SGZ and only the inner part of the GCL and constituted a clear minority of all Prox1-positive cells ($19.30 \pm 0.42\%$), whereas at this time point, calbindin expression was clearly prevalent throughout the middle and outer parts of the GCL ($71.57 \pm 1.23\%$; Figures 4D, 5A). The percentage of triple-labeled cells decreased to $0.16 \pm 0.05\%$, whereas $8.98 \pm 1.18\%$ of GCs didn't express either maturation marker (Figure 5B). Thereafter, only little change in the marker distribution took place, as on P35 $13.90 \pm 0.51\%$ of GCs were DCX-positive, $70.86 \pm 3.20\%$ exhibited calbindin expression, $0.11 \pm 0.04\%$ were labeled with both markers, and $15.13 \pm 3.37\%$ expressed neither DCX nor calbindin (Figures 4E, 5A, B). Similarly, at P42 $11.75 \pm 0.80\%$ expressed DCX, $83.61 \pm 1.32\%$ were calbindin-positive, $2.08 \pm 0.02\%$ expressed both, and $2.55 \pm 0.79\%$ exhibited neither (Figures 4F, 5A, B). These data show that the number of young, immature DCX-labeled GCs constitutes the majority of all GCs in the mouse DG at early postnatal time points P7 and P14, but their number steadily decreases over time. In contrast, mature calbindin-positive GCs are rarely found in the 7-day old mouse, whereas their number increases substantially over the next several weeks until P28 when it does not change further.

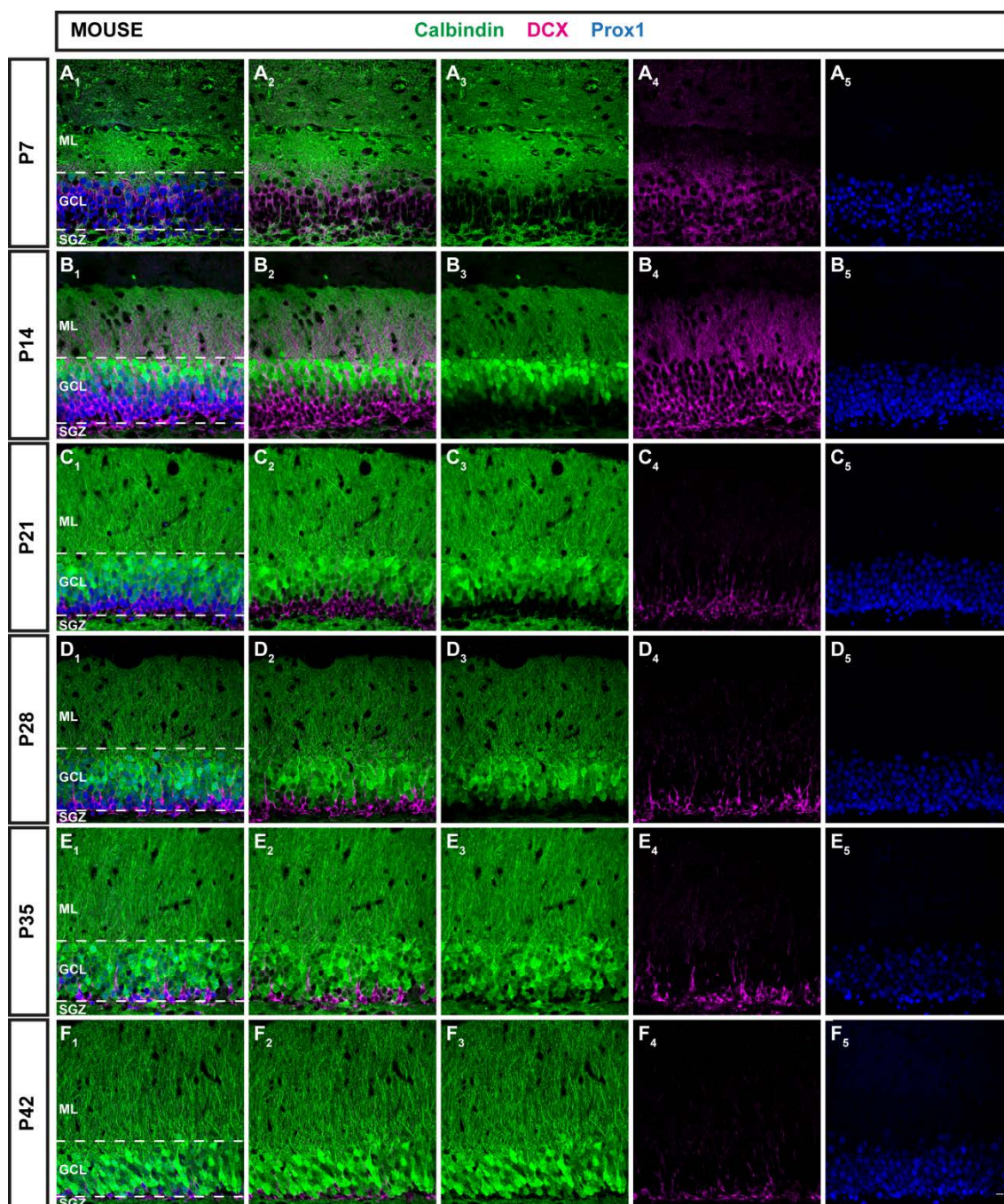


Figure 4. Immunohistochemical illustration of calbindin, DCX, and Prox1 distribution in the early postnatal DG of the mouse. (A-F) Immunostainings of the postnatal mouse DG show increasing maturation from P7 to P42, as the proportion of mature calbindin-positive cells (green) increased while the number of young, immature DCX-expressing cells (magenta) was reduced over time. The GC marker Prox1 (blue) was expressed in both mature and immature GCs at all time points (A₅-B₅). Scale bar: 10 μ m.

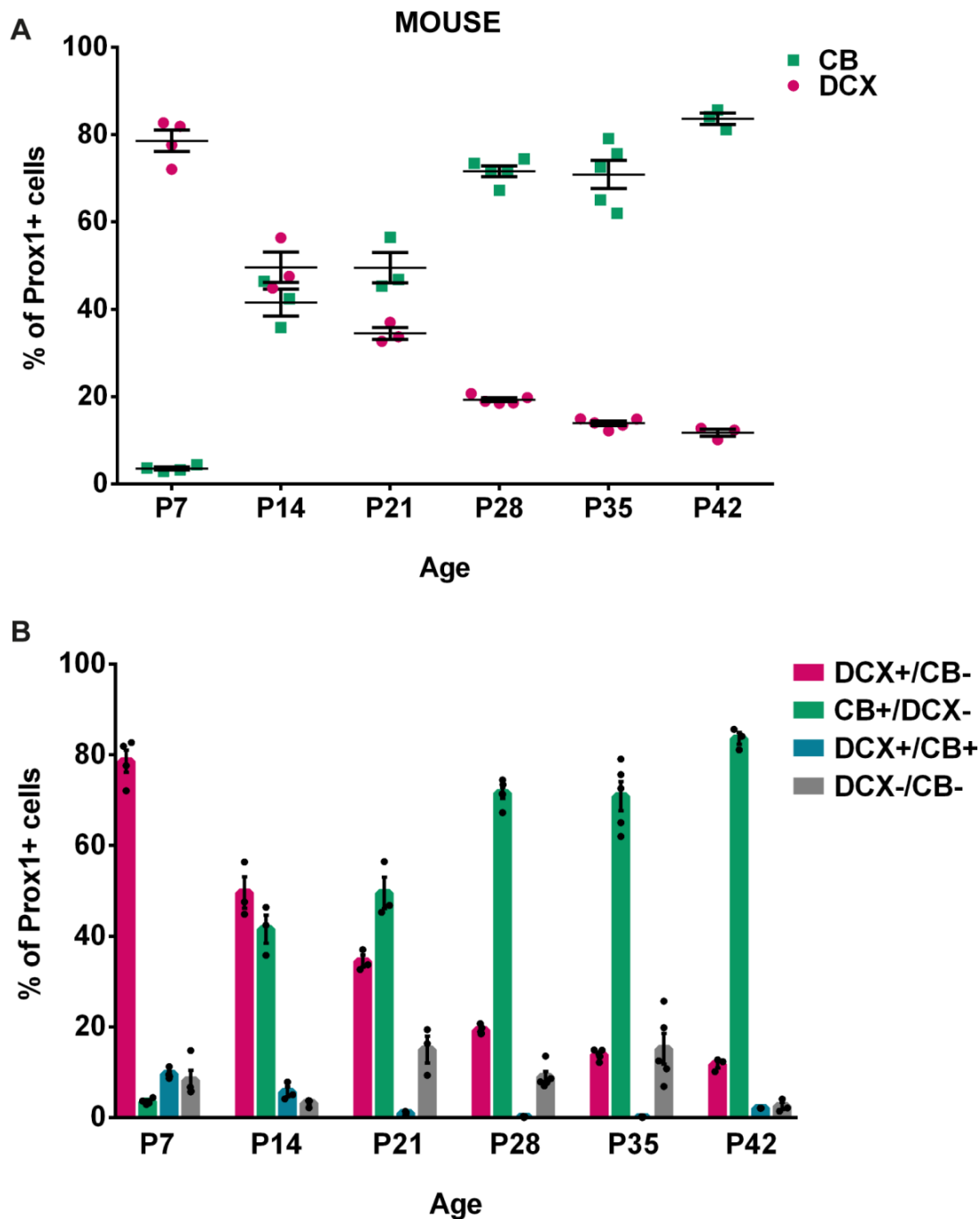


Figure 5. Quantification of DCX and calbindin expression in the early postnatal mouse DG over time. (A) At P7, nearly 80% of all Prox1-positive GCs expressed DCX while less than 4% were calbindin (CB)-positive. However, at P14, the number of DCX-positive GCs dropped to 50%, while 42% expressed calbindin. This represents the most drastic change during all time points that were examined. DCX expression continued to gradually decrease while the proportion of calbindin-expressing cells continued to increase until P42. (B) The relative distribution of DCX- and calbindin-

expressing GCs show a gradual shift toward maturity over time, particularly between P7 and P14. The number of triple-labeled cells that expressed Prox1 as well as DCX and calbindin constituted 9.62% at P7, less than 6% at P14 and P21, and between 0.11 and 2% from P28 - P42. In addition, Prox1-positive cells expressing neither maturity marker were noted. $n_{P7} = 4$; $n_{P14} = 3$; $n_{P21} = 3$; $n_{P28} = 5$; $n_{P35} = 5$; $n_{P42} = 3$. $n =$ number of animals.

5.1.2. The distribution of DCX and calbindin in the rat DG between P7 and P42

In order to study potential species differences between the mouse and the rat, the same study of the distribution of DCX and calbindin was performed within Prox1-positive cells of the rat DG. Similarly as in the mouse, DCX-expressing GCs at P7 were clearly more abundant in most parts of the rat GCL ($77.54 \pm 1.39\%$) compared with calbindin-positive GCs ($10.95 \pm 2.02\%$; Figures 6A, 7A). Again, small percentage of Prox1-positive cells expressed both, DCX and calbindin (4.24 ± 0.63), and some GCs expressed neither marker ($7.28 \pm 2.13\%$; Figure 7B). However, at P14 already, DCX-positive GCs were the minority ($29.99 \pm 2.33\%$) compared with calbindin-positive GCs ($54.81 \pm 0.50\%$; Figures 6B, 7A). At this time point, $0.20 \pm 0.05\%$ of all GCs exhibited both markers, and $15.00 \pm 2.01\%$ expressed neither (Figure 7B). At P21, the number of immature GCs decreased further, as $19.55 \pm 0.87\%$ expressed DCX, while the number of calbindin-positive GCs continued to increase with $67.33 \pm 2.69\%$ (Figures 6C, 7A). Again, a very small percentage was labeled with both markers ($0.13 \pm 0.05\%$), and some GCs ($12.99 \pm 2.30\%$) exhibited neither (Figure 7B). At P28, DCX immunoreactivity was detectable in $12.72 \pm 0.51\%$ of all Prox1-expressing cells, while the vast majority, $79.64 \pm 0.55\%$ were calbindin-positive (Figures 6D, 7A). $0.52 \pm 0.16\%$ of all GCs exhibited labeling of both maturity markers and $7.12 \pm 0.22\%$ expressed neither (Figure 7B). At P35, a very low number of DCX-positive GCs was present and located only in the SGZ and inner GCL ($6.88 \pm 0.47\%$), while most cells in the GCL were calbindin-positive and thus mature ($89.12 \pm 0.44\%$; Figures 6E, 7A). Only very few GCs were labeled with both markers ($0.14 \pm 0.01\%$), or neither ($3.86 \pm 0.72\%$; Figure 7B). Finally, at P42 there was almost no change, as $7.16 \pm 0.64\%$ of Prox1-positive cells co-expressed DCX, $86.47 \pm 1.29\%$ were calbindin-positive, $0.26 \pm 0.12\%$

Results

expressed both markers, and $6.11 \pm 0.93\%$ were labeled with neither DCX, nor calbindin (Figures 6F, 7A, B). The general expression patterns and changes in distribution of DCX and calbindin in the early postnatal rat DG over time were comparable to the mouse data. However, there were some important differences in the exact time course of these changes.

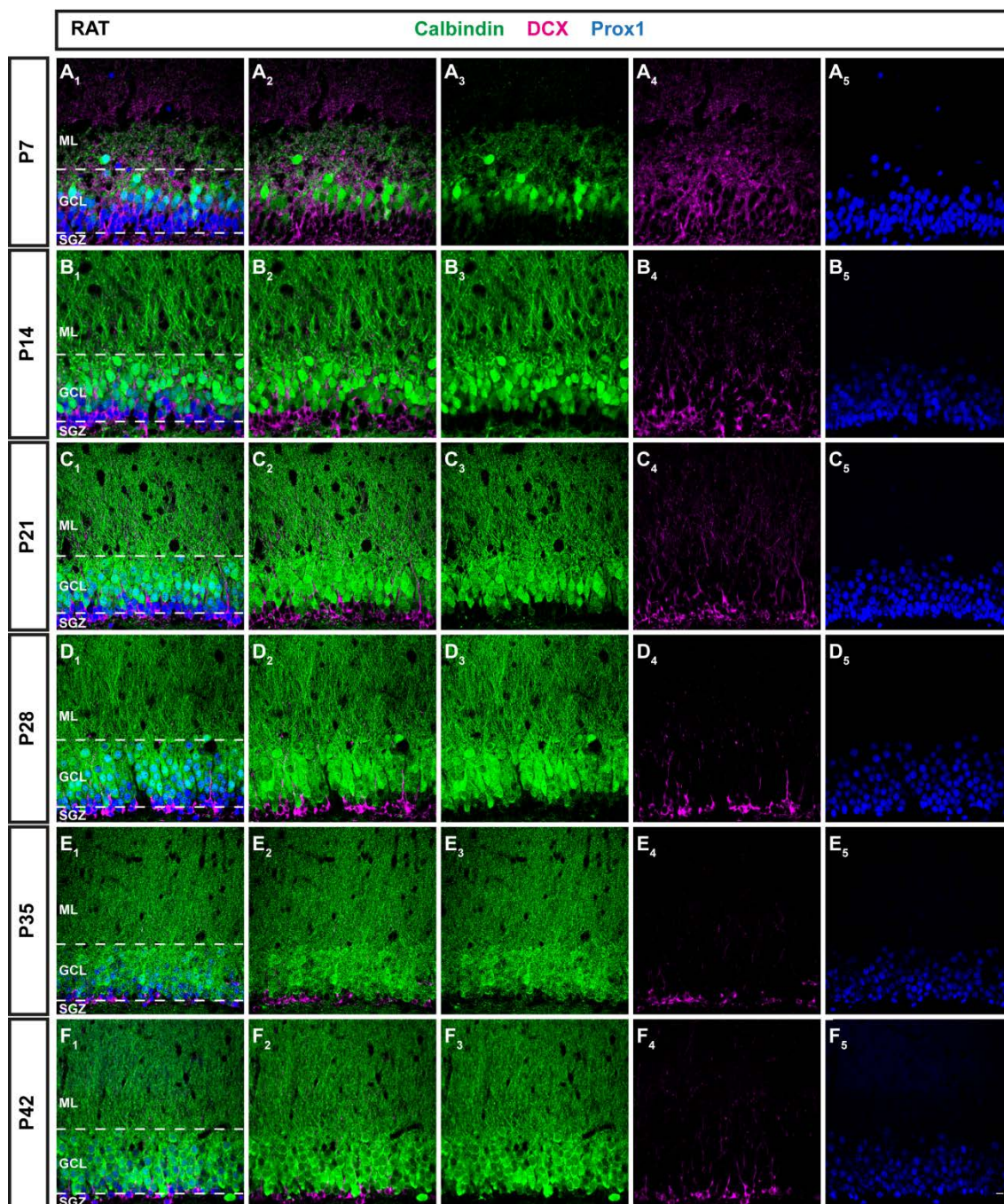


Figure 6. Immunohistochemical illustration of calbindin, DCX, and Prox1 distribution in the early postnatal DG of the rat. Immunostainings of the postnatal rat DG from P7 to P42 show increasing maturation, similarly as in the mouse. However, a larger proportion of GCs expressed calbindin (green) at early time points (A₂, B₂; A₃, B₃) and the fraction of DCX-positive cells (magenta) decreased more rapidly than in the mouse, especially between P7 and P14 (A₂, B₂; A₄, B₄). Prox1 (blue) was expressed in both mature and immature GCs at all time points (A₅-B₅). Scale bar: 10 μ m.

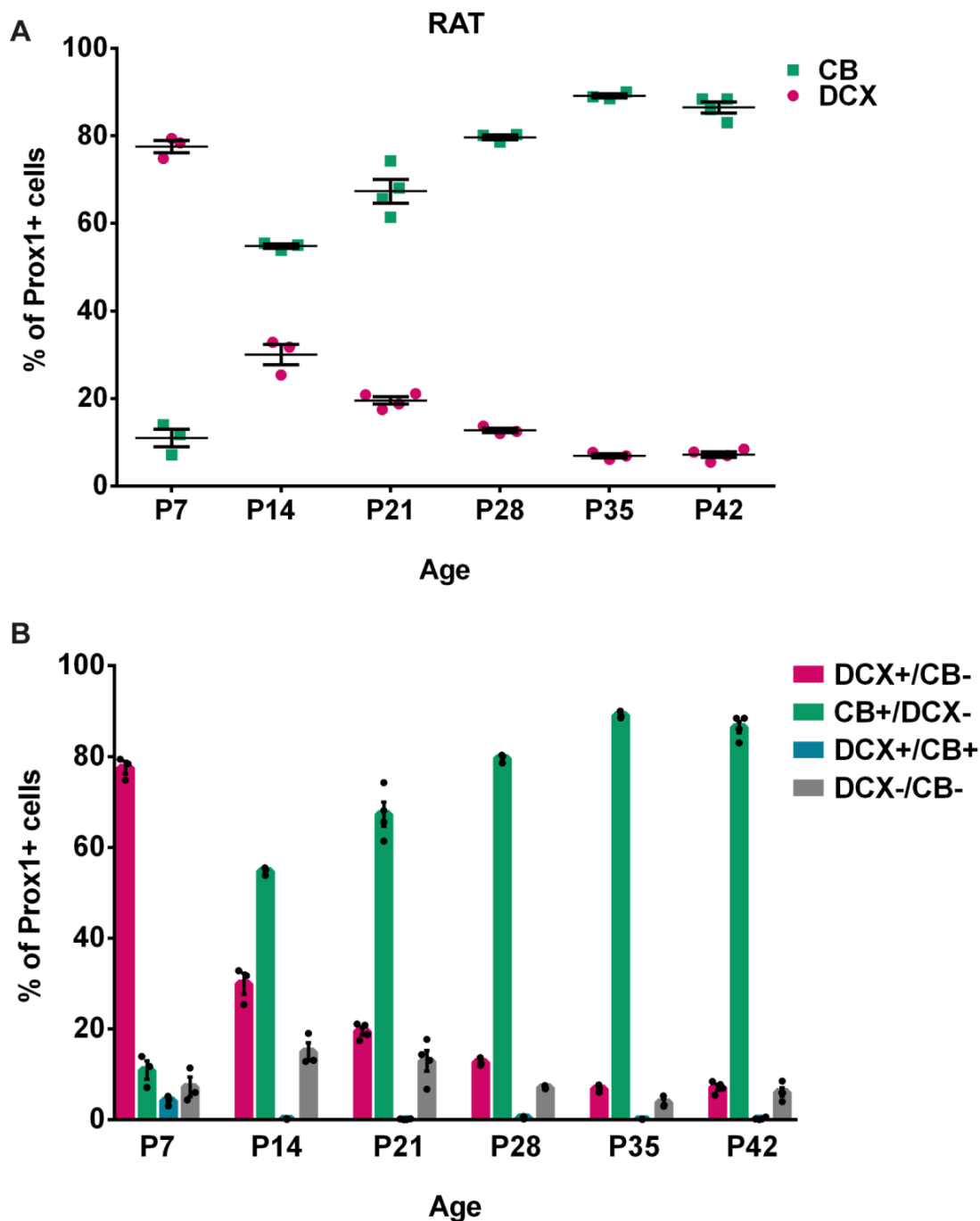


Figure 7. Quantification of calbindin and DCX expression in the early postnatal rat DG over time. (A) Similarly to the mouse DG, nearly 80% of all Prox1-positive GCs expressed DCX at P7 while 11% were calbindin (CB)-positive. At P14, the rat DG contained 30% DCX-positive and approximately 55% of calbindin-expressing GCs. Thus, the shift toward maturity between P7 and P14 was greater compared with the mouse. From then on, the proportion of DCX-positive GCs continued to decrease while the percentage of calbindin-expressing cells increased gradually until P28 after which there was only little change until P42. (B) The distributions of DCX and calbindin in GCs over time show a striking shift from immature to mature GCs between P7 and

P14. The proportion of GCs expressing both DCX and CB was extremely low at all time points, with 4% at P7 and less than 0.6% at all other time points. The fraction of GCs not expressing either maturation marker constituted between 7 - 15% at P7 - 21 and 4 - 7% at P28 - 42. $n_{P7} = 3$; $n_{P14} = 3$; $n_{P21} = 4$; $n_{P28} = 3$; $n_{P35} = 3$; $n_{P42} = 4$. n = number of animals.

5.1.3. The maturation pattern of the postnatal DG is faster in rats compared to mice

Comparing the distribution patterns of immature GCs (DCX-positive) and mature GCs (calbindin-positive) in the postnatal rat and mouse DG, it was interesting to observe that the speed of cell maturation was accelerated in the rat (Figure 8). In the rat, the percentage of DCX-positive GCs decreased significantly from P7 ($77.54 \pm 1.39\%$) to P14 ($29.99 \pm 2.33\%$, two-way ANOVA: time effect $F_{(5,31)} = 643.9$, $P < 0.0001$, followed by *post hoc* Bonferroni's test, $P < 0.0001$), and between P14 and P21 ($19.55 \pm 0.87\%$, $P = 0.0013$). In the mouse the decrease in the number of immature GCs between P7 and P14 was less drastic, albeit highly significant (P7: $78.57 \pm 2.44\%$; P14: $49.60 \pm 3.49\%$, $P < 0.0001$) as well as between P14 and P21 ($34.47 \pm 1.32\%$, $P < 0.0001$), and between P21 and P28 ($19.30 \pm 0.42\%$, $P < 0.0001$; Figure 8C).

Significant differences between the two species were observed as well. The mouse DG exhibited a significantly higher proportion of DCX-positive GCs at P14 (mouse: $49.60 \pm 3.49\%$; rat: $29.99 \pm 2.33\%$, two-way ANOVA: group effect $F_{(1,31)} = 112.6$, $P < 0.0001$, followed by *post hoc* Bonferroni's test, $P < 0.0001$; group x time interaction: $F_{(5,31)} = 10.54$, $P < 0.0001$) and P21 (mouse: $34.47 \pm 1.32\%$; rat: $19.55 \pm 0.87\%$, $P < 0.0001$; Figure 8A-C). The average age at which 50% of Prox1-positive cells were DCX-positive (i.e. $t_{50\%}$) was determined for each species using a monoexponential fit. While for mice, $t_{50\%}$ was at 14 days, in the rat, the average age was 10 days (dashed lines in Figure 8C). Hence, the decrease of immature DCX-labeled GCs was accelerated in the rat by approximately 4 days compared with the mouse.

The decrease in the number of DCX-expressing GCs as well as the increase in mature, calbindin-positive GCs was more rapid in the rat than in the mouse (Figure 8D). In the rat, the increase in calbindin-expressing GCs was significant

Results

between P7 ($10.95 \pm 2.02\%$) and P14 ($54.81 \pm 0.50\%$, two-way ANOVA: time effect $F_{(5,31)} = 350.7$, $P < 0.0001$, followed by *post hoc* Bonferroni's test, $P < 0.0001$), between P14 and P21 ($67.33 \pm 2.69\%$, $P = 0.0222$), and between P21 and P28 ($79.64\% \pm 0.55$, $P = 0.0271$). In the mouse, the increase in the proportion of calbindin-positive GCs was significant between P7 ($3.56 \pm 0.33\%$) and P14 ($41.54 \pm 3.08\%$, $P < 0.0001$) as well as between P21 ($49.52 \pm 3.50\%$) and P28 (49.52 ± 3.50 , $P < 0.0001$), and P35 ($70.86 \pm 3.20\%$) and P42 (83.61 ± 1.32 , $P = 0.0108$; Figure 8D).

A significantly higher proportion of calbindin-positive GCs was found in the rat DG at P14 (mouse: $41.54 \pm 3.08\%$; rat: $54.81 \pm 0.50\%$, two-way ANOVA: group effect $F_{(1,31)} = 79.29$, $P < 0.0001$, followed by *post hoc* Bonferroni's test, $P = 0.0248$; group x time interaction: $F_{(5,31)} = 4.065$, $P = 0.0059$), P21 (mouse: $49.52 \pm 3.50\%$; rat: $67.33 \pm 2.69\%$, $P = 0.0002$) and P35 (mouse: $70.86 \pm 3.20\%$; rat: $89.12 \pm 0.44\%$, $P < 0.0001$; Figure 8A, B, D). In the mouse $t_{50\%}$ for Prox1-positive GCs expressing calbindin was 19 days, while in the rat, $t_{50\%}$ occurred at 14 days (dashed lines in Figure 8D). Therefore, comparably to the decrease of DCX-positive GC proportion, the increase in the fraction of calbindin-positive cells was faster by 5 days in the rat compared to the mouse.

These data indicate that the early postnatal cellular maturation in the DG is faster in the rat with a higher number of mature GCs and fewer young, immature GCs at P14 and P21. However, at the last observed time point, P42, when the animals have transitioned into adulthood, the relative numbers of both mature and immature GCs are comparable between the two species.

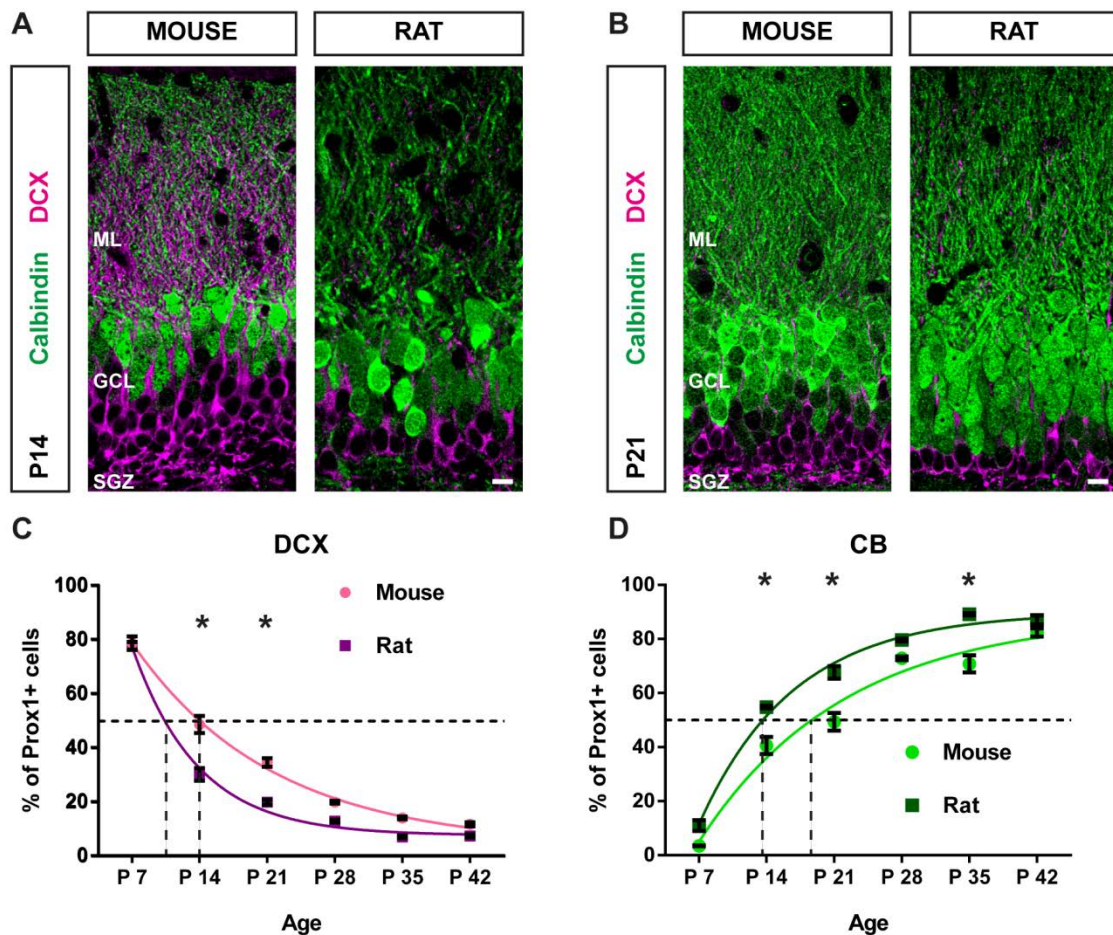


Figure 8. Postnatal maturation of the DG progresses faster in the rat compared with the mouse. (A) Immunohistochemical depiction of doublecortin (DCX)- (magenta) and calbindin (CB)-expressing GCs (green) in the mouse and rat DG at P14 and (B) at P21. (C) The comparison of DCX-positive GC distribution between mice and rats from P7 to P42 reveals that the proportion of DCX-expressing cells decreased more rapidly in the rat. Significant differences in the number of DCX-positive cells between species were found on P14 (two-way ANOVA with Bonferroni correction $P < 0.0001$) and P21 ($P < 0.0001$). A monoexponential fit was used to determine the average age at which 50% of Prox1-positive cells were DCX-positive (i.e. $t_{50\%}$) in each species (dashed lines). While for mice, $t_{50\%}$ was at 14 days, in the rat, it was 10 days. (D) Meanwhile, the proportion of CB-positive GCs increased more quickly in the rat compared with GCs in the mouse. Significant differences in the number of CB-positive cells between species were found on P14 (two-way ANOVA with Bonferroni correction $P = 0.0248$), P21 ($P = 0.0002$), and P35 ($P < 0.0001$). In the mouse $t_{50\%}$ for Prox1-positive GCs expressing CB was 19 days, while in the rat, $t_{50\%}$ occurred at 14 days. These findings suggest that GCs mature faster in the rat than in the mouse. Mouse: $n_{P7} = 4$; $n_{P14} = 3$; $n_{P21} = 3$; $n_{P28} = 5$; $n_{P35} = 5$; $n_{P42} = 3$. Rat: $n_{P7} = 3$; $n_{P14} = 3$; $n_{P21} = 4$; $n_{P28} = 3$; $n_{P35} = 3$; $n_{P42} = 4$. n = number of animals. Error bars represent SEM. * $P < 0.05$. Scale bars: 10 μ m.

5.2. Histological characteristics and marker distribution in rat OTCs

Organotypic entorhino-hippocampal slice cultures (OTCs) are characterized by the preservation of the cellular architecture and the re-establishment of the entorhino-dentate circuit *in vitro* (Gähwiler, 1984; Heimrich and Frotscher, 1993; Li et al., 1994; Kluge et al., 1998; Del Turco and Deller, 2007). Therefore, after examination of the cytological composition and the distribution of maturation markers in early postnatal dentate tissue *in vivo*, the same parameters were assessed in the OTC system for comparison. Figure 9 shows the general histological organization of an OTC at DIV 5 as depicted by the nuclear staining dye ToPro where the main hippocampal structures such as the CA areas and the DG as well as the entorhinal cortex are easily identifiable. For a more detailed description of the cytoarchitecture, specific immunocytochemical markers were applied (see also section 5.4.).

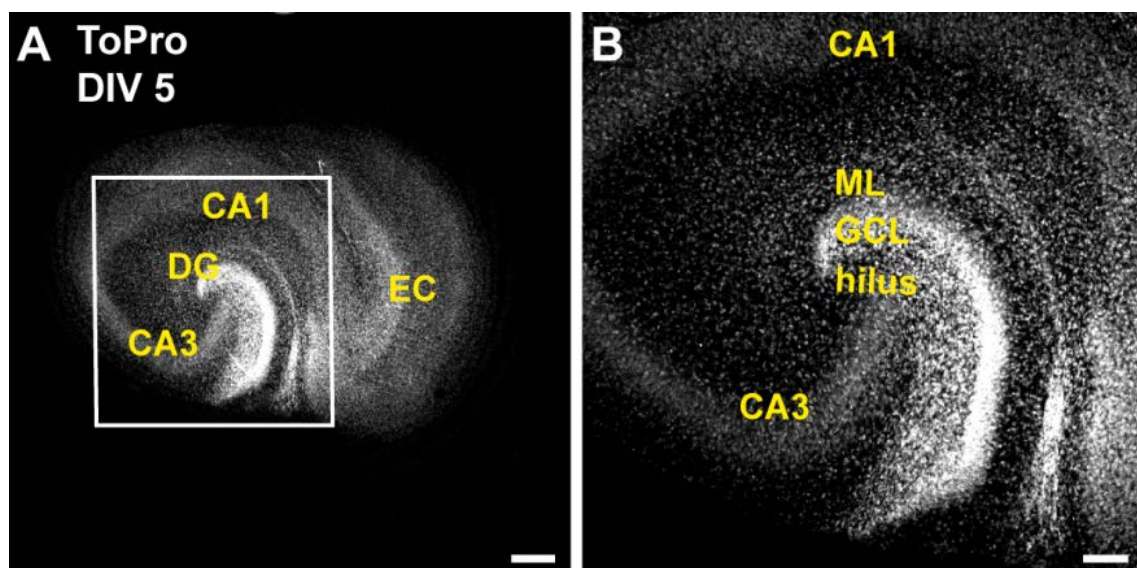


Figure 9. Histological overview of postnatal OTCs. Postnatal OTCs were treated with the nuclear dye ToPro at DIV 5. (A) A complete OTC in which the principal areas of the hippocampus are well-visible, including the dentate gyrus (DG) and the Cornu Ammonis (CA) areas as well as the attached entorhinal cortex (EC). (B) A magnified view shows the pyramidal cell layer of the CA3 and CA1 regions, the granule cell layer (GCL) consisting of densely packed granule cell nuclei, the molecular layer (ML), and the hilus. Scale bars: (A) 250 μm ; (B) 100 μm .

Because one of the main objectives of this thesis was to observe GC development over an extended period of time, the histology and the distribution of neuronal maturation markers commonly used in the study of neurogenesis was assessed in OTCs at early (DIV 7), intermediate (DIV 14), and late (DIV 28) time points.

In OTCs, at DIV 7, the GCL was clearly recognizable through a dense cellular layer of Prox1-positive cells which indicates that Prox1 is also a reliable GC marker *in vitro*. The predominant expression of DCX was striking at this time point, as the vast majority of Prox1-positive cells in the GCL, the forming SGZ, and the hilus expressed DCX, but not calbindin. In fact, only Prox1-expressing GCs in the outer bands of the GCL were calbindin-positive and did not express DCX (Figure 10). Although a formal cell count was not performed in this case, it is evident that most GCs were young and immature at this time which is comparable to the *in vivo* findings described above (section 5.1.). This is not surprising since this is still within the time period when local neurogenesis of GCs is taking place in the hilus and the forming SGZ at a high rate (Schlessinger et al., 1975; Altman and Bayer, 1990).

At DIV 14, the majority of Prox1-positive GCs in the outer and mid layers of the GCL expressed calbindin and thus displayed a mature phenotype. Nevertheless, a considerable fraction of GCs were DCX-positive and therefore young and immature (Figure 11). However, DCX expression became more confined to the SGZ and the inner part of the GCL compared to DIV 7. This suggests that OTCs were maturing *in vitro* and that there was a decrease in neurogenesis from DIV 7 to DIV 14. The two maturation markers were, again, rarely co-expressed which is best demonstrated in Figure 11B. Prox1 immunoreactivity was observed throughout the entire GCL, and co-localized with both, DCX and calbindin.

Marker distribution in OTCs at DIV 28 showed a reverse image: calbindin expression was widespread throughout the GCL, and only a few GCs located in the SGZ expressed DCX. Again, both of these cell population co-expressed Prox1 (Figure 12). These observations suggest that at this point, the rate of

neurogenesis in the OTC is rather low but nevertheless persists over several weeks, and a number of young, immature cells survive and integrate into the DG cellular network.

The fact that DCX and calbindin expression does not co-localize for the most part suggests that (i) DCX and calbindin both are useful and valid markers in the OTC system that can be employed to analyze neurogenesis and neuronal maturation in culture conditions, (ii) GC maturation in OTCs runs a comparable course to cells analyzed *in vivo*. Moreover, Prox1 was also found to be a reliable marker for both mature and immature GCs *in vitro*. Thus, neurogenesis can be studied in a well-established and easily accessible organotypic culture system under controlled conditions.

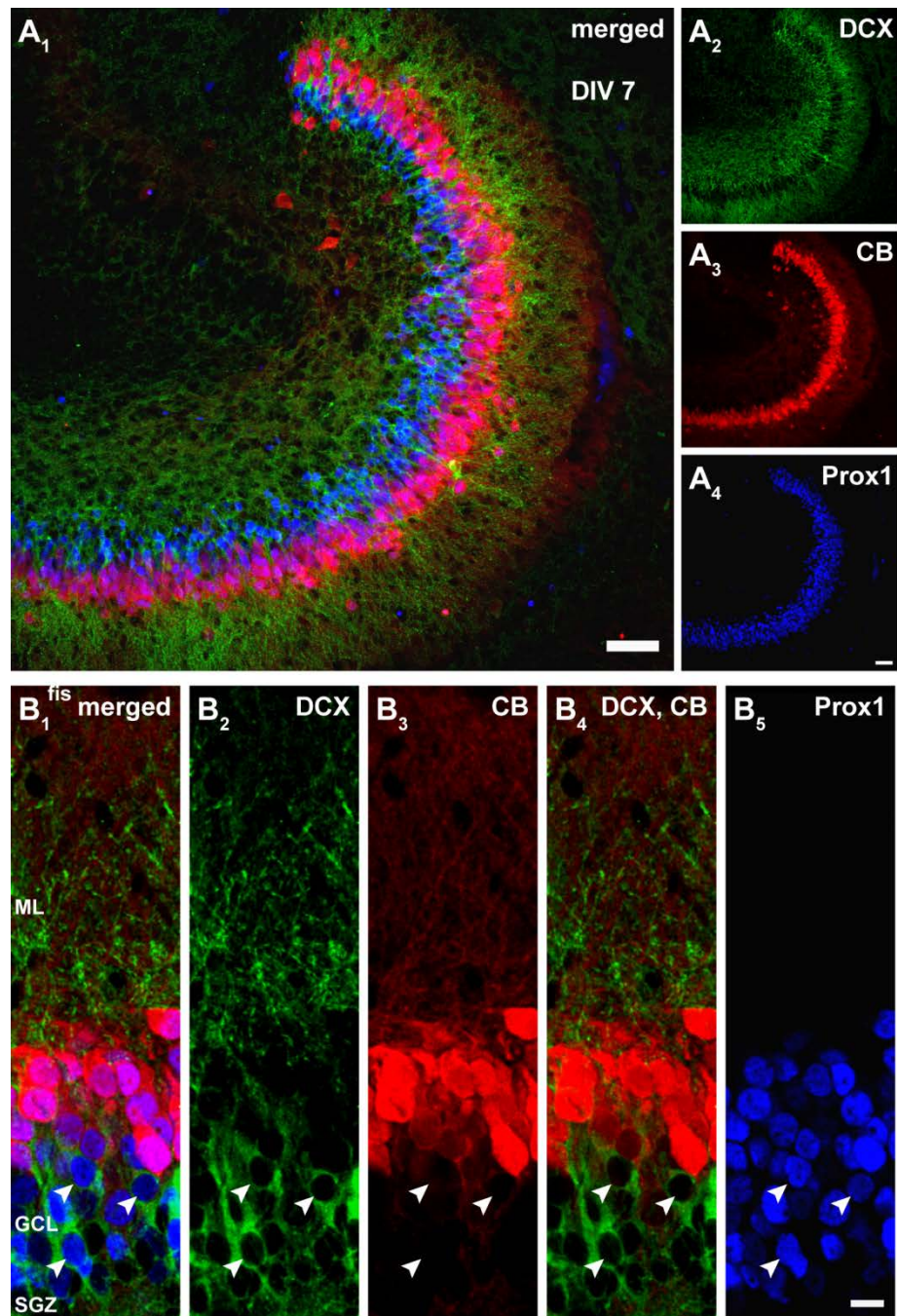


Figure 10. Immunocytochemical evaluation of postnatal OTCs at DIV 7. (A) Resliced OTC sections (50 μ m) prepared on P 4 - 5 and fixed on DIV 7 were processed for immunoreactivity of the immature neuronal marker doublecortin (DCX; green), the mature neuronal marker calbindin (CB; red), and the granule cell marker Prox1 (blue). (B) Expression of DCX was observed in the subgranular zone (SGZ), the inner and middle parts of the granule cell layer (GCL) in cell somata, as well as dendrites that extended into the molecular layer (ML). Calbindin labeling was detected in GCs that were located in the outer parts of the GCL with processes that reached the hippocampal fissure (fis). Prox1 was expressed in both, immature and more mature GCs in the GCL. DCX and calbindin co-localized only rarely, while Prox1 was co-expressed with both of these markers in addition to being present in

Results

other GCs as well. Scale bars: (A) 50 μm ; (B) 10 μm . Adapted from Radic et al. (2017).

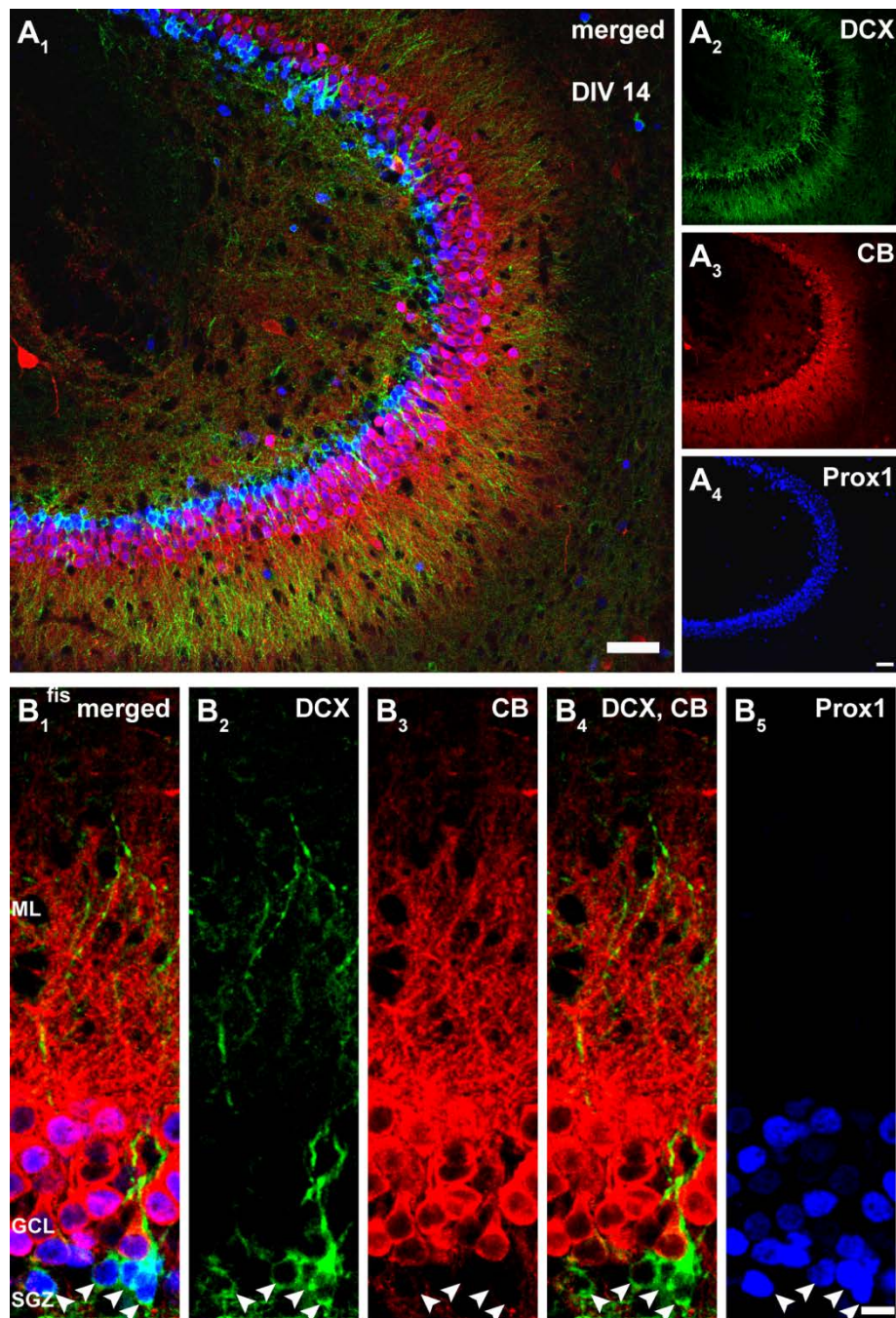


Figure 11. Immunocytochemical evaluation of postnatal OTCs at DIV 14. (A) Immunostainings of OTC sections fixed on DIV 14 illustrate a wide-ranging expression of calbindin (red) in the granule cell layer (GCL). The SGZ and the inner layers of the GCL were marked by DCX expression (green), indicating that a substantial proportion of GCs was still immature at this time point. Prox1 (blue) was expressed in the entire GCL in immature and mature GCs. (A) DCX-positive cells co-expressed Prox1, but not calbindin. A large fraction of GCs were calbindin-positive and thus mature. ML, molecular layer; fis, hippocampal fissure. Scale bars: (A) 50 μm ; (B) 10 μm .

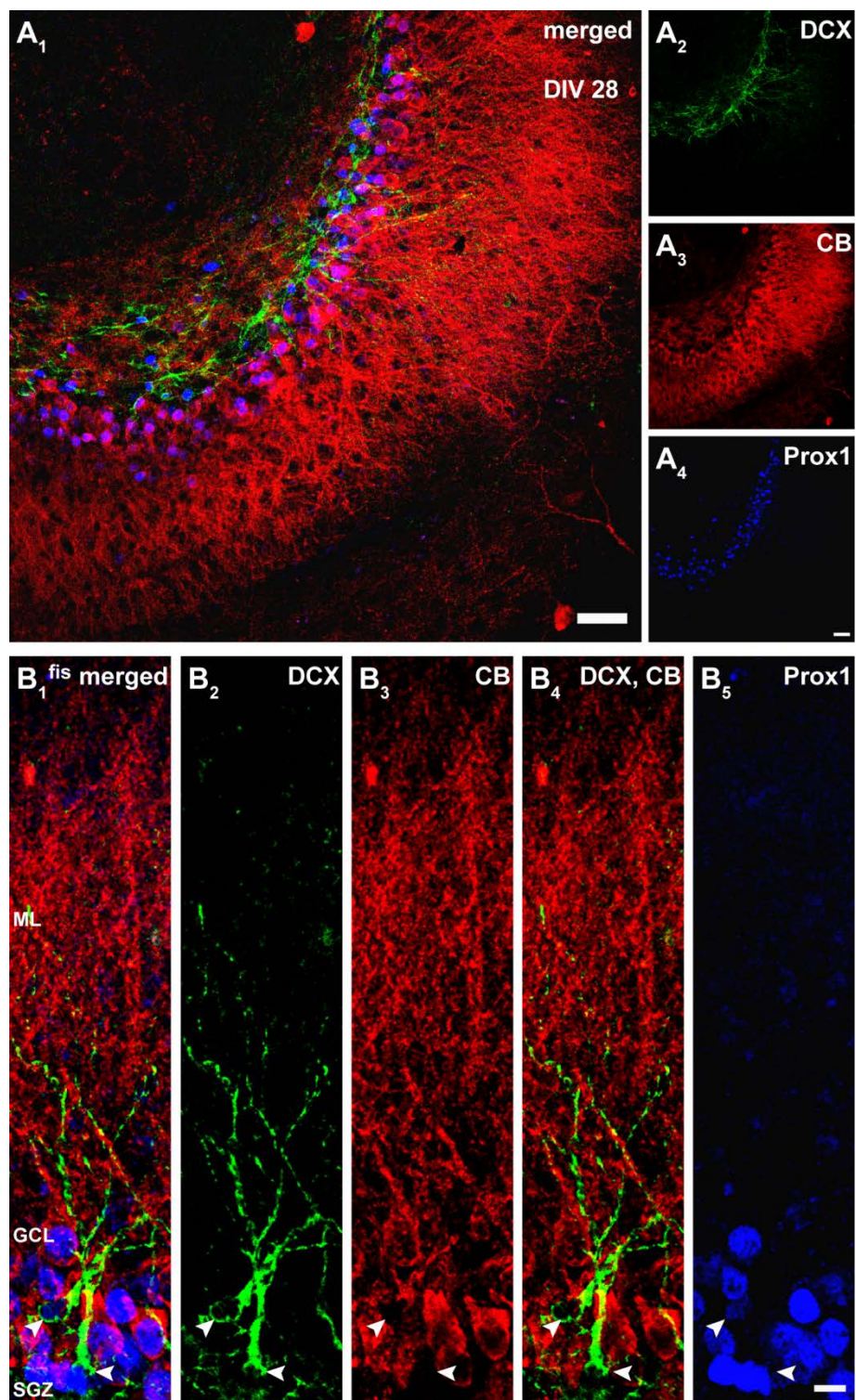


Figure 12. Immunocytochemical evaluation of postnatal OTCs at DIV 28. (A) Immunostainings of OTC sections fixed on DIV 28 displayed extensive expression of calbindin (red) throughout the granule cell layer (GCL), while there were only few DCX-positive (green) cells in the subgranular zone (SGZ). Prox1 (blue) was expressed in the entire GCL in immature and mature GCs. (B) Few DCX-positive cells were found in the SGZ in 28-day-old OTCs. Most GCs were calbindin-positive and extended their

dendrites through the molecular layer (ML) to the hippocampal fissure (fis), indicating that at this time point, most GCs are mature and the neurogenesis rate has decreased. Scale bars: (A) 50 μm ; (B) 10 μm . Adapted from Radic et al. (2017).

5.3. Retroviral transduction enables visualization of complete postnatally generated GCs in OTCs

To label newborn GCs in the OTC, a Moloney murine leukemia virus (MMLV) based retroviral (RV) vector expressing the gene for GFP under the CAG promoter (van Praag et al., 2002) was injected directly into each culture at the time of preparation (P4 - 5; DIV 0). The RV vector can only be incorporated into a cell whose nucleus is open and accessible, as is the case during mitosis (Osten et al., 2007). Therefore, all newly generated cells can potentially be transduced by the RV vector. Due to the fact that in the case of a transduction GFP is expressed under a cell-unspecific CAG promoter, all mitotic cells, including both neurons and glia, could contain the labeling. To assess the efficacy of RV transduction, OTCs were fixed and newborn GCs were identified using Prox1. Figure 13 shows RV-labeling in an OTC that was fixed at 14 days post RV injection (14 dpi). GFP-expressing cells were found throughout the DG, some of which exhibited morphologies that are characteristic of young GCs (Espósito et al., 2005; Zhao et al., 2006). The majority of these cells were found in the SGZ and the inner part of the GCL which was nicely visualized with Prox1 labeling. In fact, all of the cells with neuronal morphology co-expressed Prox1 which confirmed that these were indeed postnatally generated GCs. Moreover, the young GCs were also DCX-positive, which was expected at 14 dpi, as DCX is expressed in young neurons until approximately 4 weeks of cell age (Brown et al., 2003; Jungenitz et al., 2014; Radic et al., 2015). At 14 dpi, RV-GFP-labeled postnatally generated GCs had somata positioned in the SGZ or the inner bands of the GCL, extended dendritic processes through the GCL and into the ML, and did not contain any spine-like structures. Hence, morphologically, the labeled neurons displayed typical features of young, still maturing GCs (Espósito et al., 2005; Zhao et al., 2006). In addition to GCs, RV-GFP-labeling was also evident in cells that exhibited a glial morphology and did not express the neuronal marker DCX or the GC marker Prox1 (examples are denoted with

asterisks in Figure 13). Due to their distinct morphological characteristics, glial cells could easily be distinguished from RV-GFP-labeled neurons.

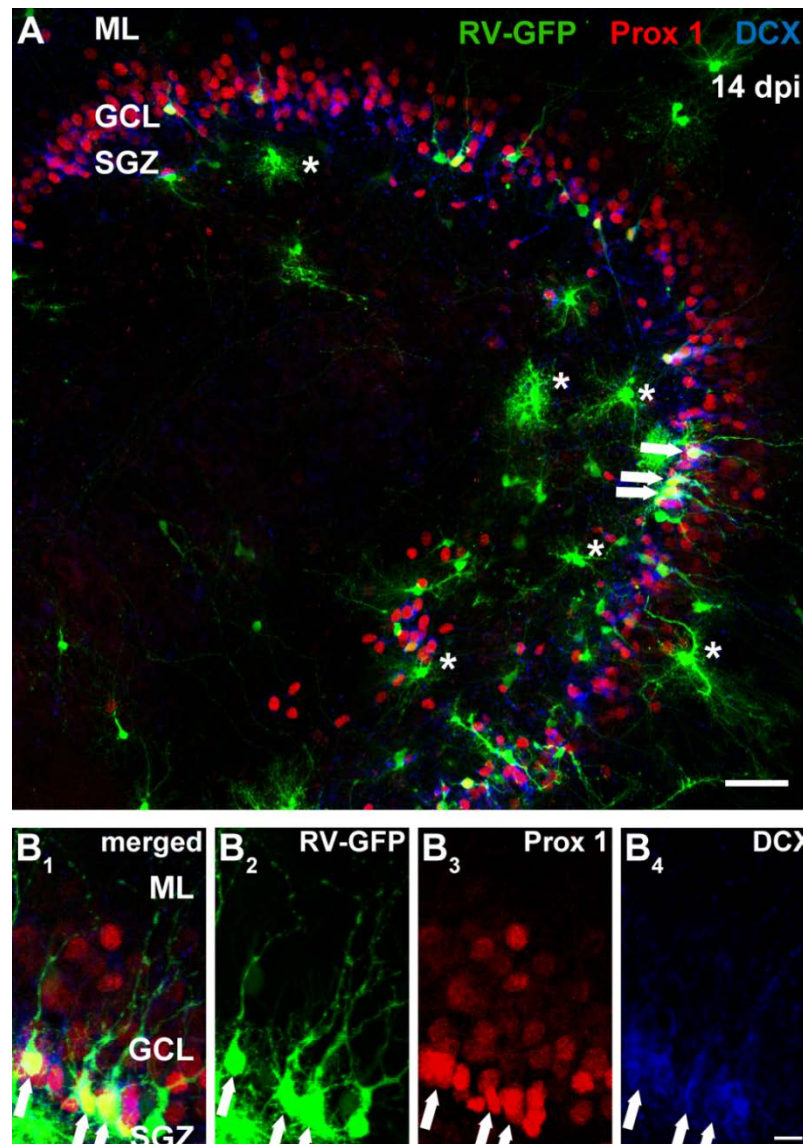


Figure 13. Retroviral (RV) transduction of newborn dentate granule cells (GCs) by local injection. (A) A triple immunostaining of an OTC that was transduced with RV-GFP on DIV 0 and fixed on 14 dpi. DCX immunoreactivity was observed in the subgranular zone (SGZ) and the inner part of the granule cell layer (GCL), while Prox1 was expressed throughout the GCL. Several RV-GFP-labeled cells located in the SGZ and inner GCL were polarized with processes extending into the GCL and the molecular layer (ML), and co-expressed Prox1 and DCX (white arrows), suggesting that a number of newborn GCs were transduced with the RV. In addition, there were RV-GFP-positive cells with glial morphology that did not express DCX, or Prox1, (examples are denoted by asterisks). (B) A magnification shows RV-GFP-labeled cells located in the SGZ and the inner layers of the GCL co-expressing both Prox1 and DCX (white arrows). Scale bars: (A) 50 μm ; (B) 10 μm . Adapted from Radic et al. (2017).

5.4. Entorhinal projection fibers innervate the molecular layer in OTCs during the development of postnatally generated GCs

One of the main sources of synaptic input to the DG derives from stellate and pyramidal neurons of the entorhinal cortex (EC). These neurons project their axons through the so-called perforant path to the hippocampus, in particular the outer molecular layer (OML) of the DG (Hjorth-Simonsen and Jeune, 1972; Steward, 1976). There, the entorhinal axon terminals establish synapses with spines of dentate GCs. It has been shown that proper development of young GCs is dependent on the presence of afferent fibers *in vitro* (Zafirov et al., 1994; Frotscher et al., 2000). Although during preparation of OTCs some of these fibers are transected, earlier studies have shown that entorhinal projections re-innervate the DG and are present in the ML within three days of explantation (Li et al., 1994; Kluge et al., 1998). In order to verify whether the projections from the EC are present in the DG during the development of RV-transduced GCs, anterograde tracing of EC fibers was performed by placing the biotinylated dextran amine Mini Ruby on the surface of layers II and III of the EC on DIV 3 and DIV 15. Cultures were fixed at different time points between DIV 8 and DIV 20. Figure 14A illustrates Mini Ruby labeling in EC neurons and their axonal projections to the ML. Neuronal markers DCX and calbindin were used to visualize the immature and mature GC populations of the GCL, respectively.

In combination with RV-labeling, it could be demonstrated that Mini Ruby-labeled EC fibers were already present in the DG at early time points (i.e. DIV 8) when 8-day-old RV-GFP-labeled newborn GCs began to extend relatively short dendrites into the IML but did not reach the axonal termination area in the OML yet (Figure 14B). At DIV 20, RV-GFP-positive GCs displayed elaborate dendritic arbors whose processes ran into the OML and intermingled with Mini Ruby-labeled perforant path fibers (Figure 14C). These findings reveal the presence of entorhinal axons in OTCs early on, when newborn GCs only begin to extend neurites toward the ML and later go on to grow into an area of entorhinal fiber plexus, similar to the situation during adult neurogenesis.

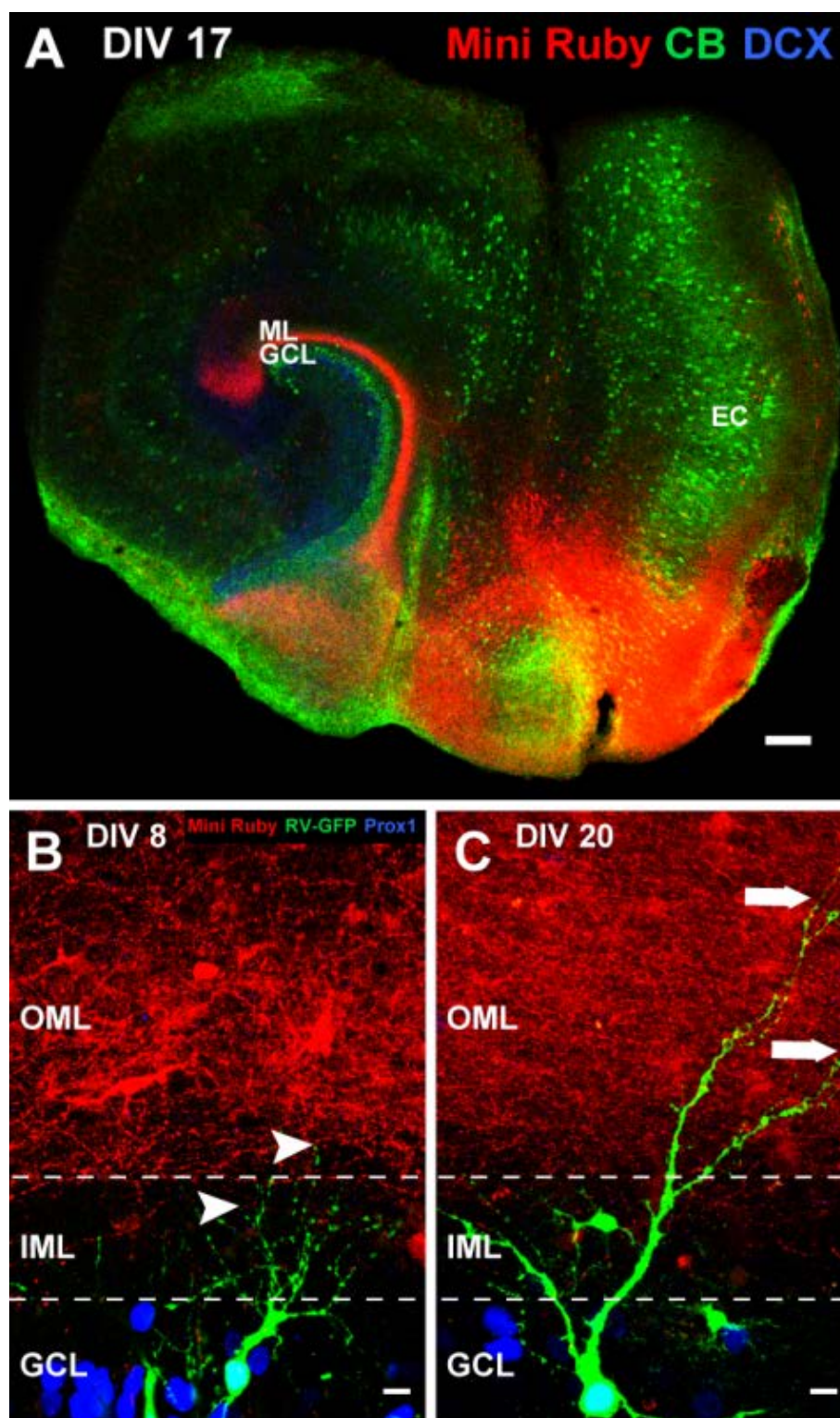


Figure 14. Perforant path fibers are present in the outer molecular layer (OML) during the development of RV-GFP-labeled GCs *in vitro*. (A) The biotinylated dextran amine tracer Mini Ruby was applied to the entorhinal cortices (ECs) of OTCs at DIV 15 and images were taken on DIV 17 showing the axons of EC neurons projecting

to the molecular layer (ML) of the dentate gyrus (red). In the granule cell layer (GCL), mature neurons were labeled with the marker calbindin (CB), while immature neurons were labeled with doublecortin (DCX). (B) Z-projection of two images (z-axis interval: 1 μm) showing an 8-day old OTC treated with the RV (green) and Mini Ruby (red). Mini Ruby was applied on DIV 3 and OTCs were fixed on DIV 8. Prox1-positive (blue) 8-day-old postnatally born RV-GFP-labeled GCs directed their growing dendrites toward the OML (white arrowheads) that was already re-innervated by Mini Ruby-labeled entorhinal fibers. (C) Z-projection of four images of an RV- and Mini Ruby-treated OTC at DIV 20. A 20-days-old RV-GFP-labeled GC exhibiting an elaborate dendritic arbor that extended well into the OML (white arrows) where labeled perforant path axons were present. Scale bars: (A) 50 μm , (B, C) 10 μm . Adapted from Radic et al. (2017).

5.5. Time-lapse imaging of postnatally generated GCs in OTCs reveals highly dynamic structural development

Since the OTC system is a highly accessible tool and RV-labeling enabled visualization of postnatally generated GCs, with the combination of the two techniques it was possible to observe and follow individual newborn GCs and analyze structural growth and maturation dynamics in the same cells over extended periods of time through live time-lapse imaging. In order to assess and understand the extent of the dynamics in structural development in newborn GCs, changes in morphology over time were compared between RV-GFP-labeled GCs and older, more mature GCs during the same time window and in the same setting. Older, presumably prenatally generated GCs were visualized by transduction with an adeno-associated viral (AAV) vector expressing tdTomato under the synapsin 1 promoter. Due to the fact that the protein synapsin 1 plays an important role in the clustering of synaptic vesicles and neurotransmitter release (Südhof et al., 1989; Greengard et al., 1993; Cesca et al., 2010), it is only expressed in neurons that engage in synaptic activity and are therefore developmentally advanced. OTCs were transduced with both, the RV-CAG-GFP (RV-GFP) and the AAV-synapsin1-tdTomato (AAV-Syn) vectors at DIV 0 (P4 - 5) which yielded labeling of newborn and older GCs in the same cultures. Figure 15A illustrates an example of an OTC containing labeled cells of both populations: While RV-GFP was expressed in newborn cells in the inner part of the GCL, tdTomato was detected throughout the GCL in GCs that were not RV-GFP-positive.

In order to track morphological changes in individual postnatally born GCs during different stages of development, time-lapse imaging was performed once a day from 8 to 28 dpi on at least 7 consecutive days ($n = 18$ GCs from 16 cultures of 13 animals, mean time of observation 13.67 ± 4.77 days; Figure 15B). The images of dendritic trees at each time point were used to create 3-D computer reconstructions (Figure 15C) using the TREES Toolbox (Cuntz et al., 2010, 2011) with which structural features and dynamic changes could be analyzed. The same procedure was applied to AAV-Syn-labeled neurons ($n = 11$ GCs from 9 cultures of 9 animals, mean time of observation 8.55 ± 2.10 days) which displayed morphological characteristics of mature GCs throughout the imaging period (Figure 15D, E), including the earliest time point (i.e. 8 dpi) studied here.

Time-lapse imaging was started at the beginning of the second week of development when postnatally generated GCs exhibited short, already polarized processes directed toward the ML. Many cells also exhibited basal dendrites extending toward the hilus as well as axonal processes with collateral branches. Here, the analysis was concentrated on the structural development and dynamic morphological changes of apical dendrites. Figure 16 shows an example of a postnatally born GC that was followed from 9 dpi to 28 dpi and its corresponding 3-D computer reconstructions at each time point.

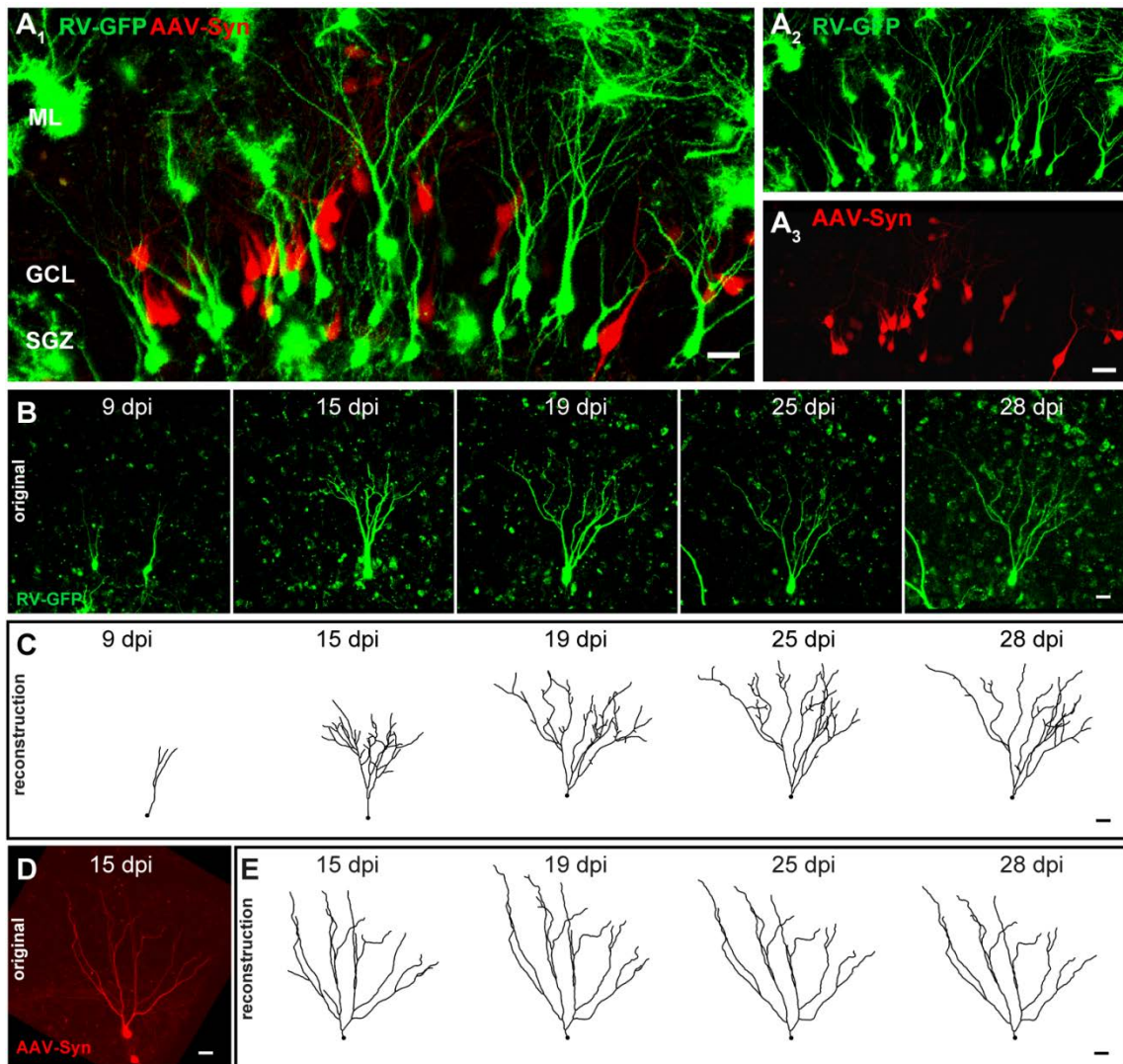


Figure 15. Time-lapse imaging and reconstruction of RV-CAG-GFP-labeled postnatally born GCs and older AAV-Synapsin1-tdTomato-labeled GCs. (A) OTCs were transduced with an RV-CAG-GFP and an AAV-Synapsin1-tdTomato vector to label newborn (RV-GFP; green) and older GCs (AAV-Syn; red) respectively. (B, C) Daily time-lapse imaging of individual RV-GFP-labeled GCs was performed over a period of three weeks between 8 and 28 days post virus injection (dpi). All cells were 3-D computer reconstructed to allow for detailed morphological analysis over time. (D, E) Example of an AAV-Syn-labeled cell with 3-D reconstructions at different time points. Scale bars: (A₁) 20 μ m, (A₂-E) 10 μ m. Adapted from Radic et al. (2017).

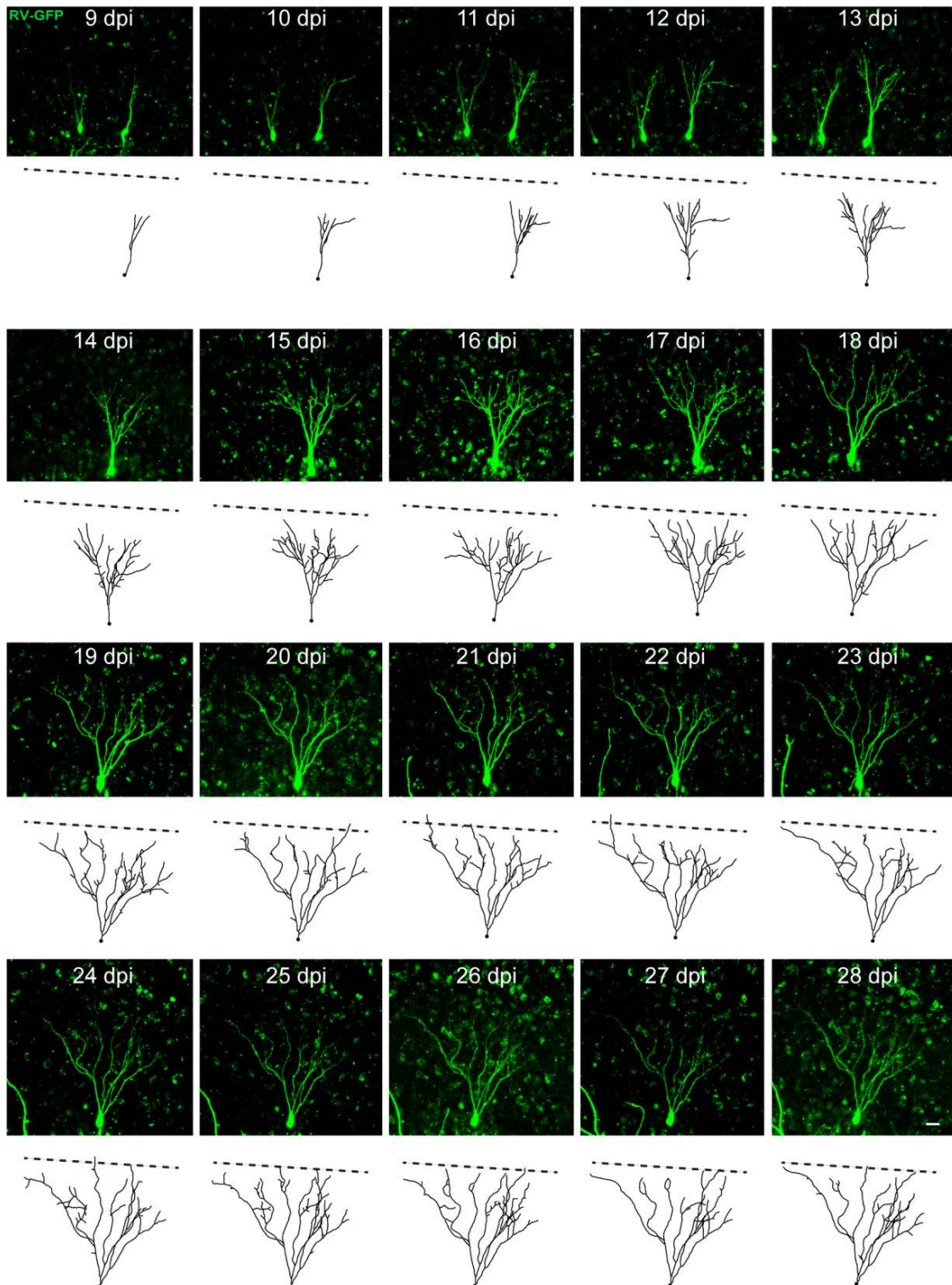


Figure 16. Time-lapse imaging of RV-GFP-labeled postnatally born GCs. Successful RV-labeling of postnatally born GCs in OTCs enabled live imaging of individual cells over extended periods of time. Daily time-lapse imaging sequences were performed between 8 - 28 dpi, up to 20 consecutive days. Three-dimensional computer reconstructions enabled detailed analysis of morphological development of

Results

individual newborn GCs. Based on immunostainings of fixed OTCs on 28 dpi, the location of the hippocampal fissure could be determined *post hoc* (dashed line). Scale bar: 10 μm . Adapted from Radic et al. (2017).

During the time period between 8 and 14 dpi, newborn GCs displayed a high degree of dendritic growth and branching (Figure 17A). In this time frame, in particular from 10 dpi on, their apical dendritic arbors became more elaborated and complex over time, and branched out into the ML. Despite the prominent overall dendritic growth, it became evident that the structural development of newborn GCs involved intricate dynamics that included both, the extension (Figure 17A, white arrowheads) and retraction of individual dendritic segments (Figure 17A, red arrowheads) at the same time. In contrast, AAV-Syn-labeled older GCs exhibited a stable dendritic arbor that did not change substantially throughout the imaging period. In an analysis of the total dendritic length (TDL) during each time of observation, older GCs did not display any changes from day to day (Figure 17B, C). In contrast, RV-GFP-labeled newborn GCs exhibited a gradual increase in TDL until approximately 21 dpi after which it remained relatively constant (Figure 17B, C). Grouped by week, there were significant differences in the mean TDL between the second and the third week (8 - 14 dpi: $931.33 \pm 90.16 \mu\text{m}$; 15 - 22 dpi: $1,361.94 \pm 87.03 \mu\text{m}$; two-way ANOVA: time effect $F_{(2,59)} = 6.365$, $P = 0.0031$, followed by *post hoc* Bonferroni's test, $P = 0.0016$) and between the second and the fourth week (8 - 14 dpi: $931.33 \pm 90.16 \mu\text{m}$; 22 - 28 dpi: $1,649.80 \pm 121.03 \mu\text{m}$; $P < 0.0001$). Newborn RV-GFP-labeled GCs had a significantly lower TDL than older AAV-Syn-labeled GCs between 8 and 14 dpi (RV-GFP: $931.33 \pm 90.16 \mu\text{m}$; AAV-Syn: $1,653.72 \pm 54.29 \mu\text{m}$; two-way ANOVA: group effect: $F_{(1,59)} = 22.40$, $P < 0.0001$, followed by *post hoc* Bonferroni's test, $P = 0.0012$) and between 15 and 21 dpi (RV-GFP: $1,361.94 \pm 87.03 \mu\text{m}$; AAV-Syn: $1,840.86 \pm 58.53 \mu\text{m}$, $P = 0.0027$), while there was no significant difference in TDL between the two cohorts between 22 and 28 dpi (Figure 17C). These results demonstrate that AAV-Syn-labeled GCs displayed larger dendritic trees even at early time points and were overall structurally more stable than RV-GFP-labeled GCs which

supports the notion that AAV-Syn-labeled GCs were older and more mature than RV-GFP-labeled GCs.

Due to the fact that RV-GFP-labeled newborn GCs underwent a very dynamic course of development during which the TDL gradually increased until it reached a plateau, the dynamics of elongation and withdrawal of dendritic segments was analyzed by the calculation of the average change in TDL from one day to the next over the entire imaging period (Figure 17D, E). Each value represents the percentage of the TDL of each previous day which was defined as 100%. The data show that the change in TDL decreased over time during the imaging period (Figure 17D). There was a high level of change in TDL during the second and the third week. In contrast, there was no change in TDL during the fourth week of development. Grouped by week, the change in TDL was significantly higher during the second week compared with the fourth week (8 - 14 dpi: $113.64 \pm 2.97\%$; 22 - 28 dpi: $100.21 \pm 0.52\%$; two-way ANOVA: time effect: $F_{(2,54)} = 2.963$, $P = 0.0601$, followed by *post hoc* Bonferroni's test, $P < 0.0001$) and during the third week compared with the fourth week (8 - 14 dpi: $109.13 \pm 2.05\%$; 22 - 28 dpi: $100.21 \pm 0.52\%$, $P = 0.0053$; Figure 17D, E). On the other hand, AAV-Syn-labeled older GCs did not exhibit substantial changes in TDL over the full imaging period (Figure 17D, E). Consequently, there were significant differences in the change in TDL between RV-GFP-labeled GCs and older GCs between 8 and 14 dpi (RV-GFP: $113.64 \pm 2.97\%$; AAV-Syn: $101.15 \pm 0.77\%$, two-way ANOVA: group effect: $F_{(1, 54)} = 11.73$, $P = 0.0012$, followed by *post hoc* Bonferroni's test, $P = 0.0106$; group x time interaction: $F_{(2,54)} = 3.428$, $P = 0.0397$) as well as between 15 and 21 dpi (RV-GFP: $109.13 \pm 2.05\%$; AAV-Syn: $99.37 \pm 0.51\%$, $P=0.0029$) but not between 22 and 28 dpi (Figure 17E). These results show that morphological growth and reorganization occurs specifically in newborn GCs in OTCs and is particularly high and dynamic during the first 3 weeks of development. At later time points, i.e. during the fourth week of development, there is only minor structural change which indicates greater stability of the dendritic arbor.

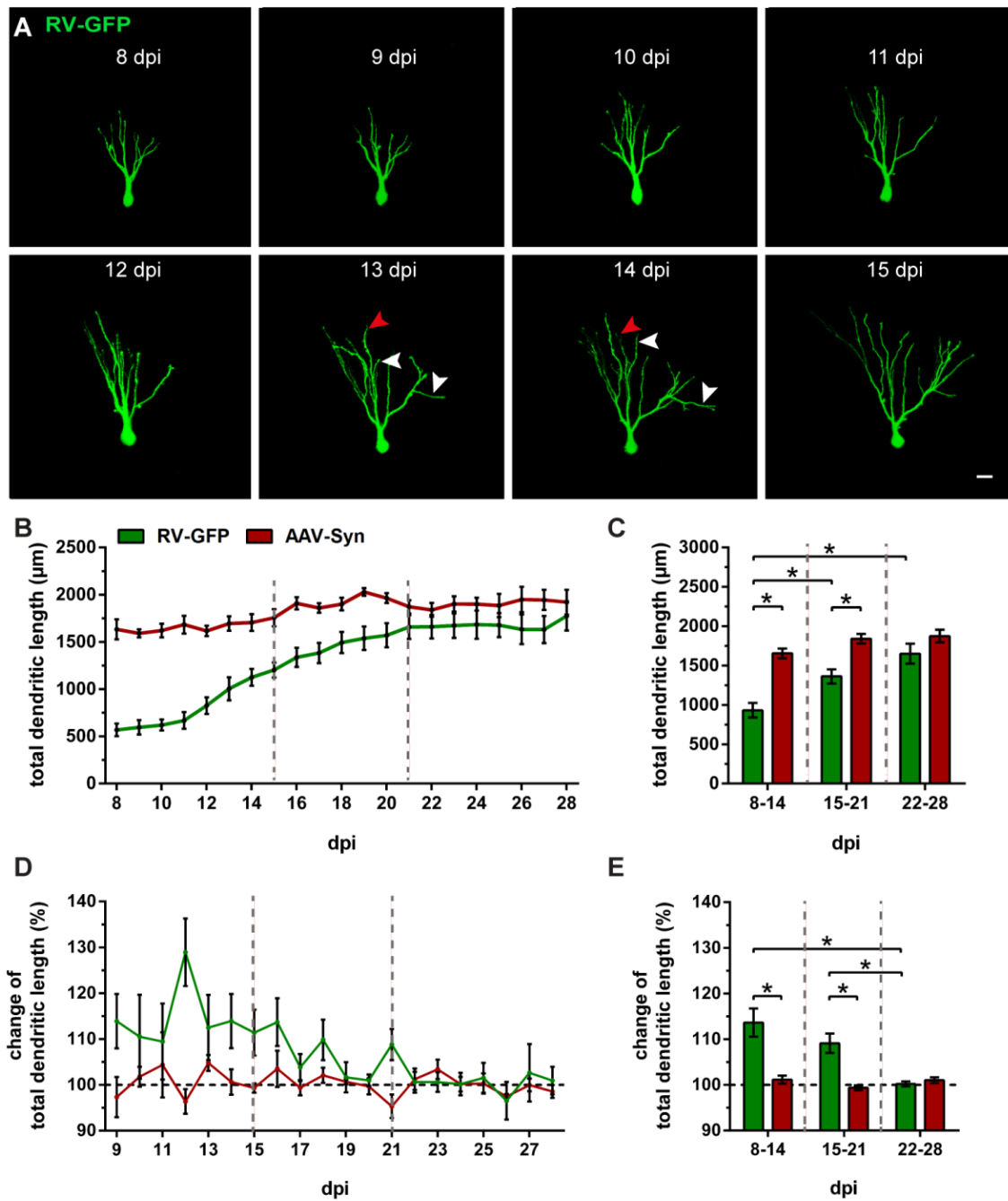


Figure 17. Newborn RV-GFP-labeled GCs exhibit higher dendritic restructuring and dynamics compared with older AAV-Syn-labeled GCs. (A) Time-lapse image sequence of a newborn cell on 8 consecutive days from 8 – 15 dpi. During this time frame, a phase of high dynamics in structural rearrangement was observed. While during the second week of development the cell exhibited considerable dendritic growth (white arrowheads), withdrawal of dendritic segments or complete branches was observed as well (red arrowheads). (B) Daily mean values of the total dendritic length (TDL) for RV-GFP-labeled GCs (green) and AAV-Syn-labeled GCs (red). (C) Mean TDL values grouped by week showed significant differences in RV-GFP-labeled GCs over time, i.e. between the second and the third week (two-way ANOVA with Bonferroni correction, $P = 0.0016$) as well as between the second and the fourth week ($P < 0.0001$). Moreover, the two cell populations displayed significant differences in the

TDL during 8 - 14 dpi (two-way ANOVA with Bonferroni correction $P = 0.0012$) and 15 - 21 dpi ($P = 0.0027$). (D) To analyze dynamic changes in dendritic development, the average change in dendritic length per day was calculated and expressed as the percentage of the TDL of each previous day which was defined as 100%. Newborn GCs exhibited significant differences in TDL change between the first and the fourth week (two-way ANOVA with Bonferroni correction $P < 0.0001$) and between the third and the fourth week ($P = 0.0053$). (E) Newborn GCs displayed a significantly higher degree of change in TDL during 8 - 14 dpi ($P = 0.0106$) and 15 - 21 dpi ($P = 0.0029$) compared with older GCs. (C, E) 8 - 14 dpi: $n_{RV-GFP} = 17$ (C), 12 (E), $n_{AAV-Syn} = 4$; 15 - 21 dpi: $n_{RV-GFP} = 18$, $n_{AAV-Syn} = 10$; 22 - 28 dpi: $n_{RV-GFP} = 11$, $n_{AAV-Syn} = 5$. n represents number of cells (1 - 2 cells per culture). Error bars represent SEM. * $P < 0.05$. Scale bar: 10 μm . Adapted from Radic et al. (2017).

Figure 18A depicts an interesting case in which the dendritic arbor of a newborn GC completely changed its shape during the second week of development. The dendritic tree of the young cell started out with one primary apical dendrite that branched out and extended toward the ML at 8 dpi. By the next day already, the soma had moved along the primary dendrite and translocated to the first branch point (white arrow). As a result, the cell had two primary dendrites at this point that had branched out further and then continued to undergo dynamic remodeling and overall growth, as it extended further into the ML between 9 and 12 dpi. However, starting at 13 dpi it could be observed that one of the primary dendrites started to retract, as it lost a number of complete segments and seemed to become thinner (Figure 18A, red arrowheads). Meanwhile, the other primary dendrite grew in overall size and number of dendritic segments (white arrowheads). The retracting dendrite degenerated completely by 14 dpi while the other continued to expand and rearrange its additional branches in a dynamic manner of extension and withdrawal of segments as described previously. By 15 dpi, the newborn GC had once again one primary dendrite that had branched out extensively and shaped a new elaborate dendritic arbor.

During the third week of development, between 15 and 21 dpi, newborn GCs continued to generally expand their dendritic arbor and rearrange their dendritic structures in a dynamic manner, albeit not as prominently as during the previous week (see Figures 16 and 18B). Overall structural changes were not as distinct anymore from one day to the next. Nevertheless, in hourly

Results

observation of individual segments at 18 dpi, it was evident that there was still dynamic movement of dendritic branches, some of which were extending and others that were withdrawing at the same time. Even neighboring branches of the same dendrite exhibited differential movement simultaneously, with one elongating (white arrowhead) and the other retracting (red arrowhead, Figure 19). This shows that substantial dynamic movement was present within 1 hour in an 11-hour time frame. During the third week of development, newborn GCs had the highest number of terminal segments (Figure 18C, D). However, between the third and the fourth week, newborn GCs exhibited a net loss of dendritic segments due to pronounced pruning. Between 22 and 28 dpi, the dynamic changes in dendritic structure decreased and gave way to a phase of stabilization and only minor refinement. As a result, the established dendritic trees of newborn GCs remained relatively stable and the overall morphology was maintained throughout the fourth week of development. Interestingly, even during the phase of stabilization, the dendrites never became completely static, but continued to display local modifications to individual segments of the dendritic tree (Figures 16 and 18B).

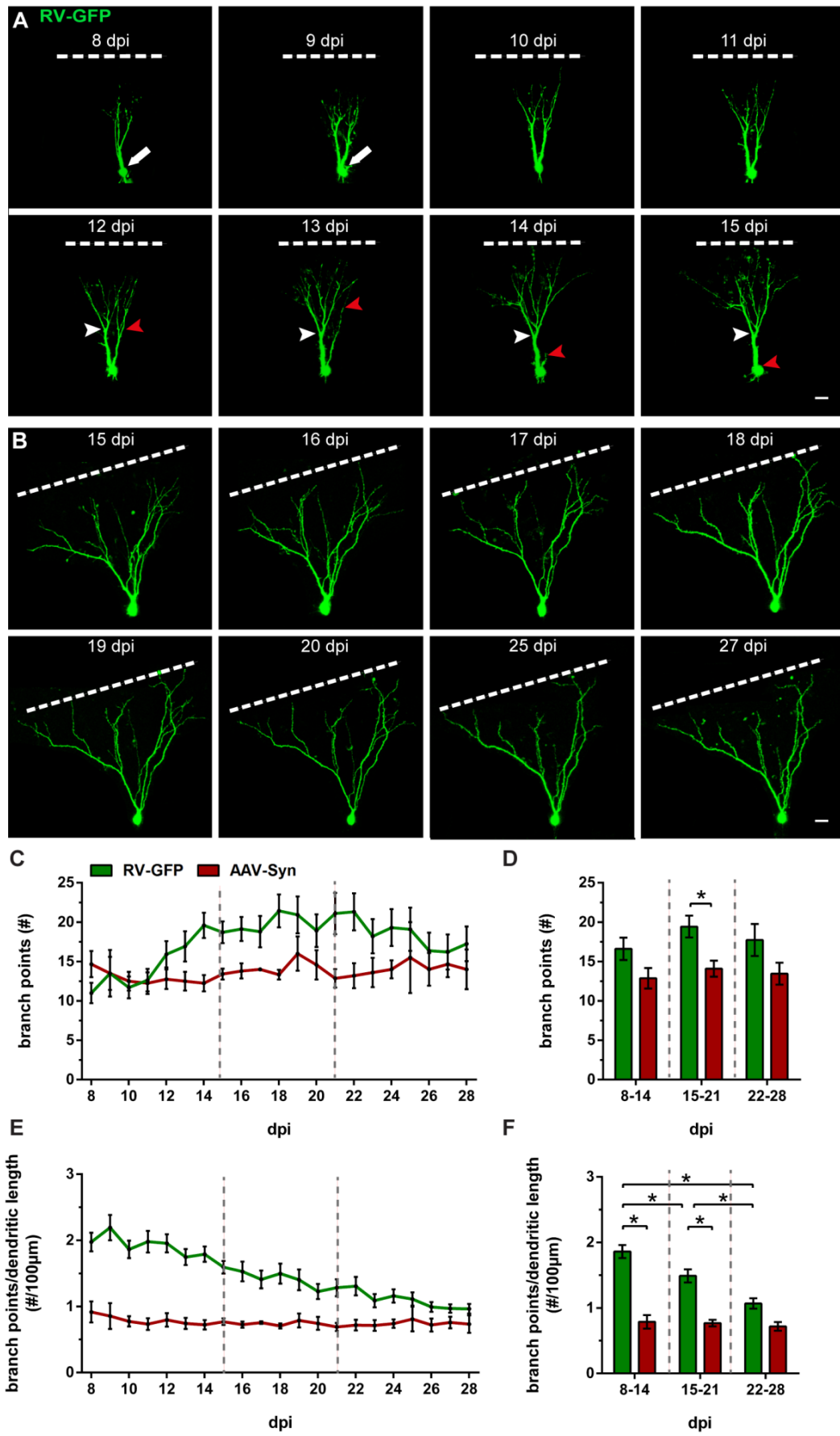
In order to analyze structural changes over time in terms of dendritic tree complexity, the number of branch points was determined for both, newborn and older GCs for each time point. During the second week of development (8 – 14 dpi), newborn GCs exhibited a continuous increase in branch points over time (Figure 18C), while the number of branch points in older GCs remained unchanged throughout the entire observation period (Figure 18C-F). No significant differences in the number of branch points occurred between the two cell cohorts during the second week of development. On the other hand, newborn RV-GFP-labeled GCs possessed a significantly higher number of branch points than AAV-Syn-labeled older GCs during the third week, between 15 and 21 dpi (RV-GFP: 19.43 ± 1.35 ; AAV-Syn: 14.09 ± 0.96 , two-way ANOVA: group effect $F_{(1,59)} = 7.963$, $P = 0.0065$, followed by *post hoc* Bonferroni's test, $P = 0.0470$; Figure 18D).

Finally, RV-GFP-labeled GCs exhibited a decrease in the number of branch points by the fourth week of development, between 22 and 28 dpi. During this

time, there were no significant differences in branch point number between RV-GFP-labeled GCs and older AAV-Syn-labeled GCs (Figure 18D).

In order to normalize the number of branch points to the changing TDL in newborn GCs, the number of branch points per 100 μm dendritic length was calculated across all time points. The data show a continuous reduction in the number of branch points per 100 μm dendritic length until the fourth week of development in newborn GCs only (Figure 18E, F). When data were grouped by week, there were significant differences between the second and the third week (8 - 14 dpi: 1.86 ± 0.10 ; 15 - 21 dpi: 1.49 ± 0.10 ; two-way ANOVA: time effect: $F_{(2,59)} = 5.374$, $P = 0.0072$, followed by *post hoc* Bonferroni's test, $P = 0.0062$), between the second and the fourth week (8 - 14 dpi: 1.86 ± 0.10 ; 22 - 28 dpi: 1.07 ± 0.08 ; $P < 0.0001$), and between the third and the fourth week (15 - 21 dpi: 1.49 ± 0.10 ; 22 - 28 dpi: 1.07 ± 0.08 ; $P = 0.0061$). In contrast, the number of branch points per 100 μm dendritic length in AAV-Syn-labeled GCs remained constant throughout the imaging period (Figure 18E, F). When the two cell populations were compared each week, RV-GFP-labeled newborn GCs exhibited a significantly higher number of branch points per 100 μm dendritic length compared to older GCs during the second week (RV-GFP: 1.86 ± 0.10 ; AAV-Syn: 0.79 ± 0.09 , two-way ANOVA: group effect $F_{(1,59)} = 52.43$, $P < 0.0001$, followed by *post hoc* Bonferroni's test, $P < 0.0001$; group x time interaction: $F_{(2,54)} = 3.759$, $P = 0.0291$) and the third week (RV-GFP: 1.49 ± 0.10 ; AAV-Syn: 0.77 ± 0.05 , $P < 0.0001$) whereas there were no significant differences between the two cohorts during the fourth week (Figure 18F). These results show that during early phases of development, newborn GCs go through a period of extensive branching, especially during the third week of development, which is followed by dendritic pruning, and finally reach a similar structural state as older, mature GCs during the fourth week.

Results



◀**Figure 18. Newborn GCs undergo periods of branching and pruning while older GCs remain structurally stable.** (A) A time-lapse image sequence of a newborn cell exemplifying the branching dynamics of the dendritic arbor during the second week of development. An example of the removal of a complete primary dendritic branch is displayed between 13 and 14 dpi (red arrowheads) while the other primary dendrite branched out and established a new dendritic structure (white arrowheads). Note the dislocation of the cell soma along the original primary dendrite toward the first branch point between 8 – 10 dpi (white arrow). (B) A time-lapse series that illustrates the dendritic growth phase which was pronounced until 20 dpi and was followed by a phase of stabilization (25 – 27 dpi). The growing dendrites reached the hippocampal fissure on 17 dpi (dashed line). (C) Daily mean values of the number of branch points. (D) At 15 - 21 dpi newborn GCs had significantly more branch points than older AAV-Syn GCs (two-way ANOVA with Bonferroni correction, $P = 0.0470$). (E) Daily mean values of the number of branch points per 100 μm of dendritic length. (F) The number of branch points per 100 μm TDL in newborn GCs was significantly reduced during each successive week, i.e. between the second and the third week (two-way ANOVA with Bonferroni correction, $P = 0.0062$), between the second and the fourth week ($P < 0.0001$) and between the third and the fourth week ($P = 0.0061$). Furthermore, newborn GCs had significantly more branch points per 100 μm TDL compared with older AAV-Syn GCs at 8 - 14 dpi (two-way ANOVA with Bonferroni correction, $P < 0.0001$) and at 15 - 21 dpi ($P < 0.0001$). (D, F) 8 – 14 dpi: $n_{\text{RV-GFP}} = 17$, $n_{\text{AAV-Syn}} = 4$; 15 – 21 dpi: $n_{\text{RV-GFP}} = 18$, $n_{\text{AAV-Syn}} = 10$; 22 – 28 dpi: $n_{\text{RV-GFP}} = 11$, $n_{\text{AAV-Syn}} = 5$. n represents number of cells (1 - 2 cells per culture). Error bars represent SEM. * $P < 0.05$. Scale bars: 10 μm . Adapted from Radic et al. (2017).

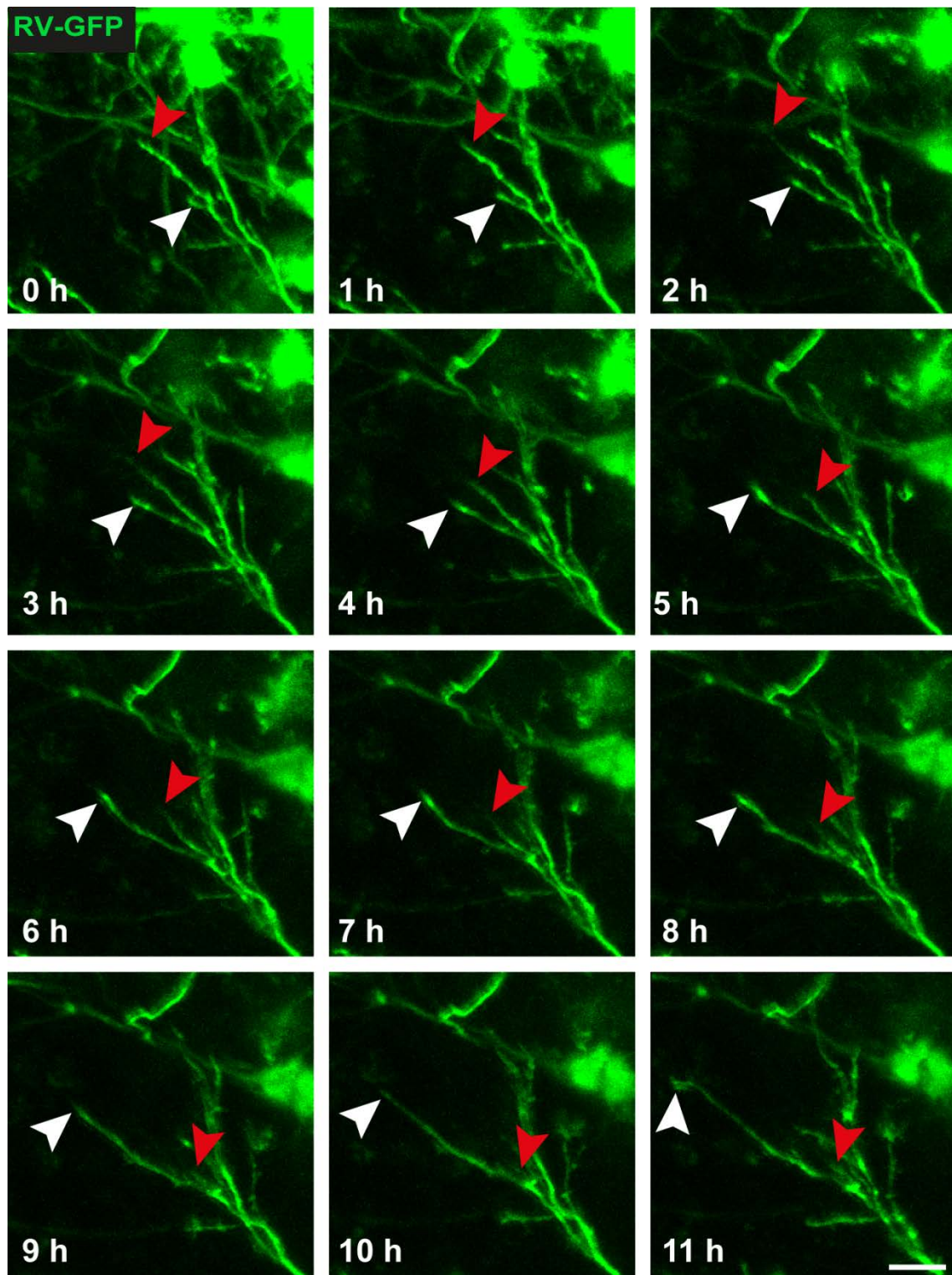


Figure 19. Hourly observation of structural dynamics in postnatally generated GCs during the third week of development. Time-lapse imaging sequence of an RV-GFP-labeled newborn GC at 18 dpi. Image stacks were taken every hour for 11 hours using a two-photon microscope (Z-projection of 40 images; z-axis interval: 2 μm). Hourly observation illustrates the rapid extension (white arrowheads) and simultaneous retraction (red arrowheads) of individual distal segments. Scale bar: 10 μm .

To determine the extent of dendritic pruning before newborn GCs reach a stable structural state, the number of maximum terminal endings which occurred during the third week of development was compared to the number of terminal endings at the last imaging time point, i.e. 28 dpi. The results show a significant reduction between the maximum number of dendritic endings (28.50 ± 2.91 endings per cell) and the number of endings at 28 dpi (18.25 ± 2.20 endings per cell, Wilcoxon paired test, two-tailed; $P = 0.0078$; $n = 8$ cells). This suggests that postnatally born GCs undergo substantial over-branching during the third week and withdraw excess segments by the fourth week of development, presumably through a homeostatic mechanism (Figure 20).

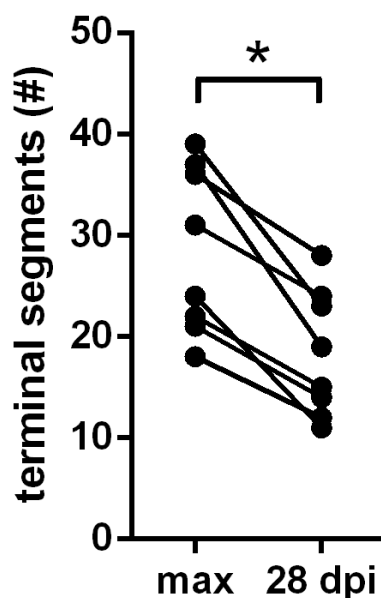


Figure 20. Dendritic pruning in postnatally born GCs between the third and the fourth week of development. Newborn GCs exhibited the maximum number of dendritic endings during the third week of development. A significant reduction in the number of endings occurred by the end of the imaging period at 28 dpi (Wilcoxon paired test, two-tailed; $P = 0.0078$; $n = 8$ cells).

5.6. The formation of spines in postnatally generated GCs

In time-lapse data between 13 and 24 dpi, the timing of spinogenesis in newborn GCs was analyzed (Figure 21A, B). First occurrences of dendritic spine-like protrusions were detectable on occasion on 14 dpi, but more prominently on 15 - 16 dpi. In the following days, between 15 and 19 dpi, the number of spine-like structures increased considerably and by 19 dpi many of them exhibited hallmark characteristics of mature dendritic spines, such as a “neck” protruding from the dendrite and a prominent, mushroom-shaped “head.” From then on, spine numbers were further increasing continuously over time. By 24 dpi, all cells that were analyzed exhibited numerous spines throughout the dendritic arbor. Remarkably, the presence of spine-like protrusions did not indicate greater dendritic structural stability, since branches that contained spiny protrusions could still withdraw or completely disappear.

In order to determine whether the newly formed spine-like protrusions established synaptic contacts with other cells, electron microscopy of 19-day-old cultures was performed which showed that, indeed, numerous RV-GFP-marked spines were involved in synapses with unlabeled axon terminals (Figure 21C). These findings indicate that newborn GCs exhibit features of structural network integration in the slice culture system.

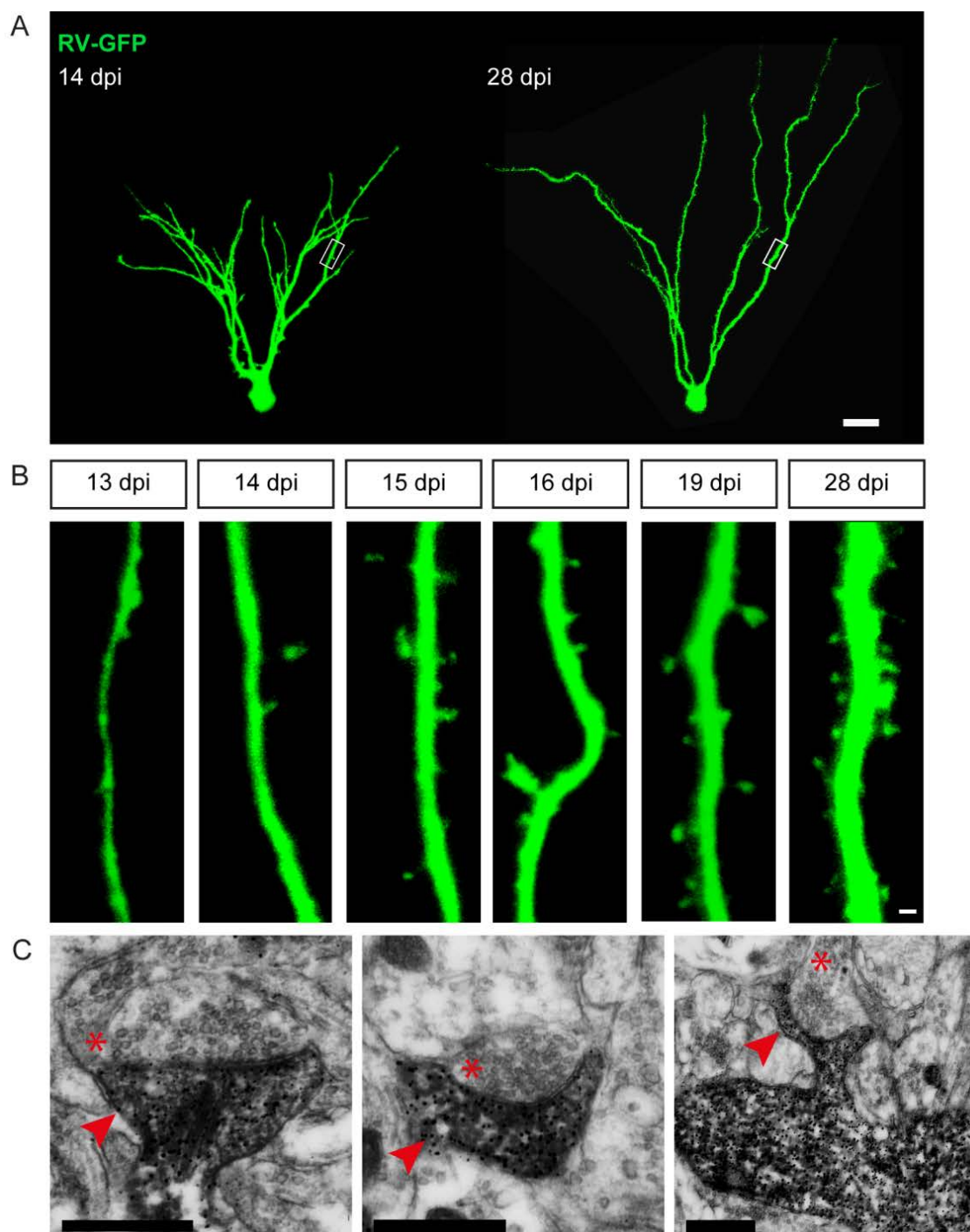


Figure 21. First spine-like structures appear between 14 and 16 dpi. (A, B) Time-lapse image series of the same dendritic segment of an RV-GFP-labeled cell at 13, 14, 15, 16, 19, and 28 dpi. The earliest presence of spine-like protrusions could be observed from 14 dpi on. Spine-like protrusions gradually increased in number and persisted throughout the remaining imaging period. (C) Electron micrographs depicting three RV-GFP-labeled dendritic segments (dark immunolabeling; $n = 3$ cells from 2 animals) at 19 dpi containing mushroom spines (arrowheads) that make synaptic contacts with GFP-negative axon terminals (asterisks) which exhibited numerous pre-synaptic vesicles. Scale bars: (A) 10 μm , (B) 1 μm , (C) 500 nm. Adapted from Radic et al. (2017).

Results

In summary of the time-lapse imaging data, the observation of individual newborn GCs over a period of three weeks, between 8 and 28 days of cell age, enabled the characterization of the dynamic course of morphological development of postnatally generated GCs. During this time, three distinct phases of dendritic maturation became evident: First, a period of rapid dendritic growth and a high degree of dynamic structural plasticity during the second week, a phase of high structural complexity during which dendritic spines begin to emerge during the third week that is followed by dendritic pruning, and a third phase marked by structural stabilization during the fourth week of development (Figure 22).

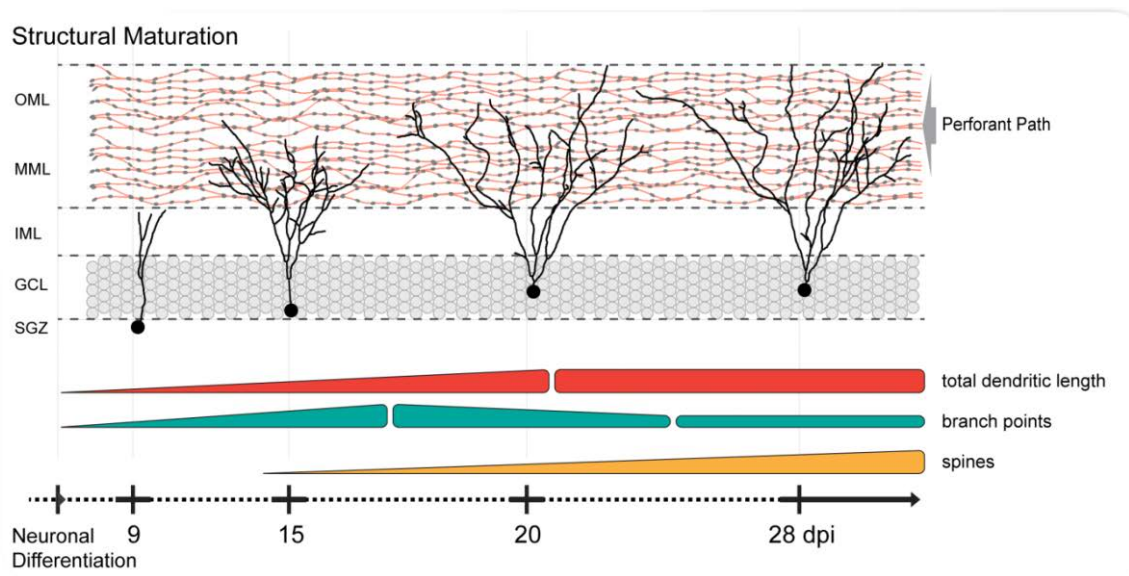


Figure 22. Time line of newborn GC development in OTCs. A schematic summary showing the temporal progression of newborn GC structural development in OTCs. During the second week of development, newborn cells exhibit a phase of dynamic dendritic extension and retraction, branching, and restructuring of the dendritic arbor with a high net increase in both total dendritic length and branch points. During the third week, newborn GCs display elaborate dendritic trees that reach a maximum level of complexity. In this time frame, the restructuring dynamics are less pronounced. First spine-like protrusions begin to emerge and continue to increase in number over time. Between the third and the fourth week, enhanced dendritic pruning is observed as the number of branches decreases. Finally, during the course of the fourth week, newborn GCs reach a phase of structural stabilization with only minor refinement to the dendritic arbor. Adapted from Radic et al. (2017).

6. Discussion

In this work, live cell imaging in organotypic slice cultures (OTCs) was used to study the structural development of newly generated granule cells (GCs) in the postnatal rat hippocampus. The early postnatal state (P7 – P42) in the rodent dentate gyrus (DG) and the distribution of GC- and neuronal maturation markers (i.e. Prox1, DCX, and calbindin) was histologically analyzed in detail in tissue from perfused animals and in OTCs which revealed substantial similarities between the *in vivo* and *in vitro* situations. Subsequently, newborn neurons were successfully transduced with an RV-GFP vector in OTCs. Using a local injection technique, complete GCs could be visualized and observed via time-lapse imaging up to 28 days following RV injection. Anterograde tracing using Mini Ruby confirmed the presence of afferent entorhinal axons in the molecular layer (ML) in OTCs which is essential for proper GC development (Zafirov et al., 1994; Drakew et al., 1999; Frotscher et al., 2000). Therefore, the postnatal OTC represents a similar situation as during adult neurogenesis in which newborn GCs grow into an existing plexus of entorhinal fibers. In addition, the structural dynamics in older GCs that were labeled with tdTomato under a synapsin 1 promoter via an adeno-associated viral vector (AAV-Syn) were examined and compared with newborn RV-GFP-labeled cells in postnatal OTCs. The results reveal that the structural development of postnatally generated GCs followed a profoundly dynamic course, especially during early time points, as could be observed during the second week of GC development. While during the third week the growth dynamics were reduced, newborn GCs exhibited a highly complex dendritic pattern with a maximum number of branch points, which was followed by dendritic pruning. Finally, a period of stability and only fine modification ensued during the fourth week. Older, AAV-Syn-labeled GCs however, exhibited a relatively stable, unchanging morphology throughout the time of analysis. This indicates that newborn GCs undergo flexible, extensive restructuring processes in order to be able to find pre-synaptic partners and thus integrate into the existing network.

6.1. Early postnatal development in intact mouse and rat brains

6.1.1. The distribution of neuronal maturation markers in the DG of mice and rats

Because early postnatal neurogenesis and the course of maturation of GCs in the early postnatal hippocampus have not been studied in detail thus far, this subject matter was addressed in the present work. The time course of early postnatal development and maturation of the DG was investigated based on the distribution patterns of the immature neuronal marker DCX and a marker for mature neurons, calbindin, at different time points from the early postnatal period until animals reached adulthood, i.e. at P7, P14, P21, P28, P35, and P42. As mice and rats represent the most widely used experimental mammals, postnatal neurogenesis was studied in both species and species-dependent differences were investigated.

At the earliest investigated time point, P7, the vast majority of neurons in both, rats and mice, was still young and immature, with almost 80% of all GCs expressing DCX. Only a very small number of cells in the outer layer of the GCL expressed the mature neuronal marker calbindin. However, between P7 and P14, a drastic change toward the mature phenotype took place in both species, as the proportion of mature GCs increased by 38% in the mouse and the percentage of immature GCs dropped by 29% (see Figure 5 for quantitative analysis). In the following weeks, this pattern continued with an ongoing increase in the proportion of mature cells and a decrease in the fraction of immature cells. However, from P14 on, these changes from week to week were much smaller. Similarly, in the rat, the proportion of mature cells increased by 44% between P7 and P14, while the number of immature cells decreased by 48% (see Figure 7 for quantitative analysis). During the following weeks, these changes constituted only 2 - 13% (see Figure 7 for quantitative analysis). Hence, the most substantial shift toward maturity of the DG, in both mice and rats, occurred in the time frame between P7 and P14. Interestingly, this is also

the time frame during which the “adult” neurogenic niche in the formative subgranular zone (SGZ) takes place as described in a recent study in which the expression patterns of key proliferation (e.g. Ki67) and developmental markers most commonly used in the study of adult neurogenesis were mapped during embryonic, early postnatal, and adult time points in the mouse (Nicola et al., 2015). These authors used a Nestin-GFP reporter mouse and additionally applied other markers including Prox1 and DCX to follow the development of the DG from E16.5 to P30. Confirming previous reports on the development of the DG in the rat (Altman and Bayer, 1990) but employing modern markers, the mouse study showed that the differentiation of the SGZ as a separate entity begins around P7 and is completed by P14, as Ki67- and Nestin-positive cells are found only within the SGZ at this point (Nicola et al., 2015). These findings support the notion that GFAP+ progenitor cells with a neuronal phenotype were mainly found in the GCL, SGZ, and hilus at P5 and were completely confined to the SGZ by P14 (Seki et al., 2014). In addition, it was reported that the distribution of DCX before P7 is diffuse in the DG, at P7 it is widely expressed in the GCL, and at P14 DCX-positive cells were detected in the GCL but not in the hilus and exhibited long processes that reached into the ML (Nicola et al., 2015) which is consistent with the results presented here. These findings in addition to the data presented in the current work suggest that from the second postnatal week on, postnatal neurogenesis is a continuous process so that the pool of newly generated cells in the early postnatal local subgranular neurogenic niche is essentially the same as in the adult hippocampus. Therefore, it is plausible that hippocampal GCs born during the early postnatal period are well-representative of adult-born GCs in their course of development. Even though the largest shift toward cell maturation occurred between P7 and P14 in both species, it took an additional week in the mouse for the majority of GCs to reach maturity and DCX-expression to drop under 50% and only by the fourth week of postnatal development were the expression patterns of maturity markers undistinguishable between the two species. These results denote important differences between mice and rats that must be considered when comparing

findings of developmental studies that were performed in different rodent species.

6.1.2. The maturation time course of the postnatal DG is faster in rats than in mice

In the mouse, the data show a very extensive distribution of DCX at P7, indicating that the vast majority (79%) of GCs was young and immature while only 4% of all GCs exhibited calbindin and were therefore mature (see Figure 8 for quantitative analysis). At this point, a number of cells exhibited both markers, which may indicate a transition phase toward maturity (Snyder et al., 2009; Jungnitz et al., 2014). Similarly, the majority of GCs in the rat were also immature (78%), but the number of matured, calbindin-positive cells constituted 11% and there were only few double-labeled cells (4%; see Figure 8 for quantitative analysis). These results suggest that during the early postnatal period, the rat DG contains a higher proportion of matured GCs compared to the mouse. Moreover, GC maturation appears to be faster as well, considering that the time of GC origin also varies between species: in the mouse first GCs are generated around embryonic day 10 (E10) and in the rat, GC production begins at E16 (Angevine, 1965; Altman and Bayer, 1990). In support of this notion, the proportion of DCX-expressing cells in the following week decreased to 30% at P14, while in the mouse, almost half of all GCs were still immature at this time point. At the same time, 55% of all GCs were mature in the rat, and 42% in the mouse (see Figure 8 for quantitative analysis). This indicates that young GCs transitioned to a mature state more quickly in rats than in mice. This pattern of relative marker distribution changes persisted until P21 whereby rats were 4 - 5 days ahead of mice in relation to GC course of maturation (see Figure 8). Interestingly, comparable differences between mouse and rat have also been found in adult animals. A detailed analysis of GC number, speed of maturation, survival, and involvement in hippocampal function during adult neurogenesis revealed striking species-dependent differences (Snyder et al., 2009). Snyder and colleagues (2009) showed that adult-born GCs in the rat were more abundant, more likely to survive and become activated during

learning tasks, and matured quicker than mouse adult-born GCs. Newborn GCs were labeled with BrdU in adult mice and rats and the proportion of BrdU-positive cells expressing various maturation markers, including DCX and calbindin, was determined at different time points. One week following BrdU injection, almost all GCs expressed DCX in both species. However, significantly more newborn neurons continued to express DCX over the following 3 weeks in the mouse than in the rat. Overall, the proportion of DCX-positive cells in the rat was decreasing more rapidly by 1 - 2 weeks (Snyder et al., 2009). The findings of the current work in postnatal and juvenile mice and rats reflect these results, as in both cases GC maturation was quicker in rats compared with mice, suggesting that similar species differences in developmental mechanisms are at play in the early postnatal as in the adult DG.

Overall, the postnatal development of the DG in both the mouse and the rat, appears to follow a clear maturation course that reflects the establishment of an outside-in pattern of the GCL with older, mature GCs positioned in the GCL part close to the ML, while young and newborn cells continue to be added to the inner parts of the GCL, closer to the hilus (Altman and Bayer, 1990; Mathews et al., 2010; Radic et al., 2015). As the DG develops, the production and presence of newborn, immature GCs gradually becomes confined to the innermost part of the GCL. The postnatal hilar zone of intrahippocampal neurogenesis, the so-called “tertiary dentate matrix,” constitutes the SGZ where neurogenesis continues as an ongoing process from the postnatal to the adult state (Altman and Bayer, 1990; Nicola et al., 2015). Knowing the situation in the postnatal period *in vivo* allows for the assessment of the histo- and cytological state of the cultured early postnatal hippocampus in the OTC.

6.2. Postnatal neurogenesis in OTCs

6.2.1. Histology of postnatal rat OTCs, a model for adult neurogenesis

An important objective of the current study was to determine whether postnatal neurogenesis in the OTC presents a useful model for the study of

adult neurogenesis. Two aspects need to be considered: (1) the difference in animal age when OTCs are prepared postnatally (P4 - 5) as opposed to conventional studies of adult neurogenesis (in at least 6-weeks-old animals) and (2) how the cultured tissue compares to the postnatal *in vivo* situation.

It has been shown that adult-born hippocampal GCs *in vivo* follow a similar maturation course as those that were generated during ontogenesis (Espósito et al. 2005; Zhao et al. 2006; Zhao et al. 2008). Espósito et al. (2005) have demonstrated that GCs born in adult mice undergo a strikingly similar developmental sequence in terms of morphological maturation as well as the establishment of afferent synaptic connections as embryonically generated GCs, even though they mature in a very different environment. This led to the supposition that the course of GC maturation is predominantly regulated by cell-autonomous processes and is not dependent on environmental conditions (Espósito et al., 2005). Therefore, GCs generated during the early postnatal period would very likely be subjected to the same mechanisms involved in structural development as adult-born GCs. Nevertheless, during the postnatal time points examined here, the neurogenic niche is already characterized by an environment that is akin to the adult SGZ.

Prior studies of postnatal neurogenesis in OTCs involved treatment with BrdU or RV after 2 - 2.5 weeks *in vitro*, and analysis up to 4 weeks following treatment (Kamada et al., 2004; Raineteau et al., 2004; Chechneva et al., 2005; Sadgrove et al., 2006). This was usually done to ensure stabilization of OTCs after preparation and to achieve a more mature state of development that would be better comparable to the adult situation (Kamada et al., 2004; Raineteau et al., 2004). However, studies in older cultures were partially limited by the severe loss of RV-labeled neurons, making live-imaging observations over a long time period very difficult (Kamada et al., 2004; Kleine Borgmann et al., 2013). In the present study, OTCs were injected with the RV construct at an early time point, i.e. DIV 0 (P4 - 5) in order to take advantage of the peak proliferative period which presumably takes place in rats between P5 and P8 (Bayer and Altman, 1974; Schlessinger et al., 1975). In that time frame, the so-called “tertiary dentate matrix” is a prominent source of newborn NSCs and consists of a

population of cells that proliferate and settle locally in the formative SGZ, the main site where hippocampal neurogenesis continues to take place throughout adulthood (Altman and Bayer, 1990). Recently, an immunohistological study showed evidence that the stem cell niche, a characteristic of the adult SGZ, is established between P7 and P14 in mice (Nicola et al., 2015). Therefore, from P7 on, postnatal neurogenesis appears to be a continuous process lasting throughout life, albeit with an age-related reduction in proliferation. Hence, since the neurogenic niche of the SGZ as it pertains to “adult” neurogenesis is being established during this period (Nicola et al., 2015), and the cells in this population essentially undergo a similar developmental process as adult-born GCs (Espósito et al., 2005; Laplagne et al., 2006; Zhao et al., 2006), it can be inferred that investigation of GCs generated during this phase could serve as a good model for studying mitosis, differentiation, structural maturation, and functional integration of newborn neurons into an existing neuronal network.

Histological analysis in postnatal OTCs showed that the DG, as well as the CA3 and CA1 regions of the hippocampus were clearly identifiable and exhibited an organotypic appearance (Figure 9). To further examine the cellular composition of these cultures, the immature neuronal marker DCX, the mature neuronal marker calbindin, and the GC marker Prox1 were applied. Prox1, a specific GC marker, is expressed early in still proliferating precursor type 2b cells, and persists throughout development and in mature GCs (Lavado and Oliver, 2007; Lavado et al., 2010; Karalay et al., 2011; Stergiopoulos et al., 2014). In postnatal OTCs, Prox1 expression was prominent in the entire GCL at all investigated time points, i.e. DIV 7, 14, and 28. Therefore, Prox1 appears to be a valid marker of GCs in postnatal OTCs. In addition, co-labeling of Prox1 and DCX represents a valuable means for identification of immature GCs in postnatal OTCs.

The well-established marker for immature neurons, DCX (Rao and Shetty, 2004), was expressed in immature GCs of the SGZ and the inner parts of the GCL, as well as neurons located in the hilus at DIV 7. On the other hand, calbindin, which labels mature neurons, was observed mainly in the outer parts of the GCL, in fewer cells (Figure 10). At DIV 14, DCX-labeled GCs were still

abundant, but the larger proportion of GCs expressed calbindin, indicating a shift to maturation of existent GCs and possibly a reduction in neurogenesis (Figure 11). At DIV 28 however, DCX-expression was limited to the SGZ and appeared in very few cells. Conversely, calbindin was present in most GCs throughout the GCL at this point (Figure 12). The expression pattern of calbindin being expressed by GCs in the outer part and DCX in the inner layers of the GCL agrees with GC outside-in pattern *in vivo*, as new GCs are continuously added to inner parts of the GCL (Altman and Bayer, 1990; Mathews et al., 2010; Radic et al., 2015). Moreover, these results are consistent with the *in vivo* findings at early time points described in section 5.2. in which the early postnatal development and expression of the same maturation markers in young mice and rats was characterized (see Figures 4 and 6) and are in line with a recent mouse study that showed DCX being widespread at P7, and becoming more confined to the inner part of the GCL over time (Nicola et al. 2015). This is presumably due to the fact that DCX is a protein that plays an important role during cell development and migration and is therefore ostensibly present in numerous cells at early postnatal time points when the rate of neurogenesis is high (Gleeson et al., 1999; Brown et al., 2003; Couillard-Despres et al., 2005). Because neurogenesis decreases over time and thus a lower number of immature cells are found at any given point in the adult hippocampus, DCX expression diminishes as well. The distribution of DCX in postnatal OTCs corresponded to the postnatal expression of DCX *in vivo* at early time points, i.e. DIV 7 and DIV 14, but was low at DIV 28. It has been reported previously that the neurogenesis rate decreases drastically during the first week of OTC cultivation (Namba et al., 2007; Gerlach et al., 2016). The reduction in the number of DCX-positive GCs over time reflects these findings. However, in the present work DCX expression was still prominent at DIV 14 and a few DCX-labeled GCs were present even at DIV 28. Since DCX expression can continue for up to four weeks post mitosis (Brown et al., 2003; Rao and Shetty, 2004; Jungnitz et al., 2014; Radic et al., 2015) these DCX-positive cells may have well been generated during early culturing time points. Although the production of new GCs may decrease substantially after the first week *in*

vitro, the survival of newborn neurons (during early time points) should not be affected (Gerlach et al., 2016). Therefore, DCX expression can persist at later time points. Alternatively, it is possible that neurogenesis continued past the first week in culture, albeit at a low rate. Namba et al. (2007) have shown that the neurogenesis rate in rat OTCs is greatly reduced when BrdU is applied at DIV 7 - 8 as opposed to DIV 0, however, they also showed that ~10% of BrdU-positive cells were neurons that persisted in culture until DIV 21. Some of these cells would presumably have been DCX-positive at DIV 21. Similarly, Gerlach et al. (2016) found that BrdU labeling at DIV 7 still yielded some surviving neurons at DIV 21, though in very low numbers. In addition, a number of studies have demonstrated that new neurons could be generated in OTCs at 2 - 2.5 weeks *in vitro* (Kamada et al., 2004; Raineteau et al., 2004; Sadgrove et al., 2006). Hence, some DCX-expressing GCs at late time points could also have been generated after the first week of cultivation. Nevertheless, as the number of DCX-positive cells clearly decreased with each successive time point, the results shown here are in line with the general notion that the rate of neurogenesis in OTCs is greatly reduced over time. Therefore, labeling of newborn neurons in OTCs should ideally occur within the first week of cultivation.

The results presented in this work show that early postnatal hippocampal cultures exhibit an organotypic structure and cellular assembly in which postnatal neurogenesis is preserved and shows considerable similarities to adult neurogenesis in marker expression and thus appears as a valuable and easily accessible tool for studying dynamic processes of neurogenesis. In a prior study using transgenic mice to visualize newborn neurons, it was shown that structural development and functional integration of newly generated GCs in OTCs could be observed over a period of several weeks (Raineteau et al., 2006). Analyses of dendritic and axonal growth as well as electrophysiological properties of newborn GCs were performed at two time points, 10 and 20 days, and revealed that new GCs became more mature morphologically over time and were functionally integrated into the hippocampal network at 20 days (Raineteau et al., 2006). Thus, using the OTC system in combination with RV

labeling of newborn GCs enables detailed investigations on the development of individual live GCs over time.

6.2.2 Retroviral labeling of newborn GCs in postnatal OTCs

Building on previous work (Kamada et al., 2004; Kleine Borgmann et al., 2013), in this study individual newborn GCs were labeled with an RV-GFP vector in OTCs with a local injection technique with which the RV solution was injected directly into the tissue, near the DG. Several cells that were successfully transduced had a neuronal morphology that was typical for maturing GCs. To identify RV-GFP-labeled GCs, the GC marker Prox1 was used (Figure 13).

RV-GFP/Prox1 positive cells displayed a polarized structure with the somata primarily located in the SGZ and the GCL while distinct apical dendrites that extended through the GCL and into the ML but did not contain any spine-like protrusions at 14 dpi (Figure 13B). The morphological traits of RV-GFP/Prox1-positive cells in OTCs are consistent with structural characteristics of developing RV-labeled GCs previously described in fixed *in vivo* samples (van Praag et al., 2002; Espósito et al., 2005; Zhao et al., 2006). Espósito et al. (2005) have characterized the structure of fixed RV-labeled newborn GCs at different time points in adult mice and found that at 14 dpi a large number of GFP-positive cells co-expressed DCX and the neuronal marker NeuN. The somata of these cells were still located in the inner GCL layers, although some had moved somewhat into the GCL. At this stage, GFP-positive cells exhibited a prominent apical dendritic tree that reached the middle molecular layer (MML) of the DG. However, their dendrites did not contain spines and still appeared immature (Espósito et al., 2005; Zhao et al., 2006). Most of these neurons also contained basal dendrites that projected to the hilus (Espósito et al., 2005). Thus, our RV-labeled cells in fixed OTCs exhibited the same characteristics as RV-labeled cells described previously in fixed *in vivo* tissue.

6.2.3. Postnatally born GCs mature within an intact entorhino-hippocampal circuitry in OTCs

Newborn GCs in postnatal OTCs differentiate in an organotypic environment. For proper GC development, the presence of afferent fibers projected from the EC and thus a functioning cellular circuitry is important (Zafirov et al., 1994; Drakew et al., 1999; Frotscher et al., 2000). However, during OTC preparation, some EC fibers are inevitably transected. It has been shown previously that the entorhino-hippocampal circuit in OTCs is re-established within three days of cultivation, as projection fibers from the EC re-innervate the ML of the DG (Li et al., 1994; Kluge et al., 1998). To verify EC projections to the ML in the current study at early time points of observation, anterograde tracing of entorhinal projection fibers was performed using the biotinylated dextran amine Mini Ruby. Our results indicate that perforant path fibers were already present in the OML at the early time point DIV 8 when observation of newborn GC development was started. At this time, the 8-day-old GCs just began to extend apical processes into the ML but had not reached the afferent fibers in the OML yet. At DIV 20, the dendrites of newly generated GCs had grown into the OML and intermingled with entorhinal fibers (Figure 14). This shows that postnatal GCs observed here grow into an existing entorhinal termination zone and mature in the entorhino-hippocampal circuitry preserved in the OTC. This situation is highly similar to the conditions in the adult brain in which newborn GCs develop and integrate into an already established entorhino-dentate network.

6.3. Time-lapse imaging of newborn GCs in OTCs uncovers the dynamics of dendritic development

To extend the scope of fixed cell data, living cells were followed from day to day using live time-lapse imaging. Longitudinal observation of the same postnatally generated GCs from the immature to the mature structural state allowed for analysis of individual dendritic growth and cellular dynamics underlying morphological development and maturation.

6.3.1. Newborn GC development during the second week is marked by highly dynamic structural changes

Successful RV-labeling of newborn GCs in OTCs enabled daily imaging and 3-D computer reconstruction of individual developing cells during different time periods (Figure 15). In an early phase of development, newborn GCs were observed between 8 and 14 dpi. During this time window, the structural development was marked by high dynamics of extension as well as retraction of neurites. Whereas the dendritic tree was growing in length and branching out toward the ML, it was also very clear that already established dendritic segments, and even complete branches, could withdraw either partially or completely (see Figures 16 and 17). The general structural features of RV-labeled GCs in OTCs are consistent with previous findings derived from fixed *in vivo* tissue from the adult mouse illustrating 7-day-old newborn GCs which were located in the SGZ or the hilus, displayed plump oval or irregularly shaped somata, and short spineless neurites (Espósito et al., 2005). At 10 dpi, fixed cells in adult mouse *in vivo* tissue exhibited immature morphological features, relatively short apical dendrites that extended into the inner molecular layer (IML), while at 14 dpi, the more elaborate dendritic tree reached into the MML (Zhao et al. 2006). The data presented in the current work are generally comparable with these *in vivo* findings from fixed adult material, and observed differences are possibly species-dependent and/or due to the fact that individual cells may develop at a different pace (Plümpe et al., 2006; Jungenitz et al., 2014; Radic et al., 2015). Therefore, it is of advantage to use a system that allows for observation of individual cells within a particular time frame and detect structural changes within one and the same cells over time. In a prior study, time-lapse imaging was performed during early cell development in slice cultures prepared from adult mice (Kleine Borgmann et al., 2013). Newborn cells were labeled with RV-RFP and live imaging was performed every 24 hours from DIV 2 up to DIV 9. The findings showed that neurites grew in different orientations and that this growth was very variable between cells. However, a prominent apical dendrite was observed at DIV 4 that continuously extended throughout the imaging period (Kleine Borgmann et al., 2013). Since the

imaging time frame encompassed only the early developing period, i.e. until DIV 9, a direct comparison between these findings and the results shown in the present study is difficult. It is possible that a longer cultivation period would reveal similar high dynamics in dendritic development in adult slice cultures as in early postnatal OTCs. Further longitudinal studies would be needed to compare the development of individual cells in these two slice culture methods.

In addition to dendritic development, movement of the soma along the primary process toward the first branching point was frequently observed during this period of highly dynamic structural changes (see Figure 18A). Somatic translocation along an apical dendrite is a well-known mechanism of neuronal migration. This process comprises distinct steps including the extension of a leading process, nuclear and somatic translocation along the leading dendrite, and the retraction of the trailing process (Edmondson and Hatten, 1987; Komuro and Rakic, 1995; Ridley et al., 2003). Since young GCs need to migrate from the hilus and the SGZ into the GCL, as was previously described in adult-born neurons in the mouse between 7 and 14 dpi (Espósito et al., 2005), somatic movement is a necessary and expected phenomenon during the initial stages of GC development.

Overall, the second week of GC development was distinguished by rapid growth as well as a high amount of dendritic motility and structural change. At this stage young GCs certainly need to find their place in a dense layer of existing and integrated older GCs and extend dendrites into ML areas where potential synaptic connections with afferent axons could be established.

6.3.2. The third week of GC development is characterized by high dendritic complexity and the emergence of dendritic spines

Time-lapse imaging between 15 and 21 dpi showed lower dynamics in neurite extension and withdrawal but elaborate dendritic arbors and further characteristics of advanced maturation (see Figures 16-20). During this time period, the distal processes of most RV-GFP-labeled GCs extended through the OML and reached the hippocampal fissure (by approximately 17 dpi; Figure

18B). This was a phase when newborn GCs exhibited a very complex dendritic arbor with the highest number of branch points compared with all other time points (see Figure 18C, D). Interestingly, this is in line with earlier findings of an *in vivo* time-lapse study of adult-born GCs in the mouse, revealing that newborn GCs contain the maximum number of endings during the third week of development, i.e. around 17 dpi (Gonçalves et al., 2016a).

Around the same time, usually at 16 dpi, dendrites started to exhibit spine-like structures (Figure 21). These data reflect previous findings that described newborn GCs in adult mice to contain spines at 16 dpi (Zhao et al., 2006; Ohkawa et al., 2012). However, in a comparison of spine growth between GCs born in the early postnatal period and in the adult, it was found that neurons born at P10 contained spines as early as 12 dpi, while cells that were born in the adult animal (7 - 10 weeks) started to exhibit spines at 16 dpi which suggests that adult-born GCs develop at a slower pace than neonatally born neurons (Zhao et al., 2006). In the present study, there were a few instances in which spines were observed as early as 14 dpi. This could be due to the fact that the neurons were generated in young animals or, more likely, simply reflect the typical variability in maturation speed between individual GCs (Plümpe et al., 2006; Jungenitz et al., 2014; Radic et al., 2015). Spines usually appeared gradually and throughout the proximal and distal parts of the dendritic arbor. It has been reported that spines stabilize the dendritic structure (Koleske, 2013). However, the emergence of spines at this point did not prevent the withdrawal of dendritic branches which indicates that the mere presence of spines does not immediately lead to dendritic stability. At early stages of development, dendritic branches of new GCs presumably extend out on the search of synaptic partners and new spines are formed at or near existent synapses of mature GCs which indicates that newborn GCs have to compete with mature GCs for synaptic input (Toni et al., 2007). Toni et al. (2007) described mature synaptic input on RV-labeled adult-born mouse GCs at 30 dpi *in vivo* on the ultrastructural level characterized by the presence of a postsynaptic density (PSD), at least four presynaptic vesicles within 100 nm of the presynaptic membrane, and a defined synaptic cleft (Toni et al., 2007). In the current study, ultrastructural imaging

was performed on 19 dpi which revealed that RV-GFP-labeled spines made synaptic contacts with axon terminals from unlabeled cells (Figure 21C). This is a further indicator that surviving postnatally generated GCs in OTCs undergo proper development and integration into the existing network. As network activity and synaptic input to newborn neurons is essential for their survival, maturation, and integration (Kempermann et al., 1997; van Praag et al., 1999b; Piatti et al., 2011; Bergami et al., 2015; Alvarez et al., 2016; Vivar et al., 2016), the establishment of synapses is crucial during their development. New spines are gradually formed over time, particularly from the third week on, as shown here and in other work conducted in our laboratory (Jungenitz et al., unpublished). It is therefore not surprising that during this time period young GCs contain a complex and extensive dendritic arbor with a high number of branches which enables the formation of new spines at pre-existing axonal boutons. During this time, when spines are immature and not stable, dendritic structures are still dynamic and can retract from areas in which no relevant synapses could be established. In this case, immature spines that do not receive substantial input can be degraded and therefore dendritic segments can become destabilized and withdraw. Over time, as young GCs begin to make relevant synaptic connections, receive substantial input, and undergo LTP at later stages of maturation (Schmidt-Hieber et al., 2004; Marín-Burgin et al., 2012; Vivar et al., 2012; Deshpande et al., 2013; Vivar and van Praag, 2013), enhanced spine and synapse stabilization may lead to dendritic stability. It would be very interesting to investigate a possible correlation between spine establishment, synapse formation, and dendritic stability in further more detailed studies using time-lapse imaging.

6.3.3. Following dendritic pruning, postnatally born GCs reach a state of structural stability by the end of the fourth week of development

Between the third and the fourth week, newborn GCs displayed enhanced net dendritic pruning (Figure 20). It has been described before that developing GCs extend their dendrites into the ML, presumably searching for pre-synaptic partners, but when afferent fibers from the EC are not available, distal dendrites

retract, even after they had already formed spines (Zafirov et al., 1994). When synaptic connections are lost or weakened, for example through long term depression (LTD), spine shrinkage or loss leads to destabilization of dendrites and thus can lead to withdrawal of entire segments (Zhou et al., 2004; Vuksic et al., 2011; Willems et al., 2016). Even though in the current work the EC fibers are present, presumably not all segments of newborn GCs establish functional connections with axonal terminations in the OML. The search for pre-synaptic partners in a “trial and error” fashion is very likely part of the maturation course of newborn GCs. The retraction of dendrites and overall pruning might be a way for the newborn neuron to optimize its connections. Segments and spines that successfully establish relevant synaptic contacts persist while those that do not, withdraw. This is in line with recent findings in adult-born GCs in the mouse (Gonçalves et al., 2016a). In that study, time-lapse imaging of newborn GCs was performed from 15 up to 60 days post RV injection in adult mice *in vivo*. The results show rapid growth of dendrites during the third and the fourth week of development. Interestingly, during the fourth week, Gonçalves et al. (2016) observed pruning of dendritic branches before the arbor reached a steady structural state by the beginning of the fifth week. In comparison, newborn rat GCs observed in the current work displayed a very dynamic growth phase during the second week, underwent a period of maximum structural complexity in the third week followed by dendritic pruning, and exhibited a stable state during the fourth week (Figures 17 and 18). The fact that according to our findings, newborn neurons developed one week in advance is likely due to species differences since newborn GCs undergo the process of maturation one week faster in the rat than in the mouse (Snyder et al., 2009). Therefore, the findings are consistent with our results, further supporting the notion that newborn GCs in the OTC system undergo similar dynamic developmental processes as *in vivo*.

In terms of dendritic tree complexity, Gonçalves et al. (2016a) found that newborn GCs displayed an average maximum number of endings of 15 at 21 dpi, while in our study newborn GCs contained a maximum of approximately 28 branches on average around 17 dpi. In both cases the numbers decreased by

the end of the observation period at 31 and 28 dpi respectively due to branch pruning. Gonçalves et al. (2016a) observed a high variability of branch growth and number among individual GCs under different conditions. The magnitude of branching seems to depend on cell-extrinsic factors such as activity and extracellular signaling, while the subsequent pruning of branches appears to be a cell-intrinsic homeostatic response to excessive branching, ultimately leading to a comparable dendritic tree structure for all GCs (Gonçalves et al., 2016a). Therefore, while the data presented in this work exhibit differences in absolute branch numbers compared to mouse data *in vivo*, a similar process of dynamic growth, over-branching, and subsequent pruning to achieve a stabilized and generally similar structure of GCs was observed during the fourth week of development (Figures 18 and 20). Differences in absolute numbers of dendritic branches could be due to different factors. It is possible that in *in vitro* conditions with generally limited neuronal activity and synaptic input to newborn GCs, dendritic trees tend to branch out more extensively in order to find and establish relevant contacts. In addition, the difference in ages of the animals could be an important aspect as well. While the *in vivo* study examined newborn GCs in adult mice, 4 - 5-day old rats were used to prepare OTCs. Although maturation processes of adult-born GCs reiterate those during early postnatal development, some differences in morphology and the speed of maturation may remain (Espósito et al., 2005; Zhao et al., 2006).

From 22 until 28 dpi, the time-lapse sequences in the present work showed a phase of structural stabilization and only minor refinement. The dynamic movement of neurites was greatly reduced and there was only little change in the overall dendritic shape. These 3 - 4-week old RV-GFP-labeled cells exhibited a characteristic morphology of mature GCs that is usually observed from 21 days on, including features such as round somata, elaborate spiny dendritic trees that extend to the hippocampal fissure, as well as axons that project through the hilus (van Praag et al., 2002; Espósito et al., 2005; Zhao et al., 2006; Beining et al., 2016). Spine-like structures remained conspicuous until the end of the imaging period. It is plausible that, as spine density increases substantially from the fourth week on (Jungenitz et al., unpublished), and young

GCs form relevant synaptic connections, the dendritic branches and thus the overall structure becomes stabilized. After the critical phase of enhanced excitation/inhibition balance in newborn GCs at 4 - 6 weeks during which they are highly excitable, they change their activity pattern and become responsive to highly specific input (Marín-Burgin et al., 2012; Temprana et al., 2015). This persisting specific input implies that lasting, stable synaptic connections have been formed which would plausibly lead to a stable structural state under physiological conditions. GC integration and stability, therefore, are dependent on network activity. Recent work from our laboratory has shown that following LTP induced by high frequency stimulation, adult-born GCs exhibit a decrease of short terminal segments (STS) at 28 and 35 dpi due to pruning while prenatally generated GCs did not change. This implies that newborn GCs undergo a phase of activity-dependent structural reorganization during a specific time frame (Beining et al., 2016). Drastic alterations in neuronal activity due to pathological states such as epilepsy, stroke, or neurodegenerative processes related to Alzheimer's or Parkinson's disease that cause dysfunction or loss of synaptic input in the hippocampal circuit may lead to dendritic destabilization, reorganization, and even apoptosis if homeostatic mechanisms fail to compensate for the dysfunction (Christian et al., 2014; Winner and Winkler, 2015). In future studies, it would be intriguing to investigate the dynamic structural and functional processes of individual postnatally generated GCs under pathological conditions, e.g. by using loss-of-function disease models of Alzheimer's disease, performing EC lesions, or by blocking network activity with pharmacological agents such as the sodium ion channel blocker tetrodotoxin (TTX). Conversely, growth factors, neurotransmitters, stimulating antibodies, or optogenetic approaches could be applied to stimulate newborn GCs at different stages of development in order to examine the effects of increased activity on dendritic growth dynamics, structural reorganization, and spine formation.

6.3.4. AAV-Syn-labeled older GCs do not exhibit the strong dynamic structural changes of newborn RV-GFP-labeled GCs

The comparison between our results and *in vivo* data is limited by the fact that all GCs in this study were cultured *in vitro*. Although the organotypic environment in the hippocampus and the entorhino-hippocampal circuitry is mainly preserved in OTCs, differences in cell development and the speed of maturation compared with the *in vivo* situation cannot be ruled out. However, the histological integrity and cellular composition in OTCs displayed a healthy appearance and were comparable to *in vivo* conditions. Additionally, the RV-GFP-labeled GCs in OTCs displayed features of structural development comparable to adult-born GCs of the same age *in vivo*. The local injection technique presumably enabled labeling of cells that were located in the depth of the tissue where the preserved neurogenic niche enabled the cells to develop organotypically. Nevertheless, one further possibility to control for environmental and culturing effects is to compare RV-GFP-labeled newborn GCs with older, more mature GCs labeled in the same conditions. Older, mature GCs were transduced with an AAV vector containing the tdTomato gene under the synapsin 1 promoter. This led to labeling of older GCs that could be observed with live imaging in the same manner as newborn GCs. These cells stayed stable concerning their morphological features and did not exhibit the high dynamic movements of neurites even during early culturing periods. This suggests that the high dynamics phase is specific to young developing GCs which appears to be a necessary precondition for a healthy progress in maturation and the establishment of synaptic contacts and is not an artifact of *in vitro* cultivation. As discussed above, newly generated GCs presumably extend their processes in the search for pre-synaptic partners and retract when no connections could be established. This suggests that the dynamic course of development is a process intended to guide dendrites to their correct synaptic partners. The dynamic structural reorganization might therefore reflect an intricate pathfinding mechanism rather than a simple growth process. In the phase of structural stabilization during the fourth week, newborn GCs reached a similar structural state as AAV-Syn-labeled older GCs since there were no

significant changes in either the average total dendritic length or total number of branch points between the two cell populations during this time. In the future, time-lapse imaging of these two different cell cohorts could be used to examine any competitive processes during spine and synapse formation of newborn GCs and how the integration of new GCs into the network affects older GCs.

6.4. Conclusion and Outlook

The current study is one of the first to show that postnatal neurogenesis can efficiently be studied in the OTC system. Individual RV-labeled postnatal GCs were followed via time-lapse imaging starting at 8 dpi, which represents an immature post-mitotic time point of neurogenesis up until 28 dpi, when newborn GCs exhibited elaborate, mature dendritic trees extending through the entire ML and dendritic spine-like processes which formed mature synapses at the ultrastructural level. Three phases of maturation were characterized: A phase of rapid growth and a high level of structural dynamics during the second week of development, a phase of maximum structural complexity and spine formation followed by dendritic pruning during the third week, and finally, a phase of structural stabilization during the fourth week (Figure 22). This work has established a basis for future research directed toward detailed, online investigation of the development of postnatally-born, living GCs over prolonged periods of time *in vitro*. This will enable observations of dynamic cellular interactions between individual newly generated GCs and their environment during their integration into the existing hippocampal network and the resulting effects on older GCs. Since OTCs are easily accessible for chronic manipulation and observation, the development, integration, structural dynamics, and spine and synapse formation of individual newborn GCs could be investigated under various conditions. For example, dendritic reorganization and the underlying mechanisms following network activity inhibition could easily be investigated with TTX treatment or by denervation of afferent fibers via EC lesion. Subsequent re-innervation by co-culturing lesioned OTC with EC cultures (Del Turco and Deller, 2007) or applying specific stimulation to lateral or medial EC afferents using optical stimulations could provide insight into the

reorganizational and homeostatic processes following injury and rescue. The application of optogenetic methods and other stimuli such as antibodies, transmitters, or growth factors would shed light on the cellular dynamics and mechanisms of developing GCs in response to increased synaptic activity. These and other approaches could easily be applied in the OTC/time-lapse paradigm which would help advance the knowledge of basic cellular processes underlying the structural and functional development and integration of individual newborn GCs in an existing neural network.

7. References

- Acheson DT, Gresack JE, Risbrough VB (2012) Hippocampal dysfunction effects on context memory: Possible etiology for posttraumatic stress disorder. *Neuropharmacology* 62:674–685.
- Aimone JB, Deng W, Gage FH (2010) Adult neurogenesis: integrating theories and separating functions. *Trends Cog Sci*:1–13.
- Aimone JB, Deng W, Gage FH (2011) Resolving new memories: a critical look at the dentate gyrus, adult neurogenesis, and pattern separation. *Neuron* 70:589–596.
- Aimone JB, Wiles J, Gage FH (2006) Potential role for adult neurogenesis in the encoding of time in new memories. *Nat Neurosci* 9:723–727.
- Akers KG, Martinez-Canabal A, Restivo L, Yiu AP, De Cristofaro A, Hsiang H-LL, Wheeler AL, Guskjolen A, Niibori Y, Shoji H, Ohira K, Richards B a, Miyakawa T, Josselyn S a, Frankland PW (2014) Hippocampal neurogenesis regulates forgetting during adulthood and infancy. *Science* 344:598–602.
- Altman J (1969) Autoradiographic and histological studies of postnatal neurogenesis. IV. Cell proliferation and migration in the anterior forebrain, with special reference to persisting neurogenesis in the olfactory bulb. *J Comp Neurol* 137:433–457.
- Altman J, Bayer SA (1990) Migration and distribution of two populations of hippocampal granule cell precursors during the perinatal and postnatal periods. *J Comp Neurol* 301:365–381.
- Altman J, Das GD (1965) Autoradiographic and histological evidence of postnatal hippocampal neurogenesis in rats. *J Comp Neurol* 124:319–335.
- Alvarez DD, Giacomini D, Yang SM, Trincherro MF, Temprana SG, Buttner KA, Beltramone N, Schinder AF (2016) A disynaptic feedback network activated by experience promotes the integration of new granule cells. *Science* (80-) 354:459–465.
- Alvarez-Buylla A, Lim DA (2004) For the Long Run: Maintaining Germinal Niches in the Adult Brain. *Neuron* 41:683–686.
- Amaral DG, Ishizuka N, Claiborne B (1990) Neurons, numbers and the hippocampal network. *Prog Brain Res* 83:1–11.

References

- Amaral DG, Scharfman HE, Lavenex P (2007) The dentate gyrus: fundamental neuroanatomical organization (dentate gyrus for dummies). *Prog Brain Res* 163:3–22.
- Amaral DG, Witter MP (1989) The three-dimensional organization of the hippocampal formation: a review of anatomical data. *Neuroscience* 31:571–591.
- Ambrogini P, Lattanzi D, Ciuffoli S, Agostini D, Bertini L, Stocchi V, Santi S, Cuppini R (2004) Morpho-functional characterization of neuronal cells at different stages of maturation in granule cell layer of adult rat dentate gyrus. *Brain Res* 1017:21–31.
- Ambrogini P, Minelli A, Lattanzi D, Ciuffoli S, Fanelli M, Cuppini R (2006) Synaptically-silent immature neurons show gaba and glutamate receptor-mediated currents in adult rat dentate gyrus. *Arch Ital Biol* 144:115–126.
- Andersen J, Urbán N, Achimastou A, Ito A, Simic M, Ullom K, Martynoga B, Lebel M, Göritz C, Frisén J, Nakafuku M, Guillemot F (2014) A transcriptional mechanism integrating inputs from extracellular signals to activate hippocampal stem cells. *Neuron* 83:1085–1097.
- Andersen P, Morris R, Amaral D, Bliss T, O'Keefe J (2006) *The Hippocampus Book* (Andersen P, Morris R, Amaral D, Bliss T, O'Keefe J, eds). Oxford University Press.
- Angevine JB (1965) Time of neuron origin in the hippocampal region. An autoradiographic study in the mouse. *Exp Neurol Suppl:Suppl* 2:1–70.
- Arruda-Carvalho M, Sakaguchi M, Akers KG, Josselyn SA, Frankland PW (2011) Posttraining Ablation of Adult-Generated Neurons Degrades Previously Acquired Memories. *J Neurosci* 31:15113–15127.
- Ashton RS, Conway A, Pangarkar C, Bergen J, Lim K-I, Shah P, Bissell M, Schaffer D V (2012) Astrocytes regulate adult hippocampal neurogenesis through ephrin-B signaling. *Nat Neurosci* 15:1399–1406.
- Barkho BZ, Song H, Aimone JB, Smrt RD, Kuwabara T, Nakashima K, Gage FH, Zhao X (2006) Identification of astrocyte-expressed factors that modulate neural stem/progenitor cell differentiation. *Stem Cells Dev* 15:407–421.
- Bayer SA, Altman J (1974) Hippocampal development in the rat: Cytogenesis and morphogenesis examined with autoradiography and low-level X-irradiation. *J Comp Neurol* 158:55–79.

-
- Beckervordersandforth R, Zhang C-L, Lie DC (2015) Transcription-Factor-Dependent Control of Adult Hippocampal Neurogenesis. *Cold Spring Harb Perspect Biol* 7:a018879.
- Beining M, Jungenitz T, Radic T, Deller T, Cuntz H, Jedlicka P, Schwarzacher SW (2016) Adult-born dentate granule cells show a critical period of dendritic reorganization and are distinct from developmentally born cells. *Brain Struct Funct*:1–20.
- Bekiari C, Giannakopoulou A, Siskos N, Grivas I, Tsingotjidou A, Michaloudi H, Papadopoulos GC (2015) Neurogenesis in the septal and temporal part of the adult rat dentate gyrus. *Hippocampus* 25:511–523.
- Ben-Ari Y (2002) Excitatory actions of gaba during development: the nature of the nurture. *Nat Rev Neurosci* 3:728–739.
- Berg DA, Belnoue L, Song H, Simon A (2013) Neurotransmitter-mediated control of neurogenesis in the adult vertebrate brain. *Development* 140:2548–2561.
- Bergami M, Berninger B (2012) A fight for survival: the challenges faced by a newborn neuron integrating in the adult hippocampus. *Dev Neurobiol* 72:1016–1031.
- Bergami M, Masserdotti G, Temprana SG, Motori E, Eriksson TM, Göbel J, Yang SM, Conzelmann K-K, Schinder AF, Götz M, Berninger B (2015) A critical period for experience-dependent remodeling of adult-born neuron connectivity. *Neuron* 85:710–717.
- Bergmann O, Liebl J, Bernard S, Alkass K, Yeung MSY, Steier P, Kutschera W, Johnson L, Landén M, Druid H, Spalding KL, Frisén J (2012) The Age of Olfactory Bulb Neurons in Humans.
- Besnard A, Sahay A (2016) Adult Hippocampal Neurogenesis, Fear Generalization, and Stress. *Neuropsychopharmacology* 41:24–44.
- Bonaguidi MA, Wheeler MA, Shapiro JS, Stadel RP, Sun GJ, Ming G, Song H (2011) In vivo clonal analysis reveals self-renewing and multipotent adult neural stem cell characteristics. *Cell* 145:1142–1155.
- Bond AM, Ming G-L, Song H (2015) Adult Mammalian Neural Stem Cells and Neurogenesis: Five Decades Later. *Cell Stem Cell* 17:385–395.
- Brandt MD, Jessberger S, Steiner B, Kronenberg G, Reuter K, Bick-Sander A, Behrens W Von Der, Kempermann G (2003) Transient calretinin expression defines early postmitotic step of neuronal differentiation in adult hippocampal neurogenesis of mice. *Mol Cell Neurosci* 24:603–613.

References

- Braun SMG, Jessberger S (2014) Review: Adult neurogenesis and its role in neuropsychiatric disease, brain repair and normal brain function. *Neuropathol Appl Neurobiol* 40:3–12.
- Brown JP, Couillard-Després S, Cooper-Kuhn CM, Winkler J, Aigner L, Kuhn HG (2003) Transient expression of doublecortin during adult neurogenesis. *J Comp Neurol* 467:1–10.
- Bruel-Jungerman E, Laroche S, Rampon C (2005) New neurons in the dentate gyrus are involved in the expression of enhanced long-term memory following environmental enrichment. *Eur J Neurosci* 21:513–521.
- Buckner RL (2010) The role of the hippocampus in prediction and imagination. *Annu Rev Psychol* 61:27–48, C1–C8.
- Burghardt NS, Park EH, Hen R, Fenton AA (2012) Adult-born hippocampal neurons promote cognitive flexibility in mice. *Hippocampus* 22:1795–1808.
- Buzsáki G (2005) Theta rhythm of navigation: link between path integration and landmark navigation, episodic and semantic memory. *Hippocampus* 15:827–840.
- Buzsáki G, Moser EI (2013) Memory, navigation and theta rhythm in the hippocampal-entorhinal system. *Nat Neurosci* 16:130–138.
- Cameron HA, Woolley CS, McEwen BS, Gould E (1993) Differentiation of newly born neurons and glia in the dentate gyrus of the adult rat. *Neuroscience* 56:337–344.
- Carleton A, Petreanu LT, Lansford R, Alvarez-Buylla A, Lledo P-M (2003) Becoming a new neuron in the adult olfactory bulb. *Nat Neurosci* 6:507–518.
- Cesca F, Baldelli P, Valtorta F, Benfenati F (2010) The synapsins: key actors of synapse function and plasticity. *Prog Neurobiol* 91:313–348.
- Chancey JH, Poulsen DJ, Wadiche JI, Overstreet-Wadiche L (2014) Hilar mossy cells provide the first glutamatergic synapses to adult-born dentate granule cells. *J Neurosci* 34:2349–2354.
- Chawla MK, Guzowski JF, Ramirez-Amaya V, Lipa P, Hoffman KL, Marriott LK, Worley PF, McNaughton BL, Barnes CA (2005) Sparse, environmentally selective expression of Arc RNA in the upper blade of the rodent fascia dentata by brief spatial experience. *Hippocampus* 15:579–586.
- Chechneva O, Dinkel K, Schrader D, Reymann KG (2005) Identification and characterization of two neurogenic zones in interface organotypic hippocampal slice cultures. *Neuroscience* 136:343–355.

-
- Christian KM, Song H, Ming G (2014) Functions and dysfunctions of adult hippocampal neurogenesis. *Annu Rev Neurosci* 37:243–262.
- Clelland CD, Choi M, Romberg C, Clemenson GD, Fragniere A, Tyers P, Jessberger S, Saksida LM, Barker R a, Gage FH, Bussey TJ (2009) A functional role for adult hippocampal neurogenesis in spatial pattern separation. *Science* 325:210–213.
- Clemenson GD, Lee SW, Deng W, Barrera VR, Iwamoto KS, Fanselow MS, Gage FH (2015) Enrichment rescues contextual discrimination deficit associated with immediate shock. *Hippocampus* 25:385–392.
- Couillard-Despres S, Winner B, Schaubeck S, Aigner R, Vroemen M, Weidner N, Bogdahn U, Winkler J, Kuhn H-G, Aigner L (2005) Doublecortin expression levels in adult brain reflect neurogenesis. *Eur J Neurosci* 21:1–14.
- Creer DJ, Romberg C, Saksida LM, van Praag H, Bussey TJ (2010) Running enhances spatial pattern separation in mice. *Proc Natl Acad Sci U S A* 107:2367–2372.
- Cuntz H, Forstner F, Borst A (2011) The TREES Toolbox — Probing the Basis of Axonal and Dendritic Branching. *Neuroinformatics* 9:91–96.
- Cuntz H, Forstner F, Borst A, Häusser M (2010) One rule to grow them all: a general theory of neuronal branching and its practical application. *PLoS Comput Biol* 6.
- Danielson NB, Kaifosh P, Zaremba JD, Lovett-Barron M, Tsai J, Denny CA, Balough EM, Goldberg AR, Drew LJ, Hen R, Losonczy A, Kheirbek MA (2016) Distinct Contribution of Adult-Born Hippocampal Granule Cells to Context Encoding. *Neuron* 90:101–112.
- DeCarolis NA, Eisch AJ (2010) Hippocampal neurogenesis as a target for the treatment of mental illness: A critical evaluation. *Neuropharmacology* 58:884–893.
- Del Turco D, Deller T (2007) Organotypic Entorhino-Hippocampal Slice Cultures—A Tool to Study the Molecular and Cellular Regulation of Axonal Regeneration and Collateral Sprouting In Vitro. *Methods Mol Biol* 399:55–66.
- Delgado AC, Ferrón SR, Vicente D, Porlan E, Perez-Villalba A, Trujillo CM, D’Ocón P, Fariñas I (2014) Endothelial NT-3 delivered by vasculature and CSF promotes quiescence of subependymal neural stem cells through nitric oxide induction. *Neuron* 83:572–585.

References

- Demars M, Hu Y-S, Gadadhar A, Lazarov O (2010) Impaired neurogenesis is an early event in the etiology of familial Alzheimer's disease in transgenic mice. *J Neurosci Res* 88:2103–2117.
- Deng W, Aimone JB, Gage FH (2010) New neurons and new memories: how does adult hippocampal neurogenesis affect learning and memory? *Nat Rev Neurosci* 11:339–350.
- Déry N, Pilgrim M, Gibala M, Gillen J, Wojtowicz JM, Macqueen G, Becker S (2013) Adult hippocampal neurogenesis reduces memory interference in humans: opposing effects of aerobic exercise and depression. *Front Neurosci* 7:66.
- Deshpande A, Bergami M, Ghanem A, Conzelmann K-K, Lepier A, Götz M, Berninger B (2013) Retrograde monosynaptic tracing reveals the temporal evolution of inputs onto new neurons in the adult dentate gyrus and olfactory bulb. *Proc Natl Acad Sci U S A* 110:E1152–E1161.
- Dieni C V, Nietz AK, Panichi R, Wadiche JI, Overstreet-Wadiche L (2013) Distinct determinants of sparse activation during granule cell maturation. *J Neurosci* 33:19131–19142.
- Dityatev A, Dityateva G, Sytnyk V, Dellling M, Toni N, Nikonenko I, Muller D, Schachner M (2004) Polysialylated Neural Cell Adhesion Molecule Promotes Remodeling and Formation of Hippocampal Synapses. *J Neurosci* 24:9372–9382.
- Döbrössy MD, Drapeau E, Aurousseau C, Le Moal M, Piazza P V, Abrous DN (2003) Differential effects of learning on neurogenesis: learning increases or decreases the number of newly born cells depending on their birth date. *Mol Psychiatry* 8:974–982.
- Doetsch F (2003) A niche for adult neural stem cells. *Curr Opin Genet Dev* 13:543–550.
- Doetsch F, García-Verdugo JM, Alvarez-Buylla A (1997) Cellular composition and three-dimensional organization of the subventricular germinal zone in the adult mammalian brain. *J Neurosci* 17:5046–5061.
- Drakew A, Frotscher M, Heimrich B (1999) Blockade of neuronal activity alters spine maturation of dentate granule cells but not their dendritic arborization. *Neuroscience* 94:767–774.
- Dranovsky A, Picchini AM, Moadel T, Sisti AC, Yamada A, Kimura S, Leonardo ED, Hen R (2011) Experience Dictates Stem Cell Fate in the Adult Hippocampus. *Neuron* 70:908–923.

-
- Drew LJ, Fusi S, Hen R (2013) Adult neurogenesis in the mammalian hippocampus: Why the dentate gyrus? *Learn Mem* 20:710–729.
- Drew LJ, Kheirbek MA, Luna VM, Denny CA, Cloyd MA, Wu M V., Jain S, Scharfman HE, Hen R (2016) Activation of local inhibitory circuits in the dentate gyrus by adult-born neurons. *Hippocampus* 26:763–778.
- Duan X, Chang JH, Ge S, Faulkner RL, Kim JY, Kitabatake Y, Liu X, Yang C-H, Jordan JD, Ma DK, Liu CY, Ganesan S, Cheng H-J, Ming G, Lu B, Song H (2007) Disrupted-In-Schizophrenia 1 regulates integration of newly generated neurons in the adult brain. *Cell* 130:1146–1158.
- Dupret D, Fabre A, Döbrössy MD, Panatier A, Rodríguez JJ, Lamarque S, Lemaire V, Oliet SHR, Piazza P-V, Abrous DN (2007) Spatial Learning Depends on Both the Addition and Removal of New Hippocampal Neurons Moser E, ed. *PLoS Biol* 5:e214.
- Edmondson J, Hatten M (1987) Glial-guided granule neuron migration in vitro: a high-resolution time-lapse video microscopic study. *J Neurosci* 7.
- Ehninger D, Li W, Fox K, Stryker MP, Silva AJ (2008) Reversing Neurodevelopmental Disorders in Adults. *Neuron* 60:950–960.
- Ekdahl CT, Claassen J-H, Bonde S, Kokaia Z, Lindvall O (2003) Inflammation is detrimental for neurogenesis in adult brain. *Proc Natl Acad Sci* 100:13632–13637.
- Eriksson PS, Perfilieva E, Björk-Eriksson T, Alborn AM, Nordborg C, Peterson DA, Gage FH (1998) Neurogenesis in the adult human hippocampus. *Nat Med* 4:1313–1317.
- Ernst A, Alkass K, Bernard S, Salehpour M, Perl S, Tisdale J, Possnert G, Druid H, Frisén J (2014) Neurogenesis in the striatum of the adult human brain. *Cell* 156:1072–1083.
- Espósito MS, Piatti VC, Laplagne DA, Ferrari CC, Pitossi FJ, Schinder AF (2005) Neuronal differentiation in the adult hippocampus recapitulates embryonic development. *Hippocampus* 25:10074–10086.
- Fanselow MS, Dong H-W (2010) Are the dorsal and ventral hippocampus functionally distinct structures? *Neuron* 65:7–19.
- Farmer J, Zhao X, van Praag H, Wodtke K, Gage F., Christie B. (2004) Effects of voluntary exercise on synaptic plasticity and gene expression in the dentate gyrus of adult male sprague-dawley rats in vivo. *Neuroscience* 124:71–79.

References

- Faulkner RL, Jang M-H, Liu X-B, Duan X, Sailor KA, Kim JY, Ge S, Jones EG, Ming G -I., Song H, Cheng H-J (2008) Development of hippocampal mossy fiber synaptic outputs by new neurons in the adult brain. *Proc Natl Acad Sci* 105:14157–14162.
- Fernando RN, Eleuteri B, Abdelhady S, Nussenzweig A, Andäng M, Ernfors P (2011) Cell cycle restriction by histone H2AX limits proliferation of adult neural stem cells. *Proc Natl Acad Sci U S A* 108:5837–5842.
- Frotscher M, Drakew A, Heimrich B (2000) Role of Afferent Innervation and Neuronal Activity in Dendritic Development and Spine Maturation of Fascia Dentata Granule Cells. :946–951.
- Fuentealba LC, Obernier K, Alvarez-Buylla A (2012) Adult neural stem cells bridge their niche. *Cell Stem Cell* 10:698–708.
- Gage FH (2000) Mammalian neural stem cells. *Science* 287:1433–1438.
- Gähwiler BH (1984) DEVELOPMENT OF THE HIPPOCAMPUS IN VITRO : CELL TYPES , SYNAPSES AND RECEPTORS. 11:751–760.
- Gähwiler BH, Capogna M, Debanne D, McKinney R a, Thompson SM (1997) Organotypic slice cultures: a technique has come of age. *Trends Neurosci* 20:471–477.
- Gao Z, Ure K, Ables JL, Lagace DC, Nave K-A, Goebbels S, Eisch AJ, Hsieh J (2009) Neurod1 is essential for the survival and maturation of adult-born neurons. *Nat Neurosci* 12:1090–1092.
- Garthe A, Roeder I, Kempermann G (2015) Mice in an enriched environment learn more flexibly because of adult hippocampal neurogenesis. *Hippocampus* 26:261–271.
- Ge S, Goh ELK, Sailor K a, Kitabatake Y, Ming G, Song H (2006) GABA regulates synaptic integration of newly generated neurons in the adult brain. *Nature* 439:589–593.
- Ge S, Yang C-H, Hsu K-S, Ming G-L, Song H (2007) A critical period for enhanced synaptic plasticity in newly generated neurons of the adult brain. *Neuron* 54:559–566.
- Gerlach J, Donkels C, Münzner G, Haas CA (2016) Persistent Gliosis Interferes with Neurogenesis in Organotypic Hippocampal Slice Cultures. 10:131.
- Gleeson JG, Lin PT, Flanagan LA, Walsh CA (1999) Doublecortin is a microtubule-associated protein and is expressed widely by migrating neurons. *Neuron* 23:257–271.

-
- Goldman SA, Nottebohm F (1983) Neuronal production, migration, and differentiation in a vocal control nucleus of the adult female canary brain. *Proc Natl Acad Sci U S A* 80:2390–2394.
- Gonçalves JT, Bloyd CW, Shtrahman M, Johnston ST, Schafer ST, Parylak SL, Tran T, Chang T, Gage FH (2016a) In vivo imaging of dendritic pruning in dentate granule cells. *Nat Neurosci* 19:788–791.
- Gonçalves JT, Schafer ST, Gage FH (2016b) Adult Neurogenesis in the Hippocampus: From Stem Cells to Behavior. *Cell* 167:897–914.
- Gould E, McEwen B, Tanapat P (1997) Neurogenesis in the dentate gyrus of the adult tree shrew is regulated by psychosocial stress and NMDA receptor activation. *J Neurosci* 17:8787–8795.
- Greengard P, Valtorta F, Czernik AJ, Benfenati F (1993) Synaptic vesicle phosphoproteins and regulation of synaptic function. *Science* 259:780–785.
- Guo W, Allan AM, Zong R, Zhang L, Johnson EB, Schaller EG, Murthy AC, Goggin SL, Eisch AJ, Oostra BA, Nelson DL, Jin P, Zhao X (2011) Ablation of Fmrp in adult neural stem cells disrupts hippocampus-dependent learning. *Nat Med* 17:559–565.
- Hafting T, Fyhn M, Molden S, Moser M-B, Moser EI (2005) Microstructure of a spatial map in the entorhinal cortex. *Nature* 436:801–806.
- Hanson ND, Owens MJ, Boss-Williams KA, Weiss JM, Nemeroff CB (2011) Several stressors fail to reduce adult hippocampal neurogenesis. *Psychoneuroendocrinology* 36:1520–1529.
- Hastings NB, Gould E (1999) Rapid extension of axons into the CA3 region by adult-generated granule cells. *J Comp Neurol* 413:146–154.
- Heimrich B, Frotscher M (1991) Differentiation of dentate granule cells in slice cultures of rat hippocampus: a Golgi / electron microscopic study. *Neuroscience* 538:263–268.
- Heimrich B, Frotscher M (1993) Slice cultures as a model to study entorhinal-hippocampal interaction. *Hippocampus* 3 Spec No:11–17.
- Hill AS, Sahay A, Hen R (2015) Increasing Adult Hippocampal Neurogenesis is Sufficient to Reduce Anxiety and Depression-Like Behaviors. *Neuropsychopharmacology* 40:2368–2378.
- Hjorth-Simonsen A, Jeune B (1972) Origin and termination of the hippocampal perforant path in the rat studied by silver impregnation. *J Comp Neurol* 144:215–232.

References

- Holick KA, Lee DC, Hen R, Dulawa SC (2008) Behavioral Effects of Chronic Fluoxetine in BALB/cJ Mice Do Not Require Adult Hippocampal Neurogenesis or the Serotonin 1A Receptor. *Neuropsychopharmacology* 33:406–417.
- Hsieh J (2012) Orchestrating transcriptional control of adult neurogenesis. *Genes Dev* 26:1010–1021.
- Huang G-J, Bannerman D, Flint J (2008) Chronic fluoxetine treatment alters behavior, but not adult hippocampal neurogenesis, in BALB/cJ mice. *Mol Psychiatry* 13:119–121.
- Hunsaker MR, Chen V, Tran GT, Kesner RP (2013) The medial and lateral entorhinal cortex both contribute to contextual and item recognition memory: A test of the binding of items and context model. *Hippocampus* 23:380–391.
- Hunsaker MR, Kesner RP (2013) The operation of pattern separation and pattern completion processes associated with different attributes or domains of memory. *Neurosci Biobehav Rev* 37:36–58.
- Igarashi KM (2016) The entorhinal map of space. *Brain Res* 1637:177–187.
- Ikrar T, Guo N, He K, Besnard A, Levinson S, Hill A, Lee H-K, Hen R, Xu X, Sahay A (2013) Adult neurogenesis modifies excitability of the dentate gyrus. *Front Neural Circuits* 7:204.
- Ishizuka N, Weber J, Amaral DG (1990) Organization of intrahippocampal projections originating from CA3 pyramidal cells in the rat. *J Comp Neurol* 295:580–623.
- Iwano T, Masuda A, Kiyonari H, Enomoto H, Matsuzaki F (2012) Prox1 postmitotically defines dentate gyrus cells by specifying granule cell identity over CA3 pyramidal cell fate in the hippocampus. *Development* 139:3051–3062.
- Jagasia R, Steib K, Englberger E, Herold S, Faus-Kessler T, Saxe M, Gage FH, Song H, Lie DC (2009) GABA-cAMP response element-binding protein signaling regulates maturation and survival of newly generated neurons in the adult hippocampus. *J Neurosci* 29:7966–7977.
- Jessberger S, Zhao C, Toni N, Clemenson GD, Li Y, Gage FH (2007) Seizure-associated, aberrant neurogenesis in adult rats characterized with retrovirus-mediated cell labeling. *J Neurosci* 27:9400–9407.
- Johnston ST, Shtrahman M, Parylak S, Gonçalves JT, Gage FH (2015) Paradox of Pattern Separation and Adult Neurogenesis: A Dual Role for

-
- New Neurons Balancing Memory Resolution and Robustness. *Neurobiol Learn Mem*.
- Julian LM, Vandenbosch R, Pakenham CA, Andrusiak MG, Nguyen AP, McClellan KA, Svoboda DS, Lagace DC, Park DS, Leone G, Blais A, Slack RS (2013) Opposing regulation of Sox2 by cell-cycle effectors E2f3a and E2f3b in neural stem cells. *Cell Stem Cell* 12:440–452.
- Jungenitz T, Beining M, Radic T, Deller T, Cuntz H, Jedlicka P, Schwarzacher SW (n.d.) Structural homo- and heterosynaptic plasticity in adult newborn rat hippocampal granule cells. unpublished.
- Jungenitz T, Radic T, Jedlicka P, Schwarzacher SW (2014) High-frequency stimulation induces gradual immediate early gene expression in maturing adult-generated hippocampal granule cells. *Cereb Cortex* 24:1845–1857.
- Kamada M, Li R-Y, Hashimoto M, Kakuda M, Okada H, Koyanagi Y, Ishizuka T, Yawo H (2004) Intrinsic and spontaneous neurogenesis in the postnatal slice culture of rat hippocampus. *Eur J Neurosci* 20:2499–2508.
- Karalay O, Doberauer K, Vadodaria KC, Knobloch M, Berti L, Miquelajauregui A, Schwark M, Jagasia R, Taketo MM, Tarabykin V, Lie DC, Jessberger S (2011) Prospero-related homeobox 1 gene (Prox1) is regulated by canonical Wnt signaling and has a stage-specific role in adult hippocampal neurogenesis. *Proc Natl Acad Sci U S A* 108:5807–5812.
- Keene CS, Bladon J, McKenzie S, Liu CD, O'Keefe J, Eichenbaum H (2016) Complementary Functional Organization of Neuronal Activity Patterns in the Perirhinal, Lateral Entorhinal, and Medial Entorhinal Cortices. *J Neurosci* 36:3660–3675.
- Kempermann G, Gast D, Kronenberg G, Yamaguchi M, Gage FH (2003) Early determination and long-term persistence of adult-generated new neurons in the hippocampus of mice. *Development* 130:391–399.
- Kempermann G, Jessberger S, Steiner B, Kronenberg G (2004) Milestones of neuronal development in the adult hippocampus. *Trends Neurosci* 27:447–452.
- Kempermann G, Kuhn HG, Gage FH (1997) More hippocampal neurons in adult mice living in an enriched environment. *Nature* 386:493–495.
- Kempermann G, Song H, Gage FH (2015) Neurogenesis in the Adult Hippocampus. *Cold Spring Harb Perspect Biol* 7.
- Kesner RP (2007) A behavioral analysis of dentate gyrus function. *Prog Brain Res* 163:567–576.

References

- Kesner RP (2013) An analysis of the dentate gyrus function. *Behav Brain Res* 254:1–7.
- Kheirbek MA, Hen R (2011) Dorsal vs Ventral Hippocampal Neurogenesis: Implications for Cognition and Mood. *Neuropsychopharmacology* 36:373–374.
- Kim JY, Liu CY, Zhang F, Duan X, Wen Z, Song J, Feighery E, Lu B, Rujescu D, St Clair D, Christian K, Callicott JH, Weinberger DR, Song H, Ming G (2012) Interplay between DISC1 and GABA signaling regulates neurogenesis in mice and risk for schizophrenia. *Cell* 148:1051–1064.
- Kippin TE, Kapur S, van der Kooy D (2005) Dopamine specifically inhibits forebrain neural stem cell proliferation, suggesting a novel effect of antipsychotic drugs. *J Neurosci* 25:5815–5823.
- Kleine Borgmann FB, Bracko O, Jessberger S (2013) Imaging neurite development of adult-born granule cells. *Development* 140:2823–2827.
- Kluge A, Hailer NP, Horvath TL, Bechmann I, Nitsch R (1998) Tracing of the Entorhinal-Hippocampal Pathway In Vitro. 68:57–68.
- Knierim JJ, Neunuebel JP, Deshmukh SS (2013) Functional correlates of the lateral and medial entorhinal cortex: objects, path integration and local–global reference frames. *Philos Trans R Soc London B Biol Sci* 369.
- Ko H-G, Jang D-J, Son J, Kwak C, Choi J-H, Ji Y-H, Lee Y-S, Son H, Kaang B-K (2009) Effect of ablated hippocampal neurogenesis on the formation and extinction of contextual fear memory. *Mol Brain* 2:1.
- Koleske AJ (2013) Molecular mechanisms of dendrite stability. *Nat Rev Neurosci* 14:536–550.
- Komuro H, Rakic P (1995) Dynamics of granule cell migration: a confocal microscopic study in acute cerebellar slice preparations. *J Neurosci* 15.
- Kornack D, Rakic P (1999) Continuation of neurogenesis in the hippocampus of the adult macaque monkey. *Natl Acad Sci*.
- Kügler S, Kilic E, Bähr M (2003) Human synapsin 1 gene promoter confers highly neuron-specific long-term transgene expression from an adenoviral vector in the adult rat brain depending on the transduced area. *Gene Ther* 10:337–347.
- Kügler S, Meyn L, Holzmüller H, Gerhardt E, Isenmann S, Schulz JB, Bähr M (2001) Neuron-specific expression of therapeutic proteins: evaluation of different cellular promoters in recombinant adenoviral vectors. *Mol Cell Neurosci* 17:78–96.

-
- Kuhn HG, Dickinson-Anson H, Gage FH (1996) Neurogenesis in the dentate gyrus of the adult rat: age-related decrease of neuronal progenitor proliferation. *J Neurosci* 16:2027–2033.
- Kunze A, Congreso MR, Hartmann C, Wallraff-Beck A, Huttmann K, Bedner P, Requardt R, Seifert G, Redecker C, Willecke K, Hofmann A, Pfeifer A, Theis M, Steinhauser C (2009) Connexin expression by radial glia-like cells is required for neurogenesis in the adult dentate gyrus. *Proc Natl Acad Sci* 106:11336–11341.
- Lacefield CO, Itskov V, Reardon T, Hen R, Gordon JA (2012) Effects of adult-generated granule cells on coordinated network activity in the dentate gyrus. *Hippocampus* 22:106–116.
- Laplagne DA, Espósito MS, Piatti VC, Morgenstern NA, Zhao C, van Praag H, Gage FH, Schinder AF (2006) Functional convergence of neurons generated in the developing and adult hippocampus. Macklis J, ed. *PLoS Biol* 4:e409.
- Larimer P, Strowbridge BW (2010) Representing information in cell assemblies: persistent activity mediated by semilunar granule cells. *Nat Neurosci* 13:213–222.
- Lavado A, Lagutin O V, Chow LML, Baker SJ, Oliver G (2010) Prox1 is required for granule cell maturation and intermediate progenitor maintenance during brain neurogenesis. *PLoS Biol* 8.
- Lavado A, Oliver G (2007) Prox1 expression patterns in the developing and adult murine brain. *Dev Dyn* 236:518–524.
- Leal SL, Tighe SK, Yassa MA (2014) Asymmetric effects of emotion on mnemonic interference. *Neurobiol Learn Mem* 111:41–48.
- Lee H, Kang E, GoodSmith D, Yoon DY, Song H, Knierim JJ, Ming G, Christian KM (2015) DISC1-mediated dysregulation of adult hippocampal neurogenesis in rats. *Front Syst Neurosci* 9:93.
- Lee J, Hollenberg S, Snider L, Turner D, Lipnick N, Weintraub H (1995) Conversion of *Xenopus* ectoderm into neurons by NeuroD, a basic helix-loop-helix protein. *Science* (80-) 268.
- Lepousez G, Nissant A, Lledo P-M (2015) Adult neurogenesis and the future of the rejuvenating brain circuits. *Neuron* 86:387–401.
- Leutgeb JK, Leutgeb S, Moser M-B, Moser EI (2007) Pattern Separation in the Dentate Gyrus and CA3 of the Hippocampus. *Science* (80-) 315:961–966.

References

- Li D, Field PM, Yoshioka N, Raisman G (1994) Axons regenerate with correct specificity in horizontal slice culture of the postnatal rat entorhino-hippocampal system. *Eur J Neurosci* 6:1026–1037.
- Lie DC, Song H, Colamarino SA, Ming G, Gage FH (2004) Neurogenesis in the adult brain: new strategies for central nervous system diseases. *Annu Rev Pharmacol Toxicol* 44:399–421.
- Lindvall O, Kokaia Z (2011) Stem Cell Research in Stroke: How Far From the Clinic? *Stroke* 42:2369–2375.
- Lois C, Alvarez-Buylla A (1993) Proliferating subventricular zone cells in the adult mammalian forebrain can differentiate into neurons and glia. *Proc Natl Acad Sci U S A* 90:2074–2077.
- Lois C, Alvarez-Buylla A (1994) Long-distance neuronal migration in the adult mammalian brain. *Science* 264:1145–1148.
- Lucassen PJ, Oomen CA, Naninck EFG, Fitzsimons CP, van Dam A-M, Czeh B, Korosi A (2015) Regulation of Adult Neurogenesis and Plasticity by (Early) Stress, Glucocorticoids, and Inflammation. *Cold Spring Harb Perspect Biol* 7.
- Luo Y, Shan G, Guo W, Smrt RD, Johnson EB, Li X, Pfeiffer RL, Szulwach KE, Duan R, Barkho BZ, Li W, Liu C, Jin P, Zhao X (2010) Fragile X Mental Retardation Protein Regulates Proliferation and Differentiation of Adult Neural Stem/Progenitor Cells Orr H, ed. *PLoS Genet* 6:e1000898.
- Ma DK, Ming G, Song H (2005) Glial influences on neural stem cell development: cellular niches for adult neurogenesis. *Curr Opin Neurobiol* 15:514–520.
- Madsen T, Kristjansen PEG, Bolwig TG, Wörtwein G (2003) Arrested neuronal proliferation and impaired hippocampal function following fractionated brain irradiation in the adult rat. *Neuroscience* 119:635–642.
- Malberg JE, Eisch AJ, Nestler EJ, Duman RS (2000) Chronic antidepressant treatment increases neurogenesis in adult rat hippocampus. *J Neurosci* 20:9104–9110.
- Mandyam CD, Harburg GC, Eisch a J (2007) Determination of key aspects of precursor cell proliferation, cell cycle length and kinetics in the adult mouse subgranular zone. *Neuroscience* 146:108–122.
- Marín-Burgin A, Mongiat L a, Pardi MB, Schinder AF (2012) Unique processing during a period of high excitation/inhibition balance in adult-born neurons. *Science* (80-) 335:1238–1242.

-
- Mathews EA, Morgenstern NA, Piatti VC, Zhao C, Jessberger S, Schinder AF, Gage FH (2010) A distinctive layering pattern of mouse dentate granule cells is generated by developmental and adult neurogenesis. *J Comp Neurol* 518:4479–4490.
- Miller BR, Hen R (2015) The current state of the neurogenic theory of depression and anxiety. *Curr Opin Neurobiol* 30:51–58.
- Miller MW, Nowakowski RS (1988) Use of bromodeoxyuridine-immunohistochemistry to examine the proliferation, migration and time of origin of cells in the central nervous system. *Brain Res* 457:44–52.
- Ming G-L, Song H (2011) Adult neurogenesis in the mammalian brain: significant answers and significant questions. *Neuron* 70:687–702.
- Mongiati LA, Espósito MS, Lombardi G, Schinder AF (2009) Reliable Activation of Immature Neurons in the Adult Hippocampus. In: Reh TA, ed. *PLoS One* 4:e5320.
- Monje ML, Toda H, Palmer TD (2003) Inflammatory Blockade Restores Adult Hippocampal Neurogenesis. *Science* (80-) 302:1760–1765.
- Moser EI, Kropff E, Moser M-B (2008) Place Cells, Grid Cells, and the Brain's Spatial Representation System. *Annu Rev Neurosci* 31:69–89.
- Mu Y, Zhao C, Toni N, Yao J, Gage FH (2015) Distinct roles of NMDA receptors at different stages of granule cell development in the adult brain. *Elife* 4:e07871.
- Mullen RJ, Buck CR, Smith AM (1992) NeuN, a neuronal specific nuclear protein in vertebrates. *Development* 116:201–211.
- Muller D, Wang C, Skibo G, Toni N, Cremer H, Calaora V, Rougon G, Kiss JZ (1996) PSA-NCAM is required for activity-induced synaptic plasticity. *Neuron* 17:413–422.
- Murphy BL, Pun RYK, Yin H, Faulkner CR, Loepke AW, Danzer SC (2011) Heterogeneous integration of adult-generated granule cells into the epileptic brain. *J Neurosci* 31:105–117.
- Nakashiba T, Cushman JDD, Pelkey KAA, Renaudineau S, Buhl DLL, McHugh TJJ, Rodriguez Barrera V, Chittajallu R, Iwamoto KSS, McBain CJJ, Fanselow MSS, Tonegawa S, Barrera VR, Chittajallu R, Iwamoto KSS, McBain CJJ, Fanselow MSS, Tonegawa S (2012) Young dentate granule cells mediate pattern separation, whereas old granule cells facilitate pattern completion. *Cell* 149:188–201.

References

- Namba T, Mochizuki H, Onodera M, Namiki H, Seki T (2007) Postnatal neurogenesis in hippocampal slice cultures: early in vitro labeling of neural precursor cells leads to efficient neuronal production. *J Neurosci Res* 85:1704–1712.
- Namba T, Mochizuki H, Suzuki R, Onodera M, Yamaguchi M, Namiki H, Shioda S, Seki T (2011) Time-lapse imaging reveals symmetric neurogenic cell division of GFAP-expressing progenitors for expansion of postnatal dentate granule neurons. *PLoS One* 6:e25303.
- Neunuebel JP, Knierim JJ (2012) Spatial firing correlates of physiologically distinct cell types of the rat dentate gyrus. *J Neurosci* 32:3848–3858.
- Neves G, Cooke SF, Bliss TVP (2008) Synaptic plasticity, memory and the hippocampus: a neural network approach to causality. *Nat Rev Neurosci* 9:65–75.
- Nicola Z, Fabel K, Kempermann G (2015) Development of the adult neurogenic niche in the hippocampus of mice. *Front Neuroanat* 9:53.
- Niibori Y, Yu T-S, Epp JR, Akers KG, Josselyn SA, Frankland PW (2012) Suppression of adult neurogenesis impairs population coding of similar contexts in hippocampal CA3 region. *Nat Commun* 3:1253.
- O'Keefe J (1976) Place units in the hippocampus of the freely moving rat. *Exp Neurol* 51:78–109.
- O'Keefe J, Dostrovsky J (1971) The hippocampus as a spatial map. Preliminary evidence from unit activity in the freely-moving rat. *Brain Res* 34:171–175.
- O'Reilly RC, McClelland JL (1994) Hippocampal conjunctive encoding, storage, and recall: avoiding a trade-off. *Hippocampus* 4:661–682.
- Ohkawa N, Saitoh Y, Tokunaga E, Nihonmatsu I, Ozawa F, Murayama A, Shibata F, Kitamura T, Inokuchi K (2012) Spine formation pattern of adult-born neurons is differentially modulated by the induction timing and location of hippocampal plasticity. *PLoS One* 7:e45270.
- Okano H, Pfaff D, Gibbs R (1993) RB and Cdc2 expression in brain: correlations with 3H-thymidine incorporation and neurogenesis. *J Neurosci*.
- Ortega F, Gascón S, Masserdotti G, Deshpande A, Simon C, Fischer J, Dimou L, Chichung Lie D, Schroeder T, Berninger B (2013) Oligodendroglial and neurogenic adult subependymal zone neural stem cells constitute distinct lineages and exhibit differential responsiveness to Wnt signalling. *Nat Cell Biol* 15:602–613.

-
- Osten P, Grinevich V, Cetin A (2007) Viral vectors: a wide range of choices and high levels of service. *Handb Exp Pharmacol*:177–202.
- Ottone C, Krusche B, Whitby A, Clements M, Quadrato G, Pitulescu ME, Adams RH, Parrinello S (2014) Direct cell-cell contact with the vascular niche maintains quiescent neural stem cells. *Nat Cell Biol* 16:1045–1056.
- Overstreet Wadiche L, Bromberg DA, Bensen AL, Westbrook GL (2005) GABAergic signaling to newborn neurons in dentate gyrus. *J Neurophysiol* 94:4528–4532.
- Owens DF, Boyce LH, Davis MB, Kriegstein AR (1996) Excitatory GABA responses in embryonic and neonatal cortical slices demonstrated by gramicidin perforated-patch recordings and calcium imaging. *J Neurosci* 16:6414–6423.
- Paez-Gonzalez P, Asrican B, Rodriguez E, Kuo CT (2014) Identification of distinct ChAT⁺ neurons and activity-dependent control of postnatal SVZ neurogenesis. *Nat Neurosci* 17:934–942.
- Pardi MB, Ogando MB, Schinder AF, Marin-Burgin A (2015) Differential inhibition onto developing and mature granule cells generates high-frequency filters with variable gain. *Elife* 4:e08764.
- Parent JM, Yu TW, Leibowitz RT, Geschwind DH, Sloviter RS, Lowenstein DH (1997) Dentate granule cell neurogenesis is increased by seizures and contributes to aberrant network reorganization in the adult rat hippocampus. *J Neurosci* 17:3727–3738.
- Piatti VC, Davies-Sala MG, Espósito MS, Mongiat L a, Trinchero MF, Schinder AF (2011) The timing for neuronal maturation in the adult hippocampus is modulated by local network activity. *J Neurosci* 31:7715–7728.
- Piatti VC, Esposito MS, Schinder AF, Espósito MS, Schinder AF (2006) The timing of neuronal development in adult hippocampal neurogenesis. *Neuroscientist* 12:463–468.
- Pleasure SJ, Collins AE, Lowenstein DH (2000) Unique expression patterns of cell fate molecules delineate sequential stages of dentate gyrus development. *J Neurosci* 20:6095–6105.
- Plümpe T, Ehninger D, Steiner B, Klempin F, Jessberger S, Brandt M, Römer B, Rodriguez GR, Kronenberg G, Kempermann G (2006) Variability of doublecortin-associated dendrite maturation in adult hippocampal neurogenesis is independent of the regulation of precursor cell proliferation. *BMC Neurosci* 7:77.

References

- Pologruto TA, Sabatini BL, Svoboda K (2003) ScanImage: flexible software for operating laser scanning microscopes. *Biomed Eng Online* 2:13.
- Radic T, Al-Qaisi O, Jungenitz T, Beining M, Schwarzacher SW (2015) Differential Structural Development of Adult-Born Septal Hippocampal Granule Cells in the Thy1-GFP Mouse, Nuclear Size as a New Index of Maturation Zheng JC, ed. *PLoS One* 10:e0135493.
- Radic T, Jungenitz T, Singer M, Beining M, Cuntz H, Vlachos A, Deller T, Schwarzacher SW (2017) Time-lapse imaging reveals highly dynamic structural maturation of postnatally born dentate granule cells in organotypic entorhino-hippocampal slice cultures. *Sci Rep* 7:43724.
- Raineteau O, Hugel S, Ozen I, Rietschin L, Sigrist M, Arber S, Gähwiler BH (2006) Conditional labeling of newborn granule cells to visualize their integration into established circuits in hippocampal slice cultures. *Mol Cell Neurosci* 32:344–355.
- Raineteau O, Rietschin L, Gradwohl G, Guillemot F, Gähwiler BH (2004) Neurogenesis in hippocampal slice cultures. *Mol Cell Neurosci* 26:241–250.
- Ramón y Cajal S (1913) Contribución al conocimiento de la neuroglía del cerebro humano. *Trab. Lab. Invest. Biol. Univ. Madrid* XI, 215-315.
- Rangel LM, Alexander AS, Aimone JB, Wiles J, Gage FH, Chiba AA, Quinn LK (2014) Temporally selective contextual encoding in the dentate gyrus of the hippocampus. *Nat Commun* 5:3181.
- Rao MS, Shetty AK (2004) Efficacy of doublecortin as a marker to analyse the absolute number and dendritic growth of newly generated neurons in the adult dentate gyrus. *Eur J Neurosci* 19:234–246.
- Reynolds BA, Weiss S (1992) Generation of neurons and astrocytes from isolated cells of the adult mammalian central nervous system. *Science* 255:1707–1710.
- Richetin K, Leclerc C, Toni N, Gallopin T, Pech S, Roybon L, Rampon C (2015) Genetic manipulation of adult-born hippocampal neurons rescues memory in a mouse model of Alzheimer's disease. *Brain* 138:440–455.
- Ridley AJ, Schwartz MA, Burridge K, Firtel RA, Ginsberg MH, Borisy G, Parsons JT, Horwitz AR (2003) Cell Migration: Integrating Signals from Front to Back. *Science* (80-) 302.
- Sadgrove MP, Laskowski A, Gray WP (2006) Examination of granule layer cell count, cell density, and single-pulse BrdU incorporation in rat organotypic

- hippocampal slice cultures with respect to culture medium, septotemporal position, and time in vitro. *J Comp Neurol* 497:397–415.
- Sahay A, Hen R (2007) Adult hippocampal neurogenesis in depression. *Nat Neurosci* 10:1110–1115.
- Sahay A, Scobie KN, Hill AS, O'Carroll CM, Kheirbek MA, Burghardt NS, Fenton AA, Dranovsky A, Hen R (2011) Increasing adult hippocampal neurogenesis is sufficient to improve pattern separation. *Nature* 472:466–470.
- Salvi R, Steigleder T, Schlachetzki JCM, Waldmann E, Schwab S, Winner B, Winkler J, Kohl Z (2016) Distinct Effects of Chronic Dopaminergic Stimulation on Hippocampal Neurogenesis and Striatal Doublecortin Expression in Adult Mice. *Front Neurosci* 10:77.
- Santarelli L, Saxe M, Gross C, Surget A, Battaglia F, Dulawa S, Weisstaub N, Lee J, Duman R, Arancio O, Belzung C, Hen R (2003) Requirement of Hippocampal Neurogenesis for the Behavioral Effects of Antidepressants. *Science* (80-) 301:805–809.
- Sargolini F, Fyhn M, Hafting T, McNaughton BL, Witter MP, Moser M-B, Moser EI (2006) Conjunctive Representation of Position, Direction, and Velocity in Entorhinal Cortex. *Science* (80-) 312.
- Saxe MD, Battaglia F, Wang J-W, Malleret G, David DJ, Monckton JE, Garcia ADR, Sofroniew M V, Kandel ER, Santarelli L, Hen R, Drew MR (2006) Ablation of hippocampal neurogenesis impairs contextual fear conditioning and synaptic plasticity in the dentate gyrus. *Proc Natl Acad Sci U S A* 103:17501–17506.
- Schindelin J, Arganda-Carreras I, Frise E, Kaynig V, Longair M, Pietzsch T, Preibisch S, Rueden C, Saalfeld S, Schmid B, Tinevez J-Y, White DJ, Hartenstein V, Eliceiri K, Tomancak P, Cardona A (2012) Fiji: an open-source platform for biological-image analysis. *Nat Methods* 9:676–682.
- Schlachetzki JCM, Grimm T, Schlachetzki Z, Ben Abdallah NMB, Ettle B, Vöhringer P, Ferger B, Winner B, Nuber S, Winkler J (2015) Dopaminergic lesioning impairs adult hippocampal neurogenesis by distinct modification of α -synuclein. *J Neurosci Res* 94:n/a – n/a.
- Schlessinger AR, Cowan WM, Gottlieb DI (1975) An autoradiographic study of the time of origin and the pattern of granule cell migration in the dentate gyrus of the rat. *J Comp Neurol* 159:149–175.
- Schmidt-Hieber C, Jonas P, Bischofberger J (2004) Enhanced synaptic plasticity in newly generated granule cells of the adult hippocampus. *Nature* 429:184–187.

References

- Seki T, Arai Y (1993) Highly polysialylated neural cell adhesion molecule (NCAM-H) is expressed by newly generated granule cells in the dentate gyrus of the adult rat. *J Neurosci*.
- Seki T, Sato T, Toda K, Osumi N, Imura T, Shioda S (2014) Distinctive population of Gfap-expressing neural progenitors arising around the dentate notch migrate and form the granule cell layer in the developing hippocampus. *J Comp Neurol* 522:261–283.
- Seri B, García-Verdugo JM, Collado-Morente L, McEwen BS, Alvarez-Buylla A (2004) Cell types, lineage, and architecture of the germinal zone in the adult dentate gyrus. *J Comp Neurol* 478:359–378.
- Shapiro LA, Korn MJ, Shan Z, Ribak CE (2005) GFAP-expressing radial glia-like cell bodies are involved in a one-to-one relationship with doublecortin-immunolabeled newborn neurons in the adult dentate gyrus. *Brain Res* 1040:81–91.
- Shelton DJ, Kirwan CB (2013) A possible negative influence of depression on the ability to overcome memory interference. *Behav Brain Res* 256:20–26.
- Shors TJ (2004) Learning During Stressful Times. *Learn Mem* 11:137–144.
- Sierra A, Encinas JM, Deudero JJP, Chancey JH, Enikolopov G, Overstreet-Wadiche LS, Tsirka SE, Maletic-Savatic M (2010) Microglia shape adult hippocampal neurogenesis through apoptosis-coupled phagocytosis. *Cell Stem Cell* 7:483–495.
- Snyder JS, Choe JS, Clifford MA, Jeurling SI, Hurley P, Brown A, Kamhi JF, Cameron HA (2009) Adult-Born Hippocampal Neurons Are More Numerous, Faster Maturing, and More Involved in Behavior in Rats than in Mice. *J Neurosci* 29:14484–14495.
- Snyder JS, Ferrante SC, Cameron HA (2012) Late maturation of adult-born neurons in the temporal dentate gyrus. *PLoS One* 7:e48757.
- Snyder JS, Hong NS, McDonald RJ, Wojtowicz JM (2005) A role for adult neurogenesis in spatial long-term memory. *Neuroscience* 130:843–852.
- Solstad T, Boccara CN, Kropff E, Moser M-B, Moser EI (2008) Representation of Geometric Borders in the Entorhinal Cortex. *Science* (80-) 322:1865–1868.
- Song J, Olsen RHJ, Sun J, Ming G-L, Song H (2016) Neuronal Circuitry Mechanisms Regulating Adult Mammalian Neurogenesis. *Cold Spring Harb Perspect Biol*.

-
- Song J, Sun J, Moss J, Wen Z, Sun GJ, Hsu D, Zhong C, Davoudi H, Christian KM, Toni N, Ming G, Song H (2013) Parvalbumin interneurons mediate neuronal circuitry–neurogenesis coupling in the adult hippocampus. *Nat Neurosci* 16:1728–1730.
- Song J, Zhong C, Bonaguidi M a, Sun GJ, Hsu D, Gu Y, Meletis K, Huang ZJ, Ge S, Enikolopov G, Deisseroth K, Luscher B, Christian KM, Ming G, Song H (2012) Neuronal circuitry mechanism regulating adult quiescent neural stem-cell fate decision. *Nature* 489:150–154.
- Spalding KL, Bergmann O, Alkass K, Bernard S, Salehpour M, Huttner HB, Boström E, Westerlund I, Vial C, Buchholz BA, Possnert G, Mash DC, Druid H, Frisén J (2013) Dynamics of hippocampal neurogenesis in adult humans. *Cell* 153:1219–1227.
- Spalding KL, Bhardwaj RD, Buchholz BA, Druid H, Frisén J (2005) Retrospective birth dating of cells in humans. *Cell* 122:133–143.
- Stergiopoulos A, Elkouris M, Politis PK (2014) Prospero-related homeobox 1 (Prox1) at the crossroads of diverse pathways during adult neural fate specification. *Front Cell Neurosci* 8:454.
- Steward O (1976) Topographic organization of the projections from the entorhinal area to the hippocampal formation of the rat. *J Comp Neurol* 167:285–314.
- Stoppini L (1991) A simple method for organotypic cultures of nervous tissue. *J Neurosci* 11:315–319.
- Strange BA, Witter MP, Lein ES, Moser EI (2014) Functional organization of the hippocampal longitudinal axis. *Nat Rev Neurosci* 15:655–669.
- Südhof TC, Czernik AJ, Kao HT, Takei K, Johnston PA, Horiuchi A, Kanazir SD, Wagner MA, Perin MS, De Camilli P (1989) Synapsins: mosaics of shared and individual domains in a family of synaptic vesicle phosphoproteins. *Science* 245:1474–1480.
- Sultan S, Gebara EG, Moullec K, Toni N (2013) D-serine increases adult hippocampal neurogenesis. *Front Neurosci* 7:155.
- Sultan S, Li L, Moss J, Petrelli F, Cassé F, Gebara E, Lopatar J, Pfrieder FW, Bezzi P, Bischofberger J, Toni N (2015) Synaptic Integration of Adult-Born Hippocampal Neurons Is Locally Controlled by Astrocytes. *Neuron* 88:957–972.
- Sun GJ, Sailor KA, Mahmood QA, Chavali N, Christian KM, Song H, Ming G (2013) Seamless reconstruction of intact adult-born neurons by serial end-

References

- block imaging reveals complex axonal guidance and development in the adult hippocampus. *J Neurosci* 33:11400–11411.
- Tashiro A, Makino H, Gage FH (2007) Experience-specific functional modification of the dentate gyrus through adult neurogenesis: a critical period during an immature stage. *J Neurosci* 27:3252–3259.
- Tashiro A, Sandler VM, Toni N, Zhao C, Gage FH (2006) NMDA-receptor-mediated, cell-specific integration of new neurons in adult dentate gyrus. *Nature* 442:929–933.
- Temprana SG, Mongiat LA, Yang SM, Trinchero MF, Alvarez DD, Kropff E, Giacomini D, Beltramone N, Lanuza GM, Schinder AF (2015) Delayed Coupling to Feedback Inhibition during a Critical Period for the Integration of Adult-Born Granule Cells. *Neuron* 85:116–130.
- Thored P, Wood J, Arvidsson A, Cammenga J, Kokaia Z, Lindvall O (2007) Long-Term Neuroblast Migration Along Blood Vessels in an Area With Transient Angiogenesis and Increased Vascularization After Stroke. *Stroke* 38:3032–3039.
- Tong CK, Chen J, Cebrián-Silla A, Mirzadeh Z, Obernier K, Guinto CD, Tecott LH, García-Verdugo JM, Kriegstein A, Alvarez-Buylla A (2014) Axonal Control of the Adult Neural Stem Cell Niche. *Cell Stem Cell* 14:500–511.
- Toni N, Laplagne DA, Zhao C, Lombardi G, Ribak CE, Gage FH, Schinder AF (2008) Neurons born in the adult dentate gyrus form functional synapses with target cells. *Nat Neurosci* 11:901–907.
- Toni N, Teng EM, Bushong EA, Aimone JB, Zhao C, Consiglio A, van Praag H, Martone ME, Ellisman MH, Gage FH (2007) Synapse formation on neurons born in the adult hippocampus. *Nat Neurosci* 10:727–734.
- Tozuka Y, Fukuda S, Namba T, Seki T, Hisatsune T (2005) GABAergic excitation promotes neuronal differentiation in adult hippocampal progenitor cells. *Neuron* 47:803–815.
- Tronel S, Belnoue L, Grosjean N, Revest J-M, Piazza P-V, Koehl M, Abrous DN (2012) Adult-born neurons are necessary for extended contextual discrimination. *Hippocampus* 22:292–298.
- Tronel S, Charrier V, Sage C, Maitre M, Leste-Lasserre T, Abrous DN (2015) Adult-born dentate neurons are recruited in both spatial memory encoding and retrieval. *Hippocampus* 25:1472–1479.
- Van Praag H, Christie BR, Sejnowski TJ, Gage FH (1999a) Running enhances neurogenesis, learning, and long-term potentiation in mice. *Proc Natl Acad Sci U S A* 96:13427–13431.

-
- Van Praag H, Kempermann G, Gage FH (1999b) Running increases cell proliferation and neurogenesis in the adult mouse dentate gyrus. *Nat Neurosci* 2:266–270.
- Van Praag H, Schinder A, Christie B, Toni N (2002) Functional neurogenesis in the adult hippocampus. *Nature* 415:1030–1034.
- Vivar C, Peterson BD, van Praag H (2016) Running rewires the neuronal network of adult-born dentate granule cells. *Neuroimage* 131:29–41.
- Vivar C, Potter MC, Choi J, Lee J-Y, Stringer TP, Callaway EM, Gage FH, Suh H, van Praag H (2012) Monosynaptic inputs to new neurons in the dentate gyrus. *Nat Commun* 3:1107.
- Vivar C, Potter MC, van Praag H (2013) All about running: synaptic plasticity, growth factors and adult hippocampal neurogenesis. *Curr Top Behav Neurosci* 15:189–210.
- Vivar C, van Praag H (2013) Functional circuits of new neurons in the dentate gyrus. *Front Neural Circuits* 7:15.
- Von Bohlen Und Halbach O (2007) Immunohistological markers for staging neurogenesis in adult hippocampus. *Cell Tissue Res* 329:409–420.
- Vuksic M, Del Turco D, Vlachos A, Schuldt G, Müller CM, Schneider G, Deller T (2011) Unilateral entorhinal denervation leads to long-lasting dendritic alterations of mouse hippocampal granule cells. *Exp Neurol* 230:176–185.
- Walter C, Murphy BL, Pun RYK, Spieles-Engemann AL, Danzer SC (2007) Pilocarpine-Induced Seizures Cause Selective Time-Dependent Changes to Adult-Generated Hippocampal Dentate Granule Cells. *J Neurosci* 27:7541–7552.
- Wang C, Liu F, Liu Y-Y, Zhao C-H, You Y, Wang L, Zhang J, Wei B, Ma T, Zhang Q, Zhang Y, Chen R, Song H, Yang Z (2011) Identification and characterization of neuroblasts in the subventricular zone and rostral migratory stream of the adult human brain. *Cell Res* 21:1534–1550.
- Willems LM, Zahn N, Ferreirós N, Scholich K, Maggio N, Deller T, Vlachos A (2016) Sphingosine-1-phosphate receptor inhibition prevents denervation-induced dendritic atrophy. *Acta Neuropathol Commun* 4:28.
- Williams PA, Larimer P, Gao Y, Strowbridge BW (2007) Semilunar granule cells: glutamatergic neurons in the rat dentate gyrus with axon collaterals in the inner molecular layer. *J Neurosci* 27:13756–13761.
- Winner B, Winkler J (2015) Adult neurogenesis in neurodegenerative diseases. *Cold Spring Harb Perspect Biol* 7:a021287.

References

- Witter MP (1993) Organization of the entorhinal-hippocampal system: a review of current anatomical data. *Hippocampus* 3 Spec No:33–44.
- Wojtowicz JM, Askew ML, Winocur G (2008) The effects of running and of inhibiting adult neurogenesis on learning and memory in rats. *Eur J Neurosci* 27:1494–1502.
- Xavier GF, Costa VCI (2009) Dentate gyrus and spatial behaviour. *Prog Neuropsychopharmacol Biol Psychiatry* 33:762–773.
- Yang SM, Alvarez DD, Schinder AF (2015) Reliable Genetic Labeling of Adult-Born Dentate Granule Cells Using *Ascl1*CreERT2 and *Glast*CreERT2 Murine Lines. *J Neurosci* 35:15379–15390.
- Ye G, Yi S, Gamkrelidze G, Pasternak JF, Trommer BL (2005) AMPA and NMDA receptor-mediated currents in developing dentate gyrus granule cells. *Dev Brain Res* 155:26–32.
- Zafirov S, Heimrich B, Frotscher M (1994) Dendritic development of dentate granule cells in the absence of their specific extrinsic afferents. *J Comp Neurol* 345:472–480.
- Zhang Z (2004) Maturation of layer V pyramidal neurons in the rat prefrontal cortex: intrinsic properties and synaptic function. *J Neurophysiol* 91:1171–1182.
- Zhao C, Deng W, Gage FH (2008) Mechanisms and functional implications of adult neurogenesis. *Cell* 132:645–660.
- Zhao C, Teng EM, Summers RG, Ming G-L, Gage FH, Jr. M, G.I, Gage FH (2006) Distinct morphological stages of dentate granule neuron maturation in the adult mouse hippocampus. *J Neurosci* 26:3–11.
- Zhou Q, Homma KJ, Poo M (2004) Shrinkage of dendritic spines associated with long-term depression of hippocampal synapses. *Neuron* 44:749–757.

List of Abbreviations

AAV	Adeno-associated virus
Ascl1	Achaete-scute homolog 1
BC	Basket cell
BDNF	Brain-derived neurotrophic factor
BLBP	Brain lipid-binding protein
BMP	Bone morphogenetic proteins
BrdU	5'-bromo-2'-deoxyuridine
BSA	Bovine serum albumin
CA1	CA1 region of hippocampus
CA2	CA2 region of hippocampus
CA3	CA3 region of hippocampus
CB	Calbindin
DCX	Doublecortin
DG	Dentate gyrus
DIV	Days <i>in vitro</i>
dgm1	First dentate migration
dgm2	Second dentate migration
dgt	Tertiary dentate matrix
DNA	Deoxyribonucleic acid
dpi	Days post injection
EC	Entorhinal cortex
EGF	Epidermal growth factor
FGF-2	Basic fibroblast growth factor
GABA	γ -aminobutyric acid
GFAP	Glial fibrillary acidic protein
GC	Granule cell
GCL	Granule cell layer
GFP	Green fluorescent protein
HCl	Hydrochloric acid
HEPES	4-(2-hydroxyethyl)-1-piperazineethanesulfonic acid
HIPP	Hilar perforant path-associated interneurons

List of Abbreviations

HICAP	Hilar commissural-associational pathway interneurons
IB	Infrapyramidal blade
IML	Inner molecular layer
IPC	Intermediate precursor cell
KCC2	Potassium-chloride co-transporter
LEC	Lateral entorhinal cortex
LTP	Long-term potentiation
MEC	Medial entorhinal cortex
MEM	Minimum essential medium
MERM	Modified Edi's Recording Medium
ML	Molecular Layer
MML	Middle molecular layer
MMLV	Moloney murine leukemia virus
MOPP	Molecular layer perforant path-associated cells
NaCl	Sodium chloride
NaN ₃	Sodium azide
NeuN	Neuron-specific nuclear protein
NeuroD	Neuronal differentiation factor
NKCC1	Sodium-potassium-chloride co-transporter
NMDAR	N-methyl-D-aspartate receptor
NSC	Neural stem cell
NSE	Neuron specific enolase
NT-3	Neurotrophin-3
OTC	Organotypic entorhino-hippocampal slice culture
OML	Outer molecular layer
PBS	Phosphate-buffered saline
PFA	Paraformaldehyde
PSC	Post-synaptic current
PV	Parvalbumin
Prox1	Prospero homeobox 1
PSA-NCAM	Polysialylated form of neural cell adhesion molecule
RGL	Radial glia-like cell

RV	Retrovirus / retroviral
SB	Suprapyramidal blade
SEM	Standard error of the mean
SGZ	Subgranular zone
Shh	Sonic hedgehog
Sox2	Sex-determining region Y-box 2
Sub	Subiculum
SVZ	Subventricular zone
Syn	Synapsin 1
TBS	TRIS-buffered saline
Tuj1	Neuron-specific class III beta tubulin
VEGF	Vascular endothelial growth factor

List of Figures

Figure 1. Principal neuron circuitry within the entorhino-hippocampal network.	23
Figure 2. Development of the dentate gyrus (DG)	27
Figure 3. The structural and functional development of newborn dentate granule cells (GCs)	44
Figure 4. Immunohistochemical illustration of calbindin, DCX, and Prox1 distribution in the early postnatal DG of the mouse	67
Figure 5. Quantification of DCX and calbindin expression in the early postnatal mouse DG over time	68
Figure 6. Immunohistochemical illustration of calbindin, DCX, and Prox1 distribution in the early postnatal DG of the rat	71
Figure 7. Quantification of calbindin and DCX expression in the early postnatal rat DG over time	72
Figure 8. Postnatal maturation of the DG progresses faster in the rat compared with the mouse	75
Figure 9. Histological overview of postnatal OTCs	76
Figure 10. Immunocytochemical evaluation of postnatal OTCs at DIV 7	79
Figure 11. Immunocytochemical evaluation of postnatal OTCs at DIV 14	80
Figure 12. Immunocytochemical evaluation of postnatal OTCs at DIV 28	81
Figure 13. Retroviral (RV) transduction of newborn dentate granule cells (GCs) by local injection	83

Figure 14. Perforant path fibers are present in the outer molecular layer (OML) during the development of RV-GFP-labeled GCs *in vitro* 85

Figure 15. Time-lapse imaging and reconstruction of RV-CAG-GFP-labeled postnatally born GCs and older AAV-Synapsin1-tdTomato-labeled GCs 88

Figure 16. Time-lapse imaging of RV-GFP-labeled postnatally born GCs 89

Figure 17. Newborn RV-GFP-labeled GCs exhibit higher dendritic restructuring and dynamics compared with older AAV-Syn-labeled GCs 92

Figure 18. Newborn GCs undergo periods of branching and pruning while older GCs remain structurally stable..... 97

Figure 19. Hourly observation of structural dynamics in postnatally generated GCs during the third week of development..... 98

Figure 20. Dendritic pruning in postnatally born GCs between the third and the fourth week of development..... 99

Figure 21. First spine-like structures appear between 14 and 16 dpi..... 101

Figure 22. Time line of newborn GC development in OTCs..... 102

List of Tables

Table 1. Primary antibodies and working concentrations used in immunostainings.....61

Table 2. Secondary antibodies and working concentrations used in immunostainings
.....61

Acknowledgements

I would like to thank PD Dr. Stephan Schwarzacher for the supervision of this interesting dissertation project as well as the support, interesting discussions, and the assistance in preparing this document.

In addition, I thank Prof. Amparo Acker-Palmer for the evaluation of this thesis.

I would like to thank Prof. Thomas Deller for his support, helpful discussions, and advice, especially during the process of writing paper manuscripts.

My special thanks go to all of my colleagues at the Institute of Clinical Neuroanatomy for a great and fun working environment, particularly Tassilo Jungenitz, Marcel Beining, Mathias Singer, Christos Galanis, and Andreas Strehl for the continuous professional and moral support, great team work, and sincere friendships. Working with you has made all of the difference!

I am especially grateful to Ute Fertig, Charlotte Nolte-Uhl, Martina Hütten, Nadine Zahn, and Anke Biczysko for all of the help and guidance regarding technical and bureaucratic matters as well as the interns who have assisted in parts of the work.

Above all, I thank my friends and family for the constant encouragement, especially my partner Michael, my brother Igor, and above all my parents Jasminka and Branko Radić for the endless support, love, and understanding.

ERKLÄRUNG

Ich erkläre hiermit, dass ich mich bisher keiner Doktorprüfung im Mathematisch-Naturwissenschaftlichen Bereich unterzogen habe.

Frankfurt am Main, den
(Tijana Radic)

Versicherung

Ich erkläre hiermit, dass ich die vorgelegte Dissertation über

„Structural development of postnatally generated dentate granule cells in organotypic entorhino-hippocampal slice cultures“

selbständig angefertigt und mich anderer Hilfsmittel als der in ihr angegebenen nicht bedient habe, insbesondere, dass alle Entlehnungen aus anderen Schriften mit Angabe der betreffenden Schrift gekennzeichnet sind.

Ich versichere, die Grundsätze der guten wissenschaftlichen Praxis beachtet, und nicht die Hilfe einer kommerziellen Promotionsvermittlung in Anspruch genommen zu haben.

Frankfurt am Main, den
(Tijana Radic)

Curriculum Vitae

TIJANA RADIĆ

Address: Offenbacher Landstr. 239
60599 Frankfurt/Main

Mobile: 0176/61458023
E-Mail: tijica@gmail.com
Date of birth: 10 March 1985
Place of birth: Tuzla, Bosnia and Herzegovina



Education

JOHANN-WOLFGANG GOETHE UNIVERSITY, Frankfurt/Main, Germany
INTERDISCIPLINARY CENTER FOR NEUROSCIENCE FRANKFURT
Master of Science, March 2012
Cumulative Grade: 1.2
Course of studies: Interdisciplinary Neuroscience
Thesis topic: Postnatal Neurogenesis in Organotypic Entorhino-
Hippocampal Slice Cultures

BALDWIN-WALLACE COLLEGE, Berea, OH, USA
Bachelor of Science, May 2008
Summa Cum Laude
Majors: Neuroscience, Psychology, German
Cumulative GPA: 3.992
Thesis topic: The Effects of Verapamil and MK-801 on Fear Extinction and
Renewal in the Explicitly Unpaired Procedure

Professional Experience

March 2012-present **Institute of Clinical Neuroanatomy, NeuroScience Center, Goethe University, Frankfurt/Main, Germany, March 2012-present**

Doctoral student / Research associate

Supervisors: PD Dr. Stephan Schwarzacher, Prof. Dr. Thomas Deller

Methods: Organotypic hippocampal slice culture (OTC) preparation; cell culture techniques; BrdU labeling; retroviral transduction in OTCs; transcardial perfusion; slicing of rodent brains and OTCs on vibratome; immunohistochemistry; fluorescent, confocal, and 2-photon microscopy; live cell imaging; 3D cell reconstruction using the TREES toolbox in Matlab; cell counting and image processing analysis using ImageJ/Fiji; statistical testing and analysis using GraphPad Prism; writing research articles.

Sept 2005-Aug 2009 **Southwest General Health Center, Middleburgh Hts., OH, USA**

CT Technician Aide, Patient Transporter

Supervisor: Brad Tarrorick

June 2007-May 2008 **B-W Animal Learning Laboratory, Berea, OH, USA**

Lab Assistant

Faculty Supervisor: Prof. Dr. Brian Thomas

Jan 2007-Aug 2007 **Center for Effective Living, Beachwood, OH, USA**

Intern

Supervisor: Dr. Michael Leach, Forensic Psychologist

Publications

Radic T, Jungenitz T, Singer, M, Cuntz H, Vlachos, A, Deller T, Schwarzacher SW. (2017). Time lapse imaging reveals highly dynamic structural maturation and spine formation of postnatally born dentate granule cells in organotypic entorhino-hippocampal slice cultures. *Sci. Rep.* 7, 43724; doi: 10.1038/srep43724

Beining M*, Jungenitz T*, **Radic T**, Deller T, Cuntz H, Jedlicka P, Schwarzacher SW. Adult-born dentate granule cells show a critical period of dendritic reorganization and are distinct from developmentally born cells. (2016). *Brain Struct. Funct.* 1-20; doi:10.1007/s00429-016-1285-y

Radic T*, Al-Qaisi O*, Jungenitz T*; Beining M; Schwarzacher SW. (2015). Differential structural maturation of adult newly born hippocampal granule cells in the Thy1-GFP mouse; nuclear size as a new index of maturation. *PLoS One* 10(8):e0135493.

Jungenitz T, **Radic T**, Jedlicka P, Schwarzacher SW. High-frequency stimulation induces gradual immediate early gene expression in maturing adult-generated hippocampal granule cells. (2014). *Cereb. Cortex.* 24(7):1845-57.

Manuscripts in preparation:

Jungenitz T*, Beining M*, **Radic T**, Deller T, Cuntz H, Jedlicka P, Schwarzacher SW. Structural homo- and heterosynaptic plasticity in adult newborn hippocampal granule cells.

Strehl A, **Radic T**, Galanis C, Schwarzacher SW, Deller T, Vlachos A. Dopamine prevents homeostatic synaptic plasticity in immature dentate granule cells during early postnatal development.

* Authors contributed equally to the work

Conferences, Oral and Poster presentations

Eurogenesis 2016, Bordeaux (France) 11. - 13. July 2016

Poster presentation: Live imaging of postnatally born dentate granule cells in organotypic entorhino-hippocampal slice cultures reveals highly dynamic structural maturation and spine formation. Radic T, Singer M, Jungenitz T, Cuntz H, Vlachos A, Deller T, Schwarzacher SW.

10th FENS Forum of Neuroscience, Copenhagen (Denmark) 02. - 06. July 2014

Poster presentation: Live imaging of postnatally born dentate granule cells in organotypic entorhino-hippocampal slice cultures reveals highly dynamic structural maturation and spine formation. Radic T, Singer M, Jungenitz T, Cuntz H, Vlachos A, Deller T, Schwarzacher SW.

Adult Neurogenesis: Evolution, Regulation and Function, Dresden (Germany) 6. – 8. May 2015

Poster presentation: Time-Lapse Imaging of Postnatally Born Dentate Granule Cells in Organotypic Entorhino-Hippocampal Slice Cultures. Radic T, Jungenitz T, Schwarzacher SW.

route28, Adult Neurogenesis work shop for PhD students, Frauenchiemsee (Germany) 5. - 11. September 2014

9th FENS Forum of Neuroscience, Milan (Italy) 5. - 9. July 2014

Poster presentation: Retroviral Labeling of Postnatally Born Dentate Granule Cells in Organotypic Entorhino-Hippocampal Slice Cultures. Radic T, Jungenitz T, Schwarzacher SW.

rmn² (rhine main neuroscience network) 3rd biennial meeting, Oberwesel (Germany) 25. - 27. June 2014

Poster presentation: Retroviral Labeling of Postnatally Born Dentate Granule Cells in Organotypic Entorhino-Hippocampal Slice Cultures. Radic T, Jungenitz T, Schwarzacher SW.

Keystone Symposia: Adult Neurogenesis, Stockholm (Sweden) 12. - 17. May 2014

Poster presentation: Radic T, Jungenitz T, Schwarzacher SW.

Oral presentation: *Retroviral Labeling of Postnatally Born Dentate Granule Cells in Organotypic Entorhino-Hippocampal Slice Cultures.*

Eurogenesis, Bordeaux (France) 24. - 26. June 2013

Poster presentation: Postnatal Neurogenesis in Organotypic Entorhino-Hippocampal Slice Cultures. Radic T, Jungenitz T, Schwarzacher SW.

rmn² (rhine main neuroscience network) 2nd biennial meeting, Oberwesel (Germany) 20. - 22. April 2012

ICNF Mini-Symposium, Frankfurt am Main (Germany) 25. November 2011

2010 Western Psychological Association, Cancun (Mexico) April 2010
Poster presentation: MK-801 Blocks Fear Expression and Increases
Fear Renewal in Rats.
Thomas BL, Novak C, Radic T, Goodwin S.

Scholarships and Stipends

FENS travel stipend from the German Neuroscience Society (NWG) – June
2016
Travel stipend from the Freunde und Förderer der Goethe Universität e.V. –
July 2016
Dr. Ernest L. Welborn Scholarship in Psychology - May 2008

Memberships

Founding member and treasurer of "Deutsche Neurowissenschaften
Olympiade (DNO) Frankfurt e.V."
Neurowissenschaftliche Gesellschaft (German Neuroscience Society)
Nu Rho Psi (Neuroscience Honor Society)
Psi Chi (Psychology Honor Society)
Dayton C. Miller Society (Academic Honor Society)

Activities

Organizer of the ICNF "Young Investigator Colloquium" 2015-present
Student representative of ICNF 2015-present
Student representative on the examination board for the master's program
"Interdisciplinary Neuroscience", Goethe University Frankfurt 2010-2012

Other Skills and Qualifications

Microsoft Office applications, Adobe Illustrator, PhotoShop
Data analysis using GraphPad Prism
Image processing and analysis with ImageJ/Fiji
3D cell reconstruction with TREES Toolbox for Matlab
Data analysis using SPSS
FELASA-B (training in experimental procedures on living animals)
Fluent in English, German, and Serbo-Croatian